Strengthening Piers to Resist Vehicular Collision

Final Report

FDOT Contract Number: BED70

Submitted to

The Florida Department of Transportation

Research Center

605 Suwannee Street, MS 30 Tallahassee, FL 32399

Project Manager Ben Goldsberry

FDOT State Structures Design Office

Submitted by

Qian Zhang, PhD	Principal Investigator
Sungmoon Jung, Ph.D	Co-Principal Investigator
Chunpeng Qu	Graduate Assistant
Md. Mashfiqul Islam	Graduate Assistant
Farhad Farzaneh	Graduate Assistant

Department of Civil & Environmental Engineering

FAMU-FSU College of Engineering, Florida State University

2525 Pottsdamer Street, Tallahassee FL 32310

Report Date

April 2024

DISCLAIMER

The opinions, findings, and conclusions expressed in this publication are those of the authors and not necessarily those of the State of Florida Department of Transportation.

Prepared in cooperation with the State of Florida Department of Transportation.

SI (MODERN METRIC) CONVERSION FACTORS

Symbol	When You Know	Multiply By	To Find	Symbol
Length				
in	inches	25.4	millimeters	mm
ft	feet	0.305	meters	m
yd	yards	0.914	meters	m
mi	miles	1.61	kilometers	km
Area				
in^2	square inches	645.2	square millimeters	mm^2
ft^2	square feet	0.093	square meters	m^2
yd^2	square yard	0.836	square meters	m^2
ac	acres	0.405	hectares	ha
mi^2	square miles	2.59	square kilometers	km^2
Volume				
fl oz	fluid ounces	29.57	milliliters	mL
gal	gallons	3.785	liters	L
ft^3	cubic feet	0.028	cubic meters	m^3
yd^3	cubic yards	0.765	cubic meters	m^3
NOTE: volumes greater than 1000 L shall be shown in m^3				
Mass				
oz	ounces	28.35	grams	g
lb	pounds	0.454	kilograms	kg
T	short tons (2000 lb)	0.907	megagrams (or "metric ton")	Mg (or "t")
Force and Pressure or Stress				
lbf	poundforce	4.45	newtons	N
kip	1000 lbf	4.45	kilonewtons	kN
lbf/in^2	poundforce per square inch	6.89	kilopascals	kPa
ksi	1000 lbf/in^2	6.89	megapascals	MPa

TECHNICAL REPORT DOCUMENTATION PAGE

1. Report No.	2. Government Accession No.	3. Recipient's Catalog No.
4. Title and Subtitle Strengthening Piers to Resist Vehicular Collision		5. Report Date April 2024
		6. Performing Organization Code
7. Author(s) Qian Zhang, Sungmoon Jung, Chunpeng Qu, Md. Mashfiqul Islam, Farhad Farzaneh		8. Performing Organization Report No. BED70
9. Performing Organization Name and Address Florida State University 874 Traditions Way, Tallahassee, FL 32306		10. Work Unit No. (TRAIS)
		11. Contract or Grant No.
12. Sponsoring Agency Name and Address Florida Department of Transportation 605 Suwannee Street, MS 30 Tallahassee, FL 32399		13. Type of Report and Period Covered Final Report June 2022 – April 2024
		14. Sponsoring Agency Code
15. Supplementary Notes		

16. Abstract

In this research, we developed dynamic finite element (FE) models to evaluate the effectiveness of three strengthening methods for bridge piers against vehicle collisions, including reinforced concrete (RC) collar, ultra-high performance concrete (UHPC) collar, and fiber-reinforced plastic (FRP) wraps. Our analysis results showed that RC collars designed for a 600-kip (2669-kN) equivalent static force (ESF) were effective in strengthening piers against heavy tractor-trailer collisions. Removing the 6-in (152-mm) spacing dowels, required by the FDOT Structures Manual, did not lead to the failure of the pier but led to a maximum deflection increase of 30%. Considering that the deflection after the increase was still minor, we concluded that the dowel bars could be eliminated. We also found that the 600-kip (2669-kN) ESF design approach for UHPC collars resulted in a conservative design. Compared to RC collars, UHPC collars were more effective in controlling damage and led to a 29% reduction in collar thickness and the elimination of collar reinforcement. Adding collar reinforcement could further reduce the necessary collar thickness. Moreover, increasing the height of RC and UHPC collars was beneficial in reducing deflection. For both RC and UHPC collars, the recommended collar height is at least 108 inches (2743 mm), about 55% of the pier height. However, FRP wrap strengthening was less effective in controlling damage and deflection of piers when compared with RC and UHPC collar-strengthening. Based on these findings, strengthening with RC and UHPC collars are identified as the two most promising methods, and a detailed experimental plan is provided for the next phase of the project.

17. Key Word	18. Distribution Statement
Vehicle collision Bridge pier Pier strengthening Finite element analysis	No restrictions

19. Security Classif. (of this report)	20. Security Classif. (of this page)	21. No. of Pages	22. Price
Unclassified.	Unclassified.	122	

EXECUTIVE SUMMARY

According to the AASHTO LRFD Bridge Design Specifications (AASHTO LRFD), vehicle collision into a pier is addressed by either providing structural resistance to the pier or by redirecting or absorbing the collision load (by protection barriers or crash walls). When the design choice is to provide structural resistance to the pier, an equivalent static force (ESF) approach is used. The AASHTO LRFD requires that the bridge piers should be designed for an equivalent static force of 600 kips, which is assumed to act in a direction of 0° to 15° with the edge of the pavement in a horizontal plane 5 ft above the ground. The 600-kip equivalent static force was adopted in 2012 AASHTO LRFD after the studies conducted by the Texas Transportation Institute found that the previously used 400-kip load at a distance of 4 ft above the ground was not conservative for design. However, many bridges were built prior to that change. The Florida Department of Transportation (FDOT) is increasingly encountering projects with existing piers that were not designed to resist the AASHTO LRFD 600-kip equivalent static design force. In addition, a pier protection barrier is often not viable due to maintenance of traffic or geometric constraints, or conflicts with utilities or other features. Pier protection barriers are also expensive due to the significant length of barrier required, and the maintenance of traffic needed during their construction. In these situations, designers must consider strengthening the existing piers.

To address the critical need for proper strengthening method of existing bridge piers for improved resistance against lateral vehicle collision to meet the AASHTO specifications, the current research applied dynamic finite element (FE) analysis to evaluate the performance of different strengthening methods for piers against vehicle collision, and identified the most promising designs for strengthening piers in Florida. Three pier strengthening methods, including conventional reinforced concrete (RC) collars, ultra-high performance concrete (UHPC) collars, and fiber-reinforced plastic (FRP) wraps, were evaluated.

This project consisted of three major tasks. First, we conducted a comprehensive literature review, synthesizing available knowledge on the dynamic behavior of bridge piers under vehicle collision. This included typically used strengthening methods, designs, and detailing, relevant code regulations, material properties, and previously developed FE models. By screening the available strengthening methods and collecting information for design and analysis, we identified RC collars, UHPC collars, and FRP wraps as the methods to be investigated. In the second step, the analysis and design of the strengthening systems were conducted. A full dynamic FE model was constructed, validated, and used to evaluate these three methods. Hand calculations were also performed to determine the preliminary design of the strengthening system and to ensure that the proposed design would meet the AASHTO code requirements. Through this, we identified RC collars and UHPC collars as the most promising strengthening methods. Designs for these strengthening methods were also presented. The final step involved planning the next phase of experimental research. In this step, we outlined a comprehensive experimental program with a test matrix and procedures to experimentally validate the proposed strengthening methods in future research projects.

TABLE OF CONTENTS

LIST OF FIGURES

LIST OF TABLES

CHAPTER 1 INTRODUCTION

1.1 Background

Currently, the design of bridge piers in the State of Florida follows the FDOT Structures Manual (FDOT, 2024), which follows mostly the AASHTO LRFD Bridge Design Specifications (AASHTO, 2020a), hereafter referred to as AASHTO LRFD. According to AASHTO LRFD (AASHTO, 2020a), vehicle collision into a pier is addressed by either providing structural resistance to the pier or by redirecting or absorbing the collision load (by barriers or crash walls). When the design choice is to provide structural resistance to the pier, an equivalent static force (ESF) approach is used. The AASHTO LRFD (AASHTO, 2020a) requires that the bridge piers should be designed for an equivalent static force of 600 kip (2669 kN), which is assumed to act in a direction of 0° to 15° with the edge of the pavement in a horizontal plane 5 ft (1.52 m) above the ground. The FDOT Structures Manual (FDOT, 2024) also requires the vehicular collision force be considered as a point load acting on the pier column (no distribution of force due to frame action within the pier, foundation, and superstructure) and the column shear capacity be checked assuming failure along two shear planes inclined at 45-degree angles above and below the point of force application.

The 600-kip (2669-kN) equivalent static force was adopted in 2012 AASHTO LRFD (AASHTO, 2012a) after the studies (Buth et al., 2010; Buth et al., 2011) conducted by the Texas Transportation Institute found that the previously used 400-kip (1779-kN) load at a distance of 4 ft (1.22 m) above the ground was not conservative for design. However, many bridges were built prior to that change. In many cases, a pier protection barrier is often not viable due to maintenance of traffic or geometric constraints or conflicts with utilities or other features. Pier protection barriers are also expensive due to the significant length of barrier required and the maintenance of traffic needed during their construction. In these cases, the piers may need to be strengthened to provide enough impact resistance.

Several potential methods, including conventional reinforced concrete (RC) collars, collars with advanced materials like ultra-high performance concrete (UHPC), and fiber-reinforced plastic (FRP) wraps, could be used to strengthen piers to resist impact loading. However, there is still a lack of comprehensive evaluation of these strengthening methods for bridge piers against vehicle collisions. Moreover, information regarding specific design, construction, and detailing requirements for these methods is limited.

1.2 Objectives

Based on the knowledge gaps and research needs, the proposed research aimed to achieve the following objectives:

- Synthesize knowledge on the strengthening methods and designs for bridge piers against vehicle collision;
- Analytically and numerically analyze the behavior of strengthened bridge piers under impact loadings and evaluate the effectiveness of the strengthening methods;
- Identify necessary detailing and quality control measures for achieving effective strengthening;

- Identify the most promising strengthening design for further experimental investigation.

1.3 Approach and Methodology

The current research developed a full dynamic FE model to evaluate and identify the most effective designs for strengthening bridge piers against vehicle collisions. The research flowchart is presented in Figure 1-1. A comprehensive literature review was first conducted, synthesizing available knowledge on the dynamic behavior of bridge piers under vehicle collisions, typically used strengthening methods, designs, detailing, relevant code regulations, material properties, and previously developed finite element models. The ultimate goal of the literature review was to screen the available strengthening methods and collect information for the design and analysis. In the second step, the analysis and design of the strengthening system were conducted. A full dynamic FE model was constructed, validated, and used to evaluate the strengthening methods. Hand calculations were also performed to determine the preliminary design of the strengthening system and to ensure that the proposed design met the AASHTO code requirement. The goal of this task was to determine the most effective and promising strengthening method and design for further investigation. The final step involved planning the next phase of experimental research. In this step, a comprehensive experimental program was outlined with a test matrix and procedures to experimentally validate the proposed strengthening methods in future research projects.

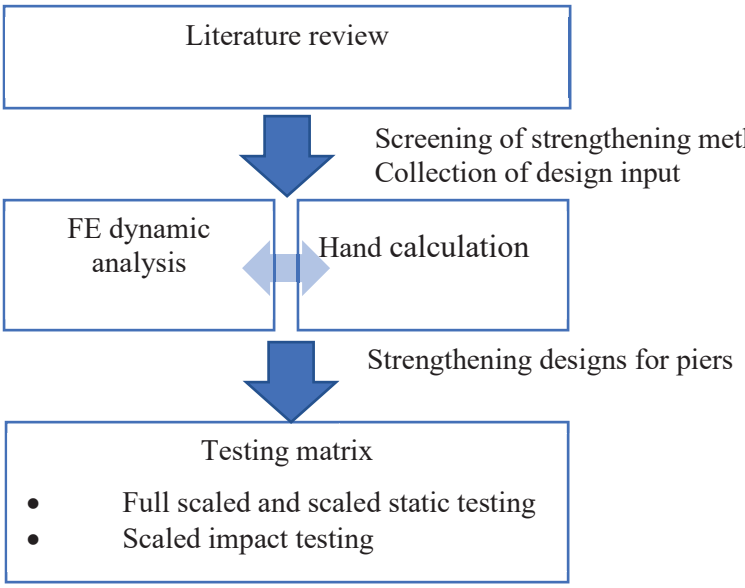

Figure 1-1 Research flow chart

The outline of this report is as follows: chapter 2 presents a comprehensive literature review that synthesizes prior research and guidelines for strengthening bridge piers with normal strength concrete collars, UHPC, FRP, and other applicable methods. Based on the conclusions of the literature review, a plan for the dynamic FE analysis and variable matrix were presented in chapter 3. Chapter 4 presents detailed strengthening designs, and hand calculations were performed to verify the proposed strengthening methods. Chapter 5 documents the validation and calibration of material constitutive models and modeling techniques, which are crucial for achieving accurate and reliable simulation results in the formal FE analysis. In chapter 6, the previously validated models are

applied to perform FE analysis of vehicle collisions with piers featuring different strengthening designs. The effectiveness of various strengthening methods was evaluated and compared. In Chapter 7, an experimental test program was outlined for the next phase of the project to increase confidence in the potential use of the strengthening methods studied in the current project. Chapter 8 presents the summary and conclusions of this research.

CHAPTER 2 LITERATURE REVIEW

2.1 Introduction

AASHTO and the bridge engineering community have emphasized on the safety of bridges by designing them to prevent or withstand excessive impact loads. According to the Federal Highway Administration, the third largest cause of bridge failure in the United States is automobile impacts or crashes (Agrawal et al., 2011). Harik et al. (1990) examined 114 bridge collapses in the United States between 1951 and 1988, determining that 17 (15%) were caused by truck collisions. In a separate study, Wardhana and Hadipriono (2003) revealed that 14 (3%) of the 503 bridge collapses in the United States between 1989 and 2000 were the result of car crashes. Buth et al. (2010) identified 19 crashes involving heavy trucks and bridge piers in Texas and Minnesota between 1965 and 2008, the majority occurring after 2000. According to statistical analysis (Sharma et al., 2008), automobile crashes caused about 210 bridge collapses between 1996 and 2005 in the US. Figure 2-1(a) shows the impact of a heavy truck on the piers of the Tancahua Street Bridge over IH-37 in Corpus Christi, Texas, on May 14, 2004. As a result of this impact, one pier of the bridge was destroyed, although the bridge did not collapse (Cao, 2019). Figure 2-1(b) shows a tractor-semitrailer impacted on SH 14 Bridge over IH-45, Corsicana, Texas and due to the impact, the bridge was collapsed.

(a) (b)

Figure 2-1 (a) Truck impact on piers of Tancahua Street Bridge over IH-37, Corpus Christi, Texas on May 14, 2004 (Cao, 2019); (b) tractor-semitrailer impact on SH-14 Bridge over IH-45, Corsicana, Texas (Buth et al., 2010).

2.1.1 Equivalent static force method for impact design

An impact event is normally characterized using the peak dynamic force (PDF) and ESF (El-Tawil et al., 2005). The PDF is defined as the largest impact force occurring throughout a single collision event which can be obtained by performing experiments or FE simulation based dynamic analysis. Conventionally, it is not considered to be an accurate representation of the demands imposed on the structure because, during the duration of the PDF, the entire structure does not have enough time to respond to the loading (El-Tawil et al., 2005; Auyeung et al., 2019). This makes the dynamic analysis very complicated for impact design of bridge piers. As a result, it is required to

transform the dynamic impact force into an ESF for engineering design in practice. This method is preferred to the PDF method, because the PDF acting on the bridge pier is subject to large variability with different types of vehicles. With different vehicles, the PDF corresponding to one value of kinetic energy can show significant variation. This variation is mainly caused by different contact areas and points of application. On the other hand, ESF is less influenced by the different contact properties of vehicles (Auyeung et al., 2019). The ESF can be calculated based on the following three methods:

- **ESF based on pier stiffness**

ESF can be determined based on the stiffness of the structure. According to Chopra (2011), the ESF is defined as an equivalent static force applied at any time to a structure that produces the same deformation as that produced under a dynamic analysis. This method equates the deformation resulting from the static loading of a structure to the deformations associated with the structure under dynamic loading (i.e., mass, stiffness, and damping). However, the stiffness-based ESF method does not provide an accurate estimate of members undergoing plastic deformations under impact, because the method assumes that the structure behaves elastically.

- **ESF based on kinetic energy and plastic deformation of bridge pier**

For structures which are designed to absorb impact energy by elastic-plastic deformations of members, the ESF may be determined by considering both plastic strength and the deformation capacity of such members. This method is widely used and discussed in Eurocode 1 Parts 1–1 and 1–7 (BSI, 2006a, Eurocode 1 - Actions on structures - Part 1-7: General actions -Accidental actions) for impact designs. Eurocode 1 describes that the design of a structure for impact can be represented by an equivalent static force providing equivalent dynamic response during the impact. In the case of hard impact, it is assumed that the structure is rigid and immovable and that the colliding object deforms linearly during the impact phase. The maximum resulting dynamic interaction force or ESF is given as $F = v_r\sqrt{(k \cdot m)}$, where vr is the object velocity at impact; k is the equivalent elastic stiffness of the object (i.e., the ratio between force F and total deformation); m is the mass of the colliding object. In the case of soft impact, if the structure is assumed elastic and the colliding object rigid and the structure is designed to absorb the impact energy by plastic deformations, provision should be made so that its ductility is sufficient to absorb the total kinetic energy of the colliding object. Thus, the assumption needs to be satisfied by the following expression $1/2(m \cdot vr2) \leq F \cdot y0$, where, F is the ESF, vr is the object velocity at impact, m is the mass of the colliding object y0 is the deformation capacity of structure, i.e., the displacement of the point of impact that the structure can undergo.

As per Eurocode 1 (BSI, 2006a), the dynamic force is the force that varies in time, and which may cause significant dynamic effects on the structure. In the case of impact, the dynamic force represents the force with an associated contact area at the point of impact (Figure 2-2). The equivalent static force is an alternative representation for a dynamic force including the dynamic response of the structure (Figure 2-2, Eurocode 1). Actions due to impact should be determined by a dynamic analysis or represented by an ESF. The forces at the interface of the impacting object and the structure depend on their interaction. The basic variables for impact analysis are the impact velocity of the impacting object and the mass distribution, deformation behavior and damping characteristics of both the impacting object and the structure. Other factors such as the angle of impact, the construction of the impacting object and movement of the impacting object after collision may also be relevant. It is assumed that the impacting body absorbs all the energy which gives conservative results (BSI, 2006a). For structures which are designed to absorb impact

energy by elastic-plastic deformations of members (i.e., soft impact), the equivalent static loads may be determined by considering both plastic strength and the deformation capacity of such members. When the colliding object is modelled as an equivalent impacting object of uniform cross-section (see Figure 2-2b) then the expressions of k and m are k=EA/L and m=ρAL, where L is the length of the impacting object; A is the cross-sectional area; E is the modulus of elasticity; ρ is the mass density of the impacting object. The Eurocode 1 Part 1-7 (BSI, 2006a, paragraph 4.5.1.4(4), Table 2-4.1 and see Annex C for more information) specifies various equivalent static design forces for different types of roads (presented in this study in Table 2-1). In the British National Annex to the Eurocode 1 (BSI, 2006b, Table 2-NA.1), the equivalent static force for vehicle impact is divided into two parts, i.e., the main force and the residual force, which should be simultaneously considered for designing piers. Furthermore, risk analysis is recommended in this code to determine the final design force.

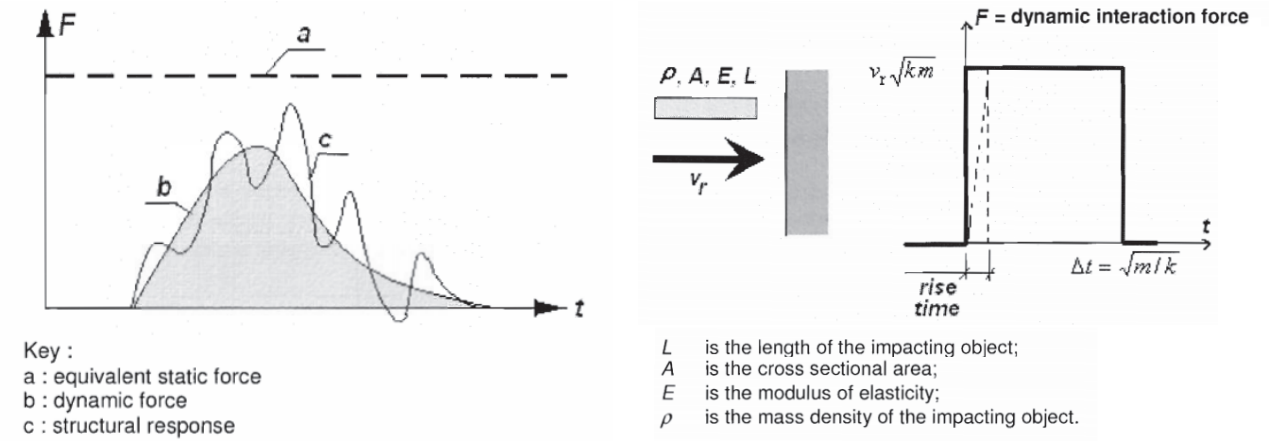

(a) (b)

Figure 2-2 (a) Schematic illustration of equivalent static force, dynamic force, and structural response; (b) impact model (Eurocode 1, BSI 2006a).

- **ESF based on impact force-time history response**

Within the automotive crash community, a common method of representing the ESF for bridge piers is to estimate the peak force of 50 ms for the moving average of the impact force-time history. This technique was used by researchers to obtain a design ESF for vehicle impacts on longitudinal barriers (Beason and Hirsch, 1989). The use of moving averages results in the filtering out of spikes in the data occurring over a short period of time, as these are associated with unusable noise in the signal. If the time interval for the moving average is too large, useful peaks in the data can also be inadvertently filtered out, resulting in lower calculated forces than those occurring. Based on this concept, a significant effort was expended in the project of Texas Transportation Institute at The Texas A&M University System Buth et al. (2011) to improve current understandings of the performance of vehicles during impacts with rigid barriers by Beason and Hirsch (1989). In particular, an effort was made by Buth et al. (2011) (discussed in detail in Section 2) to improve current procedures used to correlate the vehicle impact force (on the concrete walls instrumented with load cells and accelerometers to measure the impact force) with the vehicle acceleration data (by multiplying impact mass with impact acceleration using accelerometers mounted at the center of gravity of test vehicles).

In the above project, Buth et al. (2011) used a 25-ms moving average to filter the force-time histories. This method captured the peaks of the contact force better than a 50-ms moving average filter. The method was validated based upon simplifying assumptions that allow a relatively straightforward relationship between measured vehicle accelerations and the measured impact force. While several different methods for approximating vehicle impact forces have been developed by others, the results of their project presented a unique opportunity to advance current understandings of phenomenon of vehicle impact. In addition to the measurement of the forces by the instrumented wall, procedures have been advanced which allow the determination of the impact force from onboard vehicle accelerometers. While the vehicle impact forces determined from the vehicle accelerations were not as precise as those determined from the instrumented wall, it was believed that the procedures represent a major step forward in instrumenting test vehicles. According to 2010 AASHTO LRFD (AASHTO, 2010), the collision on bridge pier by vehicles shall be addressed by either providing structural resistance or by redirecting or absorbing the collision load, where the design choice was to provide structural resistance, the pier or abutment shall be designed for an ESF of 400 kip (1779 kN) for 50-ms average force, which was assumed to act in any direction in a horizontal plane, at a distance of 4.0 ft (1.22 m) above ground by 80000 lb (36287.3 kg) tractor impacting at 50 mph (80 km/h).

Later on, the 2012 AASHTO LRFD (AASHTO, 2012a) have increased the static design force from the original 400 kip (1779 kN) to 600 kip (2669 kN), (see Table 2-1) which was assumed to act in a direction of 0° to 15° with the edge of the pavement in a horizontal plane 5.0 ft (1.52 m) above the ground based on the full-scale crash tests of rigid columns impacted by 80000 lb (36287.3 kg) tractor trailers at 50 mph (80 km/h) performed by Buth et al. (2011) and also considers 25-ms moving average force. For individual column shafts, the 600-kip (2669-kN) load should be considered a point load. Field observations indicated that shear failures were the primary mode of failure for individual columns and columns that are 30.0 in (762 mm) in diameter and smaller were the most vulnerable (AASHTO, 2020a). This method is also followed in other bridge design codes. For example, in China, only advisory design forces are specified for designing piers against vehicle collision, that is, 224 kip (1000 kN) in the direction of normal travel or 112 kip (500 kN) in the perpendicular direction, whichever is the unfavorable circumstance (Ministry of Transport of the People's Republic of China, 2015). Table 2-1 provides a summary of ESF values followed in different bridge codes.

Table 2-1 Equivalent static forces for vehicle impact with bridge piers (Chen et al., 2020)

Ref.	Road type	Nominal force		Application position above ground (ft)	Load factors
		Direction of normal travel F_x (kip)	Perpendicular to the direction of normal travel F_y (kip)		
AASHTO LRFD (2012)	-	600	-	4.92	1.0
BSI (2006a) "Eurocode 1"	Motorway/main roads	225	112	1.64–4.92	1.0
	Rural roads	169	84	-	-
	Urban roads	112	56	-	-
BSI (2006b) "National Annex to Eurocode 1"	Motorway/main roads	337(169)	169(84)	2.46–1.4.92(3.28–9.84)	2.0 ($R_{de} \geq 2.4$)
	Other roads (speed limit ≥ 72 km/h or 45 mph)	253(127)	253(60)	-	1.0 ($0.5 \leq R_{de} \leq 2.4$)
	Other roads (speed limit≤72 km/h of 45 mph)	169(84)	84(42)	-	0.5 ($R_{de} < 0.5$)
	Minimum requirements	51(34)	51(34)	2.46–4.92 (3.28–9.84)	1.0
Ministry of Transport of the People's Republic of China, 2015	NA	224	112	3.94 (12.80)	1.0

Note: The values in and out of parentheses "()" represent the residual and main load components, respectively, which should be applied simultaneously; the design force F_x should not act simultaneously with F_y, R_{de} represents a risk factor which considers the influences of road class, traffic flow, speed limit, etc.

2.1.2 Importance of dynamic analysis for bridge pier design subjected to impact load

All the above three methods of calculating the ESF for designing bridge piers that are subject to vehicle collisions have some limitations. The stiffness-based method introduced by Chopra (2011) only considers the elastic response of the structure. In reality, the majority of the kinetic energy of the impacting vehicle is absorbed by plastic deformation of the vehicle. The remaining kinetic energy is then absorbed through plastic deformation of the pier. The method recommended by the Eurocode 1 (BSI 2006a) considers plastic deformation in the structural components exposed to the kinetic energy of the vehicle; however, it fails to account for the inertial forces that play a large role

in the load-resisting mechanisms of a structure undergoing dynamic loads. Lastly, the ESF obtained by filtering the contact force-time history data using moving averages may underestimate the actual dynamic load event that may result in under-design (including strengthening design) of bridge piers against vehicular impact force.

Auyeung et al. (2019) reported that, the pier that underwent the dynamic collision load experienced much larger displacements and damage levels. According to their study, the ESF recommended by AASHTO was only able to produce the same displacements and contact forces as a dynamic collision for a truck traveling less than 30 mph (48.3 km/h). At higher vehicle speeds, the static analysis greatly underestimates the displacement and force demand experienced by a bridge pier in a collision. They also noted that the current design provisions are that the ESF is based on a single vehicle traveling at 50 mph (80 km/h). As potential impact conditions are dependent on local traffic conditions, piers may be overdesigned in areas with generally low vehicle speeds and under-designed in areas with high vehicle velocities and a high volume of heavy commercial vehicles. Agrawal et al. (2013) performed a comparison between behavior of piers subjected to 2007 AASHTO LRFD (AASHTO, 2007) prescribed static load (ESF of 1800 kN or 400 kip) and dynamic loads by moving trucks by FE analysis. It is observed from Figure 2-3(a) that the peak displacements because of truck impacts are much higher than that because of the static cases for different impact velocities. The displacement because of the static load corresponds more closely to the displacement because truck impact at 30 mph (48.3 km/h). It is also observed in Figure 2-3(b) that the impact force on bridge piers increases drastically with the increase of the truck impact velocity. At 30 mph (48.3 km/h) truck velocity, impact force on bridge piers is approximately 700 kip (3114 kN), which is much higher than the 400 kip (1800 kN) ESF recommended by the AASHTO LRFD (AASHTO, 2007) and 600-kip (2699-kN) ESF recommended by the latest AASHTO LRFD (AASHTO, 2020a) as well. Therefore, it is observed that the prescribed ESF of AASHTO LRFD (AASHTO, 2020a) is only comparable to the actual dynamic impact load applied by a truck moving at speed less than 30 mph (48.3 km/h). Thus, the AASHTO prescribed ESF significantly underestimated the actual impact event. This proves that only ESF based design and strengthening of RC bridge pier should be avoided.

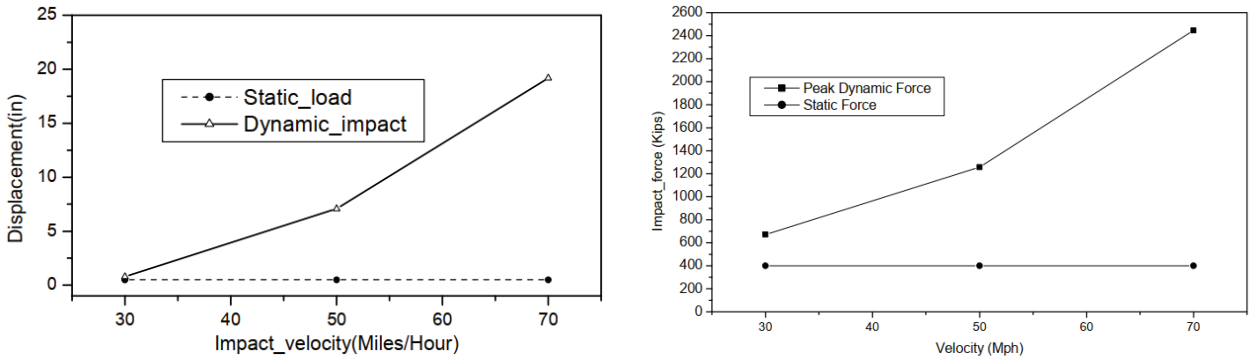

(a) (b)

Figure 2-3 (a) Comparison between peak displacement because of static and dynamic truck impact loads at different speeds; (b) comparison between impact force subjected to static and peak dynamic truck impact loads at different speeds (Agrawal et al., 2013).

2.1.3 Scope of the current study

Before the new ESF value was adopted by AASHTO LRFD (AASHTO, 2012a) in 2012, there were bridges built prior to that change all over the country including Florida. Moreover, there are many bridges in the USA those were built before introducing the concept of ESF by 1994 AASHTO LRFD (AASHTO, 1994), which may not be adequate for vehicular impact load on the bridge piers. The FDOT frequently encounters highway bridges with piers that were not designed to withstand the design ESF of 600 kip (2669 kN) as per the AASHTO LRFD (AASHTO, 2012a). Furthermore, providing the pier protection measures including pier protection barriers are costly to construct as well as the construction is not always suitable due to traffic maintenance, geometric restrictions, conflicts with the utilities, etc. In this situation, the only option left for the structural designers is to strengthen the existing bridge piers to withstand the new design ESF adopted by AASHTO LRFD (AASHTO, 2012a). To this end, it is necessary to conduct a detailed review on the behavior of unstrengthened and strengthened RC bridge piers subjected to vehicular impact force from existing bridge design standards and available literature to fully understand the responses of piers to perform the strengthening design.

There exist very limited number of experimental study and finite element simulation on the vehicular impact based dynamic behavior of unstrengthened (Thilakarathna et al., 2010; Do et al., 2018; Zhou et al., 2018; Zhou and Li, 2018; Sohel et al., 2020; Chen et al., 2021a; Li et al., 2022a; Chen et al., 2022) and strengthened (Fuhaid et al., 2022; Liu, T et al., 2022; Isaac et al, 2011; Sha and Hao, 2015; Liu, X et al., 2022; Mohammed and Parvin, 2020; Al-Bukhaiti et al., 2021; Fan et al., 2018; Liu, X et al., 2022) RC bridge pier due to vehicular collision. There are several strengthening methods employed by the researchers, such as, conventional RC collar (Fuhaid et al., 2022), fiber reinforced polymer (FRP) wrap (Liu, T et al., 2022; Isaac et al., 2011; Sha and Hao, 2015; Liu, X et al., 2022; Mohammed and Parvin, 2020; Al-Bukhaiti et al., 2021), ultra-high performance concrete (UHPC) collar (Fan et al., 2018), and other hybrid strengthening methods (Liu, X et al., 2022). The experimental investigations along with dynamic analysis via FE simulation outcomes of these strengthening method showed promising results to resist the AASHTO LRFD (AASHTO, 2012a) specified impact load due to vehicular collision by the RC bridge piers. Since there is only a limited number of studies available, it is still difficult to assess the performance of these strengthening methods under dynamic impact loads, and the required design and detailing considerations.

To address the critical need for proper strengthening method of existing bridge piers in Florida for an improved resistance against the lateral vehicle collision to meet the AASHTO LRFD (AASHTO, 2012a) specifications, a detailed review of all relevant literature is conducted. The failure behavior and pattern of unstrengthened RC bridge piers subjected to vehicular impact load are discussed. The impact force-time history responses are also explained and discussed based on different vehicle type and engine weight. Corresponding ESF along with finite element modeling based dynamic responses are also discussed. Moreover, different strengthening methods for existing RC bridge piers and their performance are also discussed based on experiment investigation of scaled specimen and loading environment. Finally, a list of conclusions is presented based on the review of existing literature and standards and provided future recommendations. To address the demand for proper strengthening method, the current research proposes to apply FE based dynamic analysis of bridge pier subjected to vehicular impact load to evaluate the performance of different strengthening methods, and to identify the most promising designs for strengthening bridge piers in Florida.

2.2. Review of Vehicle Collision with Unstrengthened Bridge Piers

In the current state of the art, there are very few full-scale crash tests of large vehicles impacting RC bridge pier structures. However, there has been numerous research studies on the dynamic responses of RC columns due to vehicle collision, based on customized experimental impact tests (lateral impact, drop impact, pendulum impact, etc.), theoretical analysis, and numerical simulations. In general, the impact force due to vehicular collision is influenced by the physical characteristics of RC piers (i.e., shape and dimensions, cross-section, bearing capacity, etc.) along with the impact conditions (e.g., location of impact, impact speed, type of impacting vehicle, the mass of the engine and overall mass of the vehicle, etc.).

2.2.1 Dynamic response in the impact-time history curve

Beason and Hirsch (1989) conducted 10 oblique impact tests on vertical walls and found that the impact force-time histories generally have two main peaks (Figure 2-4a). The highest peak ("engine-impact peak") was caused by the collision of the front of the truck, including engine. The next distinct peak (cargo-impact peak" was caused by the container (including cargo). A small peak that precedes the engine-impact peak was caused when the truck bumper contacts the wall. Figure 2-4b shows how the speed of the truck affected the timing and intensity of the impact. Figure 2-5 (Chen et al., 2020) shows impact force-time histories for three types of truck: a Chevrolet C2500 pickup (2 ton), a Ford F800 box truck (12 ton), and a tractor-trailer truck (23 ton). Note that as expected the engine-impact peak for the tractor-trailer truck is much larger than for the smaller trucks; however, the cargo-impact peak for the tractor trailer truck is larger than its engine-peak, in contrast to the smaller trucks, where the cargo-impact peak is smaller than the engine-impact peak.

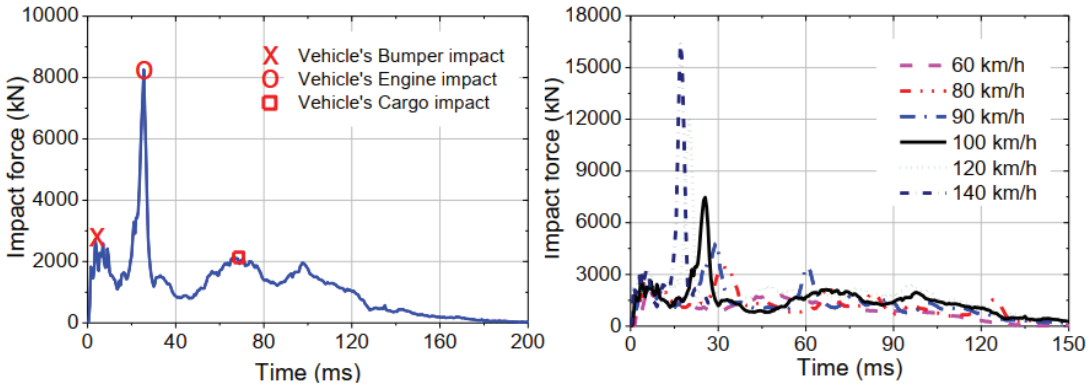

(a) Vehicle velocity of 100 km/h (b) Different vehicle velocities

Figure 2-4 Impact force time history under Ford truck model (7258 kg or 8 ton) collision (Do, 2019)

The first peak of the impact force history (due to engine impact) will increase when the impact velocity or engine mass increases; however, it is hardly influenced by the overall mass of a specific type of impacting vehicle (Do et al., 2018). It is worth noting that the first peak of impact force is barely influenced by the damage state (or bearing capacity) of RC piers, but the damage state of piers after engine impact greatly influences the second peak of impact force. If the pier can sustain the impact load from the engine, then the second peak of impact force history would increase with the increase of impact speed, the overall mass of the vehicle, or stiffness of vehicle structure (Chen et al., 2016). On the other hand, if the bridge pier experiences considerable damage during engine

impact, the second peak of impact force history would reduce due to the reduction of the stiffness and load bearing capacity of the pier; furthermore, if the pier totally fails during the engine impact stage, the second peak of impact force would not even occur (Chen et al., 2020). From the literature, it can be noted that, for most trailer-trucks, the first peak is much higher than the remaining peaks. Therefore, the ESF was chosen as the maximum of the 25-ms moving average, which was longer than the duration of the major peaks from the impact force-time history.

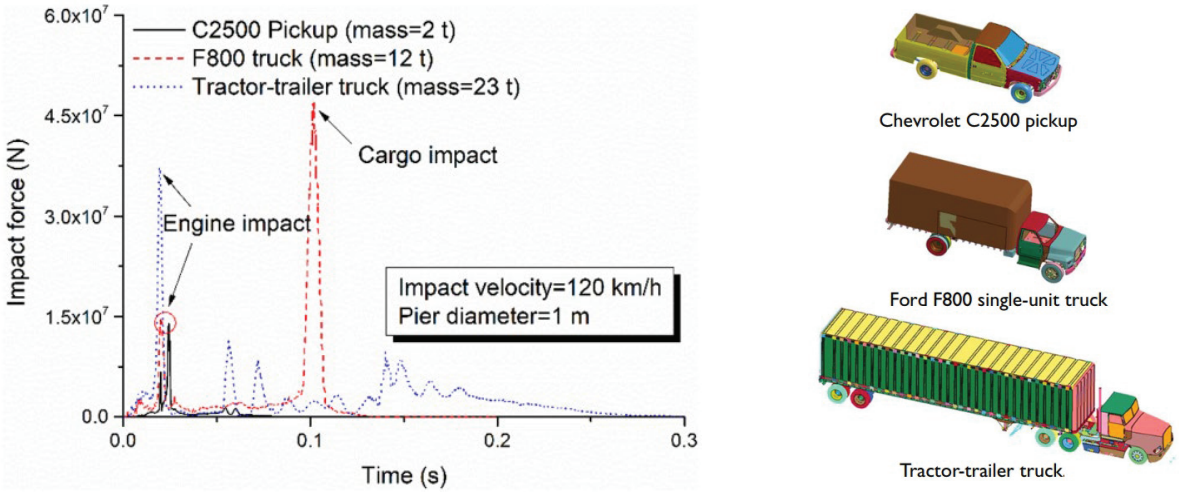

Figure 2-5 Vehicular impact forces on the rigid column from FE simulations (Chen et al., 2020)

There exists a complex relationship between the cross-sectional dimensions of piers on the impact force (Chen et al., 2020). If the cross-sectional size of piers increases that increases the deforming area of the vehicle, then such a cross-section decreases the residual kinetic energy of the vehicle when the cargo hits. Therefore, the peak impact force on a rigid pier caused by cargo impact decreases as the cross-sectional size of the pier increases (Chen et al., 2016). On the other hand, increasing the cross-sectional dimension of the RC pier would enhance its stiffness and impact load-bearing capacity, which might lead to a higher response in the impact force history. The influence of vehicle type on the impact force is also complicated. Chen et al. (2016) reported that larger and heavier vehicles did not necessarily produce larger impact force. As shown in Figure 2-5, despite being heavier and larger than the single-unit truck, the tractor-trailer collision induces a smaller second peak of impact force. This is because the distance between the trailer and the front of the truck is longer, resulting in larger energy consumption of the truck body so that its cargo would hardly collide with the pier (Chen et al., 2020). Regarding RC piers with normal sizes (e.g., with a diameter larger than 30 in (762 mm) subjected to vehicular impact, simulation results showed that the gravity loads from the superstructure, boundary conditions of the superstructure as well as the characteristics of the foundation have little effect on the engine-induced peak of impact force (Do et al., 2018).

Zhou and Li (2018) conducted FE based dynamic analysis and described the vehicle collision events for a single unit truck (11.88-m or 39-ft long, 2.46-m or 8-ft wide, 4.04-m or 13.3-ft high vehicle and the maximum total weight of 50 ton or 45359 kg including the maximum cargo weight of 42.84 ton or 38864 kg at 60 km/h or 37.3 mph) on a bridge pier which are divided in four phases as follows: (i) Initial peak impact force phase (0–50 ms): In most of the cases, the first major peak lies within 25 ms, However, in this phase at the impact position of the affected pier, initially no evident damage or displacement occurred since the vehicle front's stiffness was much lower than the

RC piers (Figure 2-6a). The vehicle travelled towards the pier with an initial impact velocity and the pier collided with the engine the first time. It is found that the deformation is mainly from vehicle deformation since the stiffness of the vehicle front was much smaller than that of the RC pier. Therefore, no obvious damage or displacement was generated at the impact location of the impacted pier; (ii) Impact force of development phase (50–150 ms): At the impact location, concrete began to spall. Displacement can be observed at the impact location (Figure 2-6b). The impact force and displacement increase steadily in this phase in the impact force time history plot (Figure 2-7); (iii) Maximum peak impact force phase (150–200 ms): Shear failure happened at the point of collision (Figure 2-6c). Furthermore, the majority of the concrete at the impact location was damaged, and the stirrups were ruptured. The shear failure occurred at the impact location. In this phase, a great amount of kinetic energy was transferred from the vehicle into the internal energy of the pier in a short period as the pier was impacted by the cargo the second time. In addition, most concrete at the impact location was broken and stirrups were fractured. The displacement increased significantly and the vertical settlement at the top of the pier was generated, which caused the superstructure to collapse. The impact force and displacement reached the maximum at the same time (Figure 2-7); (iv) The impact force of attenuation phase (200–300 ms): The pier's shear and axial bearing capacities were reduced. There was evident residual horizontal displacement and vertical settlement. The vehicle separated from the pier (Figure 2-6d). The pier lost shear capacity and axial bearing capacity. Obvious residual horizontal displacement and vertical settlement remained (Figure 2-7b). Finally, the impact force decreased to zero (Figure 2-7a) along with a residual displacement of 5.67 in (144 mm).

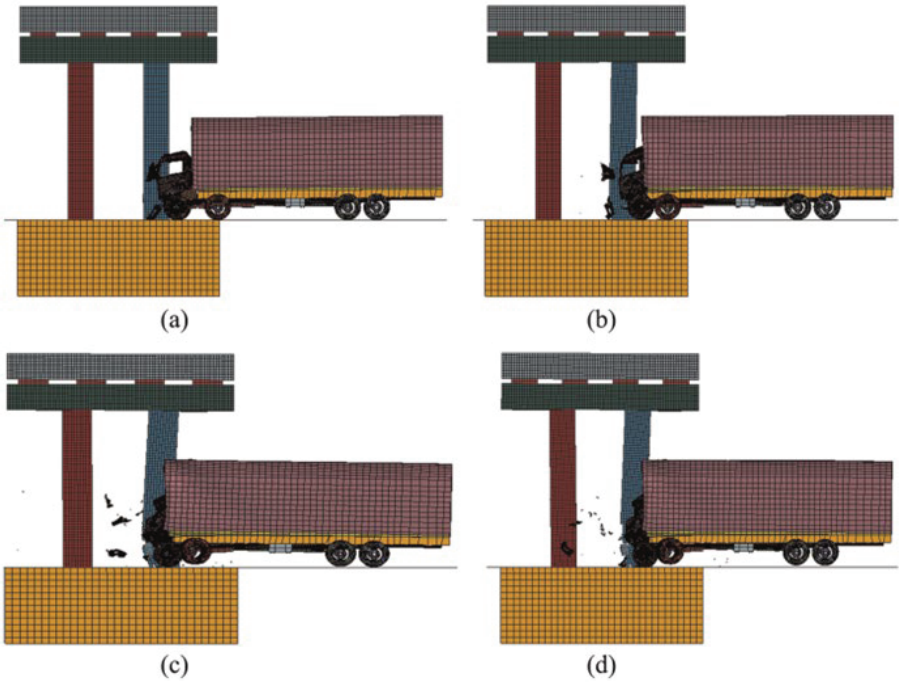

Figure 2-6 Failure process and damage state of the impacted pier in the FE modeling and analyses: (a) 0–50 ms; (b) 50–150 ms; (c) 150–200 ms; (d) 200–300 ms (Zhou and Li, 2018)

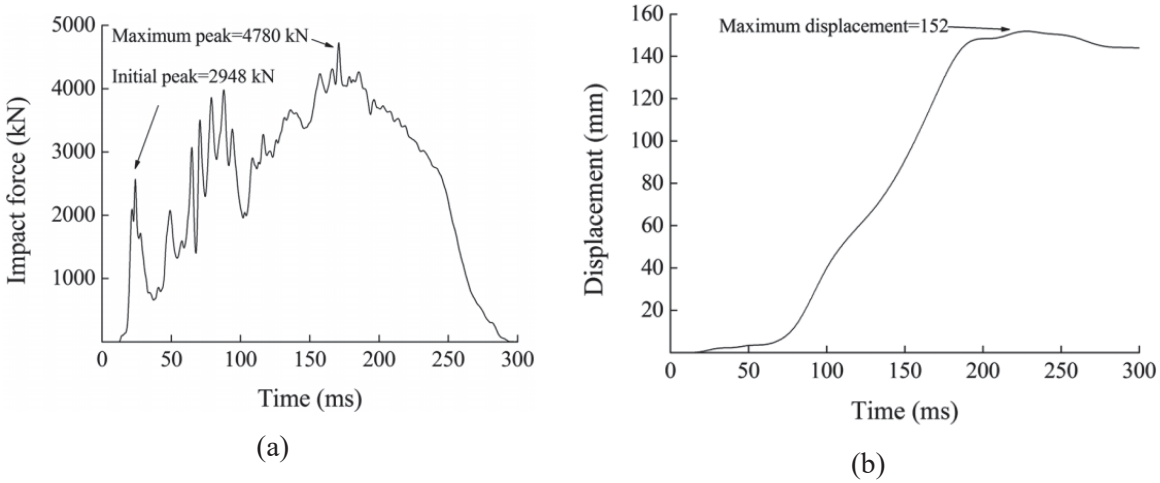

Figure 2-7 (a) Typical impact force time history; (b) typical displacement at the impact location time history (Zhou and Li, 2018)

2.2.2 Review of the experimental work and dynamic FE simulation results

Several full-scale experimental studies were conducted in the past to determine the impact forces during vehicular collisions. A pioneering study was conducted by Popp (1961) who carried out 14 actual vehicle collision tests on unstrengthened RC and steel columns, with vehicle masses from 1.4 ton to 24.0 ton (1270 kg to 21772.4 kg) and collision speed from 30 mph to 52 mph (50.0 km/h to 84.3 km/h) and was able to measure only the column reaction forces. Due to lack of instrumentation, the displacement and acceleration were not measured, yet this study was still of historical importance. They reported that the peak dynamic was up to 2.7 times that of the static reactions at failure, indicating that the impact dynamics can strongly differ from static conditions Since those tests were conducted about 60 years ago, the structure and material characteristics of the collision truck might differ from those of today's vehicles as well as the design, materials, and the construction of RC columns.

Beason and Hirsch (1989) conducted 10 crash tests using vehicles obliquely impacting a vertical rigid wall and obtained the contact force time histories on the wall, that is, vehicular impact force. The vehicle mass and collision speed were from 2 ton to 36.3 ton (1814.4 kg to 32931 kg), and from 44.7 mph to 65.9 mph (71.9 to 105.9 km/h), respectively. It was observed that the impact force time histories during the vehicular collision generally had two main peaks, which were caused by the collision of the front of the truck (including engine) and the container (including cargo) respectively. Based on the maximum impact force (after filtering) of 408 kip (1815 kN) for 50-ms average obtained from the above tests for a tractor tank-trailer of weight 79.8 kip (355 kN) impact velocity 55 mph (88 km/h), the first edition of the AASHTO specification was developed to specify the equivalent static force or ESF (i.e., 1,800 kN or 400 kips) for the bridge pier design against vehicle collision which was in use until 2012.

McGuinn et al. (1996) performed a destructive crash test on an RC pier using a tanker-type tractor-trailer, however, no force was measured. The work was carried out in two phases. In the first phase relatively simple finite element computer models of heavy good vehicles (HGVs) colliding with bridge structures were built and analyzed. Following this work a program of full-scale physical testing was initiated, which consisted of head-on collision of a tanker (typical HGV) to a representative prestressed concrete bridge supported by RC column at 40 mph (64.4 km/h). The peak

horizontal force was 1259 kip (5600 kN) and the average force during total duration of the impact (0.18 sec) was 517 kip (2300 kN). When the force of the engine started to be applied to the column the force suddenly increased. The impact force caused the column to drift along impact direction. However, at about 100 ms into the event there was another large increase in force due to the tanker itself, which caused the column to collapse.

Buth et al. (2011) carried out two frontal crash tests on a rigid column using van-type tractor-trailers under Texas Transportation Institute to evaluate the magnitude of the design force in modernizing the design codes, e.g., AASHTO LRFD (AASHTO, 2012a). They performed two full-scale crash tests with approximately 80000 lbm (36287 kg) van-type tractor-trailer impacting an instrumented, simulated bridge pier at 80 km/h (50 mph) and 15-degree approach angle. The pier was 36 in (914 mm) in diameter and 14-ft (4.27-m) tall and was supported in the longitudinal direction by two load cells. Based on their study, an ESF of 600 kip (2669 kN) based on 25-ms moving average was recommended and later accepted by the AASHTO LRFD (AASHTO, 2012a).

Chen et al. (2021b) investigated an actual medium-duty truck to perform a head-on collision test on a full-scale unstrengthened RC bridge pier to examine the dynamic responses and damage characteristics of the pier and vehicle. The mass of the truck was 7.76 ton (7040 kg) with no ballast and the truck engine weighed approximately 1 ton (907 kg). The height and diameter of the RC column was 15.88 ft (4.84 m) and 3.28 ft (1.0 m), respectively and was supported by a pile of length and diameter of 36.09 ft (11.0 m) and 3.94 ft (1.2 m) respectively. The speed during the collision was maintained 56 mph (90 km/h). The static shear capacity (with a single shear plane) of the column was 234 kip (1042 kN) according to AASHTO LRFD (AASHTO, 2012a), however the ESF was 575 kip (2559 kN) which was much larger than the static shear capacity. Yet, the column only sustained minimal damage in the test, e.g., scratches, dents, and small cracks appeared on the bridge pier due to the impact of the truck as shown in Figure 2-8. They reported that vehicle impact increased the axial compression force at the bottom section of RC piers, which significantly increased the shear capacity of the piers; in addition, the strain rate effects enhanced the material strength. Therefore, the actual shear capacity of the pier was greater than 234 kip (1042 kN).

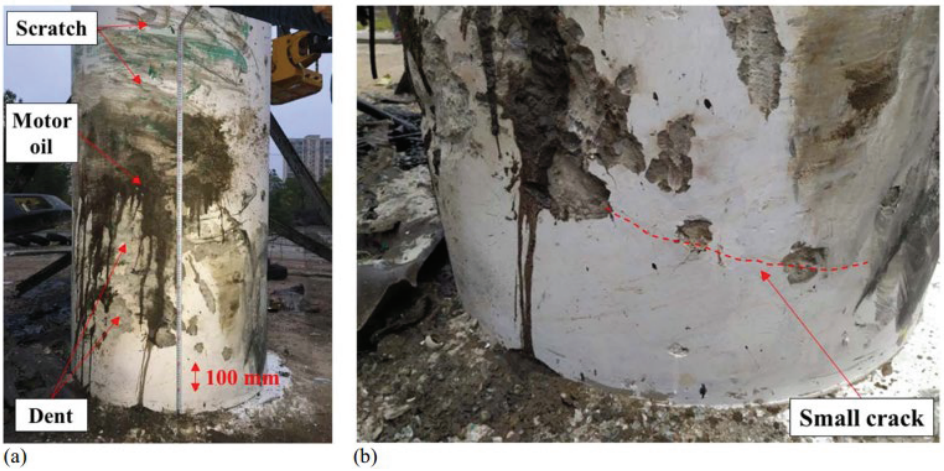

Figure 2-8 Damage of pier after the collision: (a) scratches and dents; (b) small crack (Chen et al., 2021b)

Chen et al. (2022) conducted an impact test on a full-scale RC bridge pier including a monopile foundation subjected to six repeated impact consecutively using a rigid model vehicle accelerated by a self-designed large-size slide device (see Figure 2-9). In addition, FE model was developed and validated against the experimental results. The impact velocities were 7.1, 13.6, 15.5,

15.8, 18.4, and 17.6 mph (11.4, 21.8, 25.0, 25.5, 29.6 and 28.4 km/h) with corresponding ESF of 442, 1012, 1280, 1274, 1406, and 1309 kip (1966, 4501, 5695, 5670, 6252, and 5824 kN), respectively. It can be seen from the Figure 2-9 that the pier did not show obvious cracks after the first impact test attributed to the relatively low impact energy. Horizontal flexural cracks and oblique shear cracks started to appear in the second and third tests, respectively. In general, the number and width of the cracks increased with the number of impacts. In the last (sixth) impact test, the model vehicle overturned after impact and deformed the track, thus the tests were terminated. Figure 2-10(a) shows the final damage of the pier after all six impacts. The FE models established in this study generally reproduced the damage pattern, peak positive displacement, and vibration period of the RC pier under multiple successive collisions as shown in Figure 2-10(b).

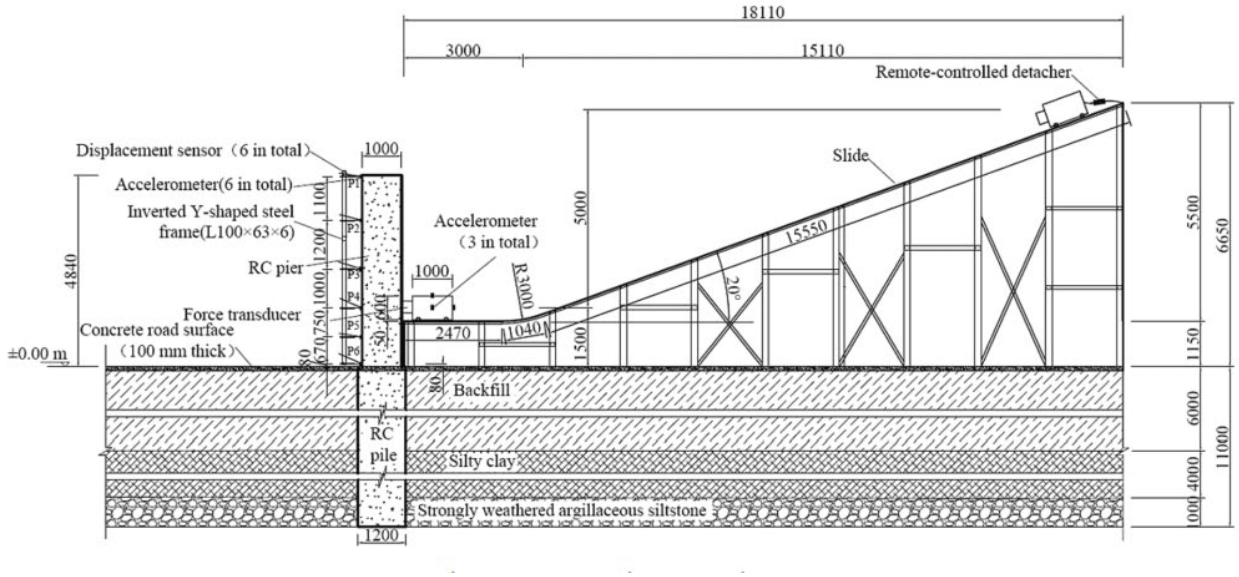

Figure 2-9 Test setup and measuring devices (Chen et al., 2022)

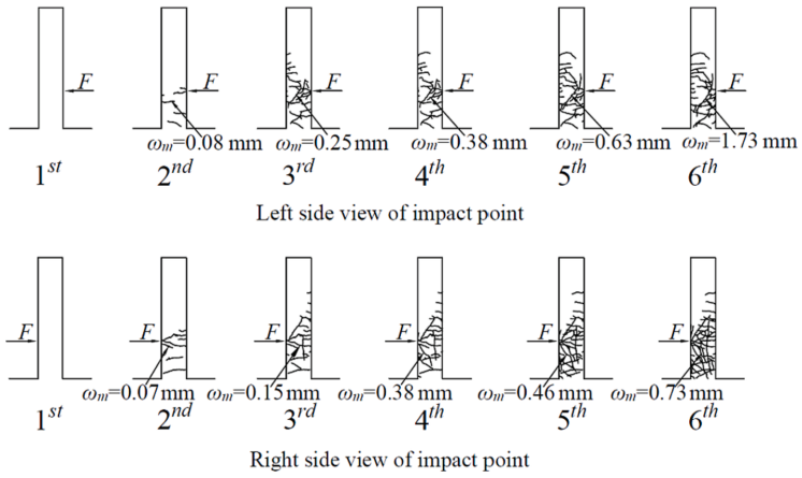

(a)

Figure 2-10 (a) Damage evolution of the RC pier under all the six impact tests; (b) damage contours of the RC pier under all the six impacts (T = 0.25 s) from FE analysis (Chen et al., 2022)

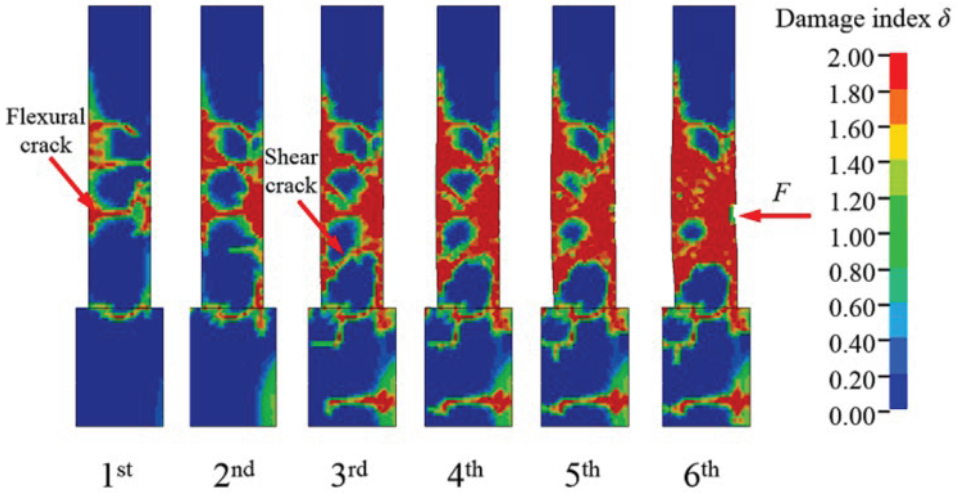

(b)

Figure 2-10 (a) Damage evolution of the RC pier under all the six impact tests; (b) damage contours of the RC pier under all the six impacts (T = 0.25 s) from FE analysis (Chen et al., 2022)

As the actual full-scale crash test using the real vehicle is very expensive and difficult to conduct, the drop impact test of RC pier is performed by several researchers to simulate the vehicular collision of the member (Thilakarathna et al., 2010; Zhou and Li, 2018). Experimental data from the RC column impact tests of the Ph.D. research of Feyerabend (1988) were used in the validation process of FE models by many researchers (Thilakarathna et al., 2010; Zhou and Li, 2018). The typical parameters of Feyerabend (1988) test specimen and setup were: cross-section of column 0.98 ft x 0.98 ft (0.3 m x 0.3 m), span 13.12 ft (4.0 m), initial axial load 45 kip (197 kN), striker force 2.6 kip (11.18 kN), and impact velocity 6.7 mph (10.8 km/h) (Figure 2-11). The columns showed tension cracks initiated at the bottom and top of the section followed by the crushing of the material beneath the impacted zone.

Thilakarathna et al. (2010) modeled the specimens of Feyerabend (1988) using the LS-DYNA finite element program and validated the impact force, deflection, and failure behavior (Figure 2-12a, b). Then they conducted a comprehensive impact analysis of axially loaded columns of 12 inch to 20 inch (300 mm to 500 mm) diameter and evaluated the capacity for the collision of different small vehicles in medium-rise buildings (5 to 20 storied). The impact force produced the ESF of 225 kip (1000 kN). They reported that the failure due to vehicle impact varies from the usual flexural type of failure under midspan impact. Hence, a conventional hypothesis based on the energy absorption capacity of the column may not be applicable as the energy absorption characteristics mainly depend on the flexural deformation of the column. Since the column has not been subjected to flexural deformations, the column has failed due to shear failure initially and subsequently by flexural failure leading to collapse. The observed failure modes can be categorized as shear or shear flexural types of failures depending on the test variables as observed during the many simulations. They also reported that excessive shear forces are generated at the contra-flexure points located close to the supports. This observation may be cited as a potential reason for the failure of the column shown in Figure 2-12(d) which indicates a typical shear critical situation. The Figure 2-shows that laps forming in this region worsen the consequences. Thus, the authors recommended that the conventional design of axial member and respective detailing practices need modification to prevent damages due to impact force. They also suggested that the laps of rebar should be avoided in the

case of axial member with a probable impact load and an adequate transverse reinforcement should be provided close to the supports where shear strength is vital to resist impact load. These recommendations should apply for strengthening design of bridge piers as well.

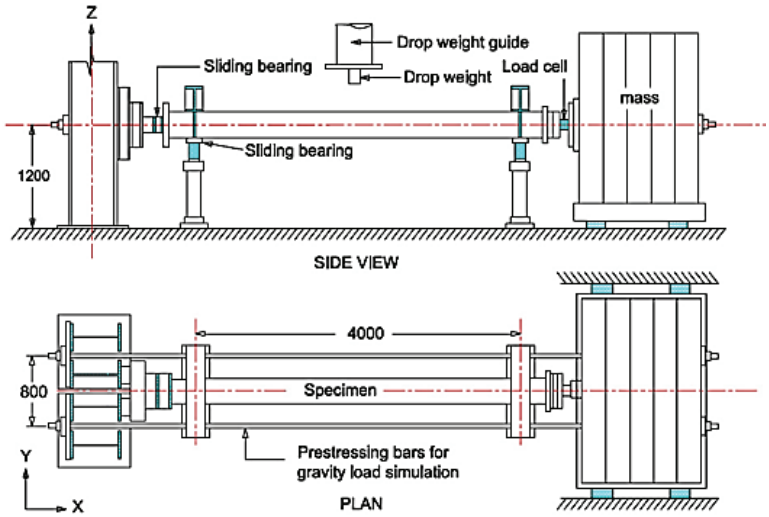

Figure 2-11 The test set-up by Feyerabend (1988)

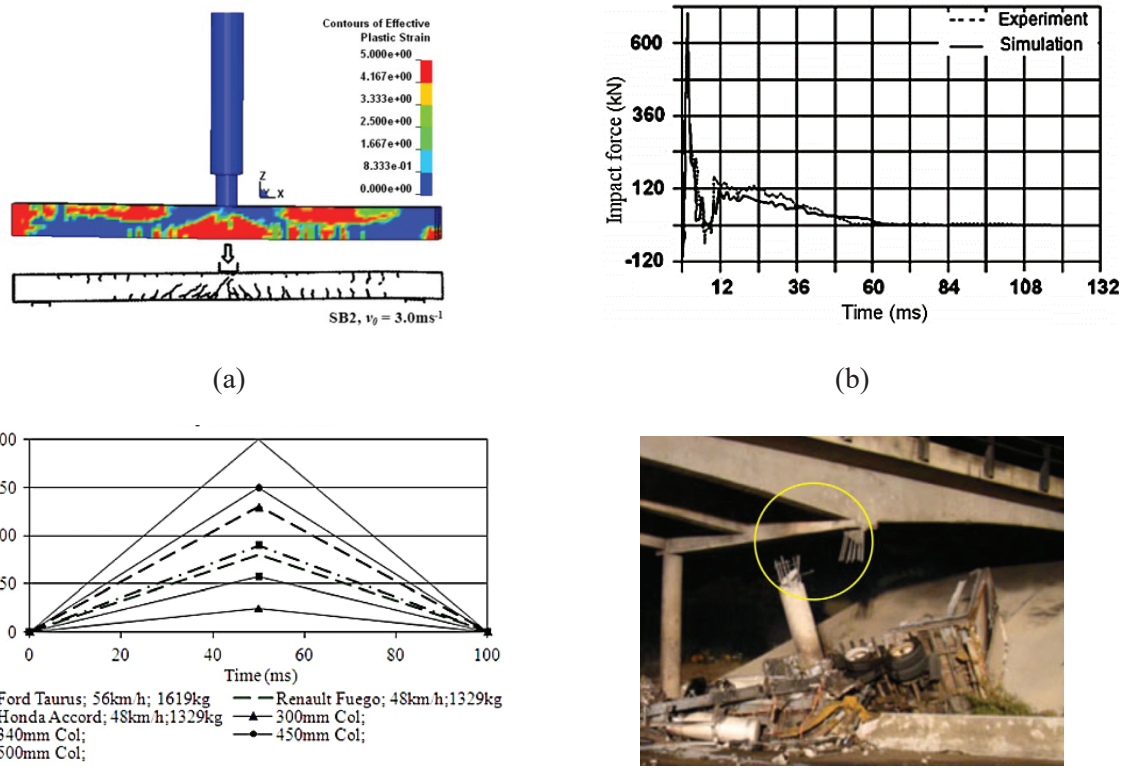

Figure 2-12 (a) Crack propagation of the impacted column and numerical simulation; (b) comparison of the resultant impact force; (c) comparison of impact capacities of columns with full-scale crash tests; (d) damaged column under vehicle impact (Thilakarathna et al., 2010)

Zhou and Li (2018) followed a similar approach to Thilakarathna et al. (2010) and developed a detailed numerical model of vehicle–pier collision using LS-DYNA followed by validation of the experimental results, failure mode, and crack development conducted by Feyerabend (1988). The weight of the vehicle model was 50 ton (45359 kg) including the maximum cargo weight (42.84 ton or 38864 kg) and the impact velocity was 37 mph (60 km/h). The impact force produced the ESF of 1079 kip (4780 kN) which conform to the AASHTO LRFD (AASHTO, 2012a) specification minimum requirement. They divided the failure process of the impacted pier into four phases, the initial peak impact force phase, the impact force of the development phase, the maximum peak impact force phase, and the impact force of the attenuation phase.

Do et al. (2018) investigated the impact responses and performances of bridge columns under vehicle collision with a detailed 3D model which was built with the commercial software LS-DYNA. The accuracy of the numerical model was verified against the testing results of the pendulum impact tests on a conventional column by Zhang et al. (2016). The numerical simulation was performed to reproduce the common failure modes observed in vehicle collision of mass 8 ton (7258 kg) with velocity varied from 25 to 87 mph (40 to 140 km/h). When the impact velocity increases to 75 mph (120 km/h) producing a peak impact force (PIF) of 2697 kip (12,000 kN), flexural cracks are observed at the impact point and column mid-height by a positive bending moment and at the two ends by a negative bending moment. When the vehicle velocity increases to 87 mph (140 km/h) with the PIF of about 3687 kip (16,400 kN), a large diagonal shear crack at the column top is observed on the negative side, which is caused by a combination of the huge flexural bending moment and shear force at the column top. Diagonal shear failure at the column base was experienced under the vehicle collision when the column was collided by the truck model with a velocity 62 mph (100 km/h) and the engine's mass 2 ton (1814 kg). In addition, the large peak impact force yields a huge negative bending moment near the impact area. That bending moment together with the large shear force results in another huge diagonal shear crack at the two third of the column. The loading in this study conformed AASHTO LRFD (AASHTO, 2012a) specification minimum requirement.

Sohel et al. (2020) performed numerical simulations of impact of car model (mass of 2203 kg) with an axially loaded square RC column. The results of the numerical analysis showed that the column-foundation joint was highly affected by the lateral impact force when the impact velocity was more than 19 mph (30 km/h). A shear fracture occurred at the joint when the speed exceeded 25 mph (40 km/h) for columns with dimensions 15.75 inch (400 mm) or less. The axially loaded RC column had a higher impact resistance than columns without axial loads. From the impact force-time histories, the equivalent static forces (ESFs) have been calculated for the different ranges of impact velocities and different sizes of columns (up to 287 kips or 1277.2 kN). They reported that the calculated ESF values were higher than the recommended values given by Eurocode 1 (BSI. 2006a: Eurocode 1: actions on structures-Part 1-7: general actions – accidental actions, 2006, paragraph 4.5.1.4(4)). The ESF values for various conditions are provided in Table 2-1.

Table 2-2 Summary studies on the impact responses of unstrengthened RC bridge piers to vehicle

Studies	Test methods	Vehicle	Protection on bridge piers	ESF (kip)	Failure modes
Thilakarathna et al., (2010)	FE	Car	NO	225 kip	Shear or shear flexural failure
Do et al., (2018)	PT + FE	Ford SUT	NO	2697 kip	Flexural and shear cracks, Punching shear
Zhou and Li (2018)	FE	Dong feng Truck	NO	1079 kip	Shear failure
Sohel et al., (2020)	DT + FE	Ford Econoline vehicle	NO	287 kip	Shear failure
Chen et al., (2021b)	FE	Ford F800 truck	NO	234 kip	Shear failure, minor overall flexural damage
Chen et al., (2022)	PT + FE	Ford F800 truck	NO	Up to 1309 kip	Shear failure

Note: FT = Full scale crash tests, PT = Pendulum impact tests, FE = FE simulation, DT = Drop-hammer impact tests.

2.2.3 Review of failure behavior of unstrengthened piers

In the maximum peak impact force phase, the shear failure took place in the impacted pier. However, the vehicle impact force for engineering design was yet difficult to be defined since it always varied over the collision process. Zhou and Li (2018) developed quantitative division of the damage based on the damage index "λ" where $\lambda=ESF/F_v$, They investigated the ESF as the equivalent impact force based on 50-ms moving average, and F_v is the shear capacity of the impacted pier. They proposed the equation of 50-ms moving average based $ESF = \int_{t_{p-25}}^{t_{p+25}} p(i)di/50$, where p(i) is the instantaneous impact force and t_p is the moment of the peak dynamic force (PDF) in the impact-time history plot. Using the equation of λ, Zhou and Li (2018) obtained 40 damage indexes of FE specimen. By analyzing these damage indexes, the reported that there was no significant damage or obvious displacement for the impacted piers (see Figure 2-13a) when λ was in the range from 0 to 0.2. This damage state was consistent with the damage description of the slight damage (Table 2-3). Several cracks developed at the impact location, and a few concretes spalled with reinforcement bending (see Figure 2-13b) when λ was in the range from 0.2 to 0.6. This damage state can be accurately reflected as the moderate damage. The shear failure occurred in the impact pier with several significant cracks developing at the impact location when λ was in the range from 0.6 to 1.0 (Table 2-3). Most concrete spalled and several stirrups suffered obvious deformation (see Figure 2-13c). The pier stiffness was decreased significantly, leading to excessive residual displacement at the impact location. This damage state was the same as the damage description of the severe damage (Table 2-3). The pier was destroyed with broken concrete and fractured stirrups (see Figure 2-13d) when λ was greater than 1.0. At this stage, at the top of the pier, a vertical settlement was observed and the superstructure inclined. In particular, the impacted pier lost the shear capacity and the superstructure could collapse for the damage index $\lambda > 1.0$.

The axial capacity of the impacted piers significantly decreased due to a large vertical settlement caused by the excessive displacement at the top end, as a result, the final damage

assessment results as shown in Figure 2-14 can be divided into four levels. Based on the calculation of λ from FE analyses, they categorized the damage into four levels with the increase of the vehicle impact force, e.g., slight damage, moderate damage, severe damage, and collapse. Table 2-3 lists these damage states and the corresponding damage descriptions. Slight damage indicated that the impacted pier could be smoothly used without repairing. Moderate damage indicated that the impact pier should be repaired in order to be used. Severe damage and collapse indicated that the impacted pier was completely destroyed and required reconstruction (shown in Figure 2-13).

Table 2-3 Damage state and damage description of the impacted pier (Zhou and Li, 2018)

Damage state	**Damage description**	**Damage index λ**
Slight damage	Insignificant damage or microcracks occurred at the impact location. No obvious displacement at the impact location.	0 to 0.2
Moderate damage	Minor concrete fell off and reinforcement bent at the impact location. Small residual displacement remained at the impact location.	0.2 to 0.6
Severe damage	The shear failure took place in the impacted pier. Significant cracks occurred at the impact location with stirrups fractured. Obvious residual displacement at the impact location and a small vertical settlement at the top of the pier remained.	0.6 to 1.0
Collapse	Piers were destroyed with broken concrete and fractured stirrups. Excessive residual displacement and vertical settlement remained, resulting in superstructures being inclined badly or collapsing.	> 1.0

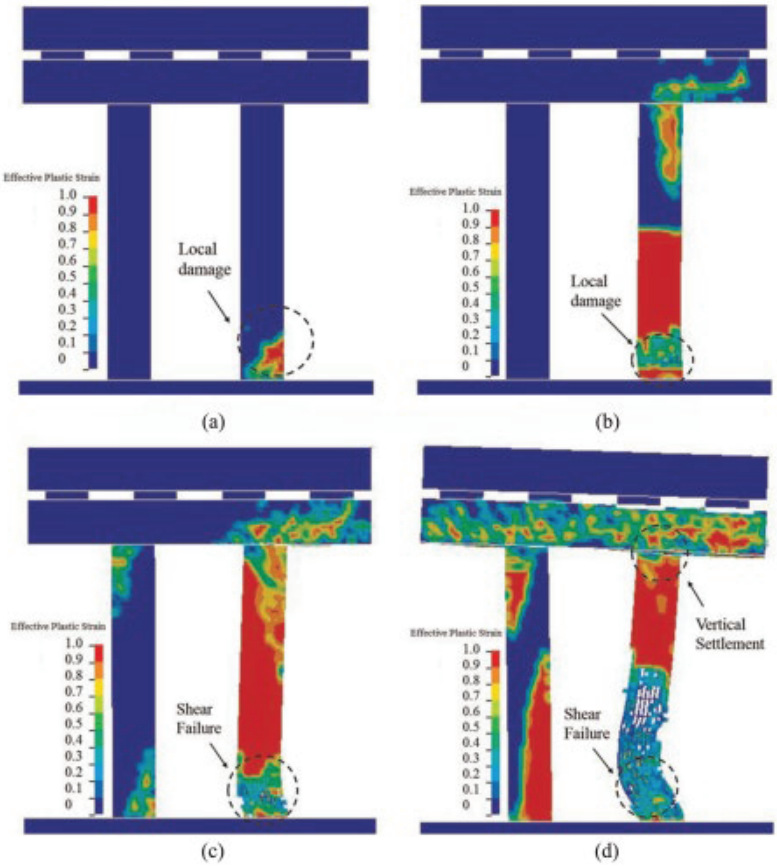

Figure 2-13 (a) slight damage; (b) moderate damage; (c) severe damage; (d) collapse (Zhou and Li, 2018)

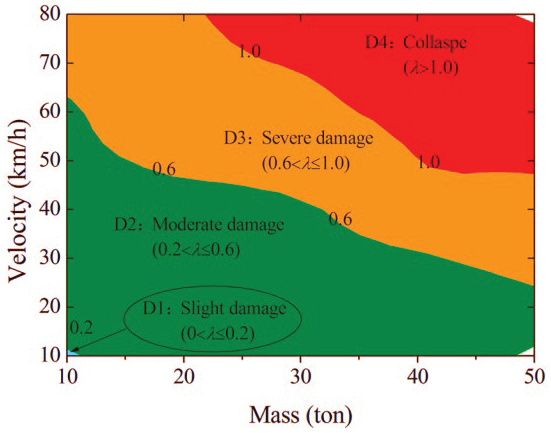

Figure 2-14 Damage assessment results of the impacted piers (Zhou and Li, 2018)

There are several failure modes of unstrengthened RC bridge piers subjected to a vehicle collision, i.e., flexural cracks, shear failure, punching shear failure, and total collapse, which were observed in real impact events as shown in Figure 2-15 (Buth et al., 2010). The high shear force from the truck collision exceeds the shear capacity of the pier, thus resulting in a shear failure mechanism in the pier (Figure 2-15d) that consisted of two shear failure planes: one extending upward from the applied load at approximately 45 degrees and the other extending downward at approximately 45 degrees. In fact, shear failures are commonly found for flexural RC members under impact. Several authors (Saatci and Vecchio, 2009; Ožbolt and Sharma, 2011; Micallef et al.,

2014) found that even RC beams which failed in a ductile flexural manner under static loading shifted to a brittle shear failure when subjected to impact loading. As a result, the shear strength of RC bridge piers is critical when considering the resistance to vehicle collision. The shear mechanism of the concrete structures under impact loads has been experimentally and numerically investigated in previous studies (e.g., Do et al., 2018, 2019). In these studies, the punching shear failure is the most common failure scenario of the concrete beams under severe impact loading conditions. Likewise, the example rectangular RC columns impacted by a vehicle model showed punching shear failure at the impact area when the peak impact force (PIF), caused by the engine impact (Do et al., 2018), reached 26,855 kips (30,000 kN), which is larger than the shear capacity of the column section. Figure 2-16 shows the typical shear mechanism of the RC bridge pier under vehicle impact via FE-based dynamic analysis (Do et al., 2018) and simplified punching shear model of the RC bridge pier under impact load (Do et al., 2019).

Nevertheless, some research also indicates that other damage modes, such as flexural or shear failure at column ends could happen depending on the actual collision (Thilakarathna et al., 2010) and retrofitting or strengthening of the pier could also shift the failure modes from shear-dominated to flexural-dominated in certain cases (Zhou et al., 2021). The failure modes vary dramatically under different loading circumstances. Moreover, when the vehicle speed rises, a significant diagonal shear fracture develops on the column top's negative side due to the large flexural bending moment and shear force. It is usual that as vehicle velocity increases, the damage to the bridge pier increases, from minor local concrete damage at the impact region to the total collapse of pier. The first peak impact force rises as the engine's mass increases, resulting in increased moment and shear force in the column. Consequently, the weight of the engine must be taken into account when designing the RC bridge columns to withstand vehicle impact in the case of tractor-trailer trucks.

(a) (b) (c) (d) (e) (f)

Figure 2-15 Failure modes of bridge columns under vehicle collision: (a) flexural crack; (b) shear failure at the column top; (c) shear failure at the impact point (d) punching shear failure; (e) shear failure; (f) total collapse (Do et al., 2018)

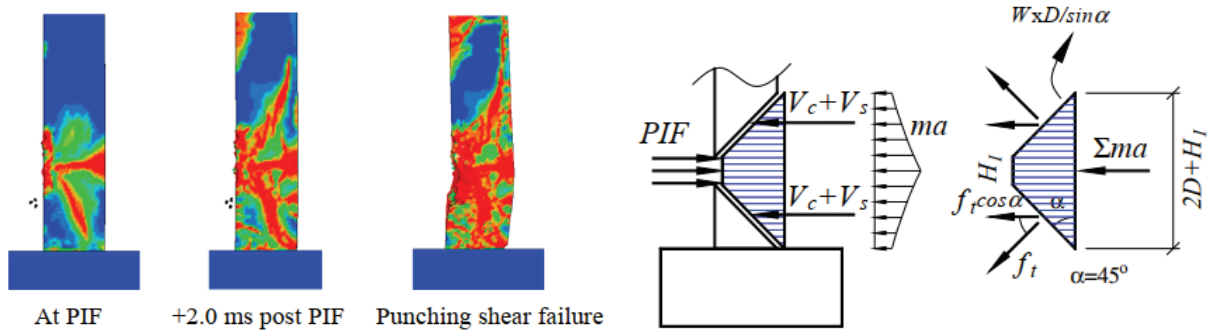

(a) (b)

Figure 2-16 Shear mechanism of the RC bridge pier under vehicle impact: (a) column punching shear failure (Do et al., 2018); (b) simplified punching shear model of the RC bridge pier under impact load (Do et al., 2019)

Based on the observed failure mechanism of pier columns involved in large truck collisions, an acceptable method of calculating the column strength to resist the vehicular collision force is to assume failure along two shear planes inclined at 45-degree angles above and below the point of force application. The FDOT Structures Manual (FDOT, 2024) recommends checking the column shear capacity assuming failure along two shear planes inclined at 45-degree angles above and below the point of force application. However, AASHTO LRFD (AASHTO, 2020a) does not consider this method in impact design for bridge piers. .

After reviewing the above literature, the following conclusions can be drawn:

- The vehicular collision can be divided into four important phases, e.g., (a) initial peak impact force phase (0–50 ms): At the impact position of the affected pier, no evident damage or displacement occurred since the vehicle's front's stiffness was much lower than the RC piers, (b) impact force of development phase (50–150 ms): due to the engine hitting the column, at the impact location, concrete started to spall., (c) maximum peak impact force phase (150–200 ms): Shear failure happened at the point of collision, (d) impact force of attenuation phase (200–300 ms): the pier's shear and axial bearing capacities were reduced, and residual horizontal displacement and vertical settlement occurs.

- Most of the unstrengthened RC bridge piers showed shear failure under impact loading. In most cases, the columns failed due to shear failure initially and subsequently by flexural failure leading to collapse. The observed failure modes can be categorized as shear or shear flexural types of failures depending on the test variables. In some cases, excessive shear forces were generated at the contra-flexure points located close to the supports. These observations may be cited as a potential reason for the failure of the column. Some researchers recommended avoiding the lapping joint of steel reinforcement on the pier and applying adequate transverse reinforcement to avoid complete separation of pier from the structure.

- There exists a complex relationship between the cross-sectional dimensions of piers on the impact force. If the cross-sectional size of piers increases that increases the deforming area of the vehicle, and hence decreases the residual kinetic energy of the vehicle when the cargo hits. Therefore, the peak impact force on a rigid pier caused by cargo impact decreases as the cross-sectional size of the pier increases. On the other hand, increasing the cross-sectional dimension of the RC pier would enhance its stiffness and impact load-bearing capacity, which might lead to a higher response in the impact force history.

- The influence of vehicle type on the impact force is also complicated. The larger and heavier vehicles may not necessarily produce larger impact force. It was observed from the FE simulation based dynamic analysis that, despite being heavier and larger than the single-unit truck, a tractor-trailer collision induced a smaller second peak of impact force in the impact-time history response. This is because the distance between the trailer and the front of the truck is longer, resulting in larger energy consumption of the truck body so that its cargo would hardly collide with the pier.

- Regarding RC piers with normal sizes (e.g., with a diameter larger than 762 mm or 30 inch) subjected to vehicular impact, FE simulation results showed that the gravity loads from the superstructure, boundary conditions of the superstructure as well as the characteristics of the foundation have little effect on the engine-induced peak of impact force.

- The researchers employed different method to apply the impact force experimentally on the bridge pier specimens, e.g., full scale crash tests, pendulum impact tests, drop-hammer impact tests, horizontal impact test. Very few literature were found where the authors are able to create the ESF by applying the impact force using these methods as per the AASHTO LRFD (AASHTO, 2012a) specification minimum requirement (2669 kN or 600 kip). However, the researchers showed promising simulation results and validation of failure modes and dynamic behavior of bridge piers due to the collision between the FE models of bridge pier and heavy vehicle with various mass and impact speed using the nonlinear FE modeling platform of LS-DYNA.

- Due to high cost of the full-scale impact test experiments, the researchers mostly investigated the influence of different factors, e.g., vehicle weight, vehicle speed, column size, etc. on the impact force and failure mechanism of RC bridge pier based on the dynamic analysis via FE simulation. However, to gather more confident in performance-based design and verification of the failure behavior, more experimental investigation is required to fill the fundamental knowledge gap.

2.3. Review of Vehicle Collision with Strengthened Bridge Piers

A very limited study exists on the strengthening of bridge piers to improve resistance against lateral impact induced by a vehicle collision. Several piers strengthening methods including conventional RC collars, collars with advanced concrete materials (e.g., ultra-high performance concrete or UHPC), and fiber reinforced polymer (FRP) wraps have been investigated for impact strengthening of piers and showed promises. Figure 2-17 shows examples of these common strengthening practices. However, due to the limited number of studies, there is still a lack of adequate understanding of the performance of these strengthening methods under dynamic impact loading, and the necessary design and detailing requirements for these strengthening methods.



(a) (b) (c)

Figure 2-17 Typical strengthening methods of bridge piers: (a) pier strengthening of Milton Madison bridge, KY, using RC encasement (showing the steel reinforcement prior to casting of the concrete, photo courtesy: Michael Baker International); (b) repair of the Canadian Railway bridge pier using UHPC, Montreal, QC; (c) repair of bridge pier on South Carolina's I-385 using CFRP wrap (photo courtesy: Milliken Infrastructure)

2.3.1 RC collar-strengthening and code recommendations

The FDOT Structures Manual (FDOT, 2024) has related sections on RC collar-strengthening detailing. In the case of RC collars to strengthen the piers against lateral impact, the manual has the following detailing requirements regarding the concrete collar construction:

- Provide a grid of mechanical connections between the existing concrete and the concrete collar at a maximum horizontal and vertical spacing of 6 inches (150 mm).
- Use a shrinkage-reducing admixture for the collar concrete.
- Roughen the existing concrete interface surface to a minimum amplitude of 0.2 inch (6 mm).
- The existing concrete interface surface shall have a Saturated Surface Dry (SSD) condition when placing the concrete collar.

These detailing requirements are intended to enhance the bond between the existing piers and the added collar, and such measures have been considered in many retrofitting projects and studies in the literature. Nevertheless, whether these requirements are necessary and whether they are applicable to retrofitting methods other than conventional concrete collars, such as when advanced concrete materials, e.g., ultra-high performance concrete (UHPC), are used, requires further verification. The FDOT has designed and constructed RC collars as a regular strengthening practice for bridge piers, such as in the piers of Campbell Drive Interchange on Florida's Turnpike. The circular piers were modified with an 8 inch (200 mm) thick RC collar. The 32 and 36 inch (813 mm and 914 mm) diameter piers were modified to 40 and 44 inch (1213 mm and 1314 mm) diameter respectively. However, the AASHTO LRFD (AASHTO, 2020a) does not provide any guideline for RC collar-strengthening design or requirements to prevent delamination for bridge piers against vehicular impact.

Only the following study reported the dynamic behavior of RC columns strengthened with RC collars under impact load due to vehicular collision. Fuhaid et al. (2022) developed an FE model in LS-DYNA to investigate the maximum lateral load due to car collisions at speeds up to 40.4 mph (65 km/h) with building columns located in parking garages and evaluated strengthening methods to prevent damages. The cross-section and clear span of the columns were 12 inch x 12 inch x 120 inch (300 mm x 300 mm and 3000 mm), respectively. In the FE modeling, they considered a Ford van

(Econoline-2007, weight 2031 kg) and a Ford Explorer (weight 2254 kg). The recorded maximum ESF was 326 kip (1450 kN) for 37 mph (60 km/h). They compared between the aramid fiber reinforced polymer (AFRP) wrap strengthening (up to 0.04 inch or 1 mm thickness and bottom 6.6 feet of the column) and RC collar (1.6 inch or 40 mm thickness and bottom 4.3 feet) strengthening (Figure 2-18). However, they did not follow any guide or recommendation for AFRP wrap or RC collar application for preventing debonding or delamination. They reported that the AFRP wrap can reduce the damage of the column but cannot completely eliminate the residual damage for a slender column at moderate car impact velocity (more than 31 mph or 50 km/h). On the other hand, RC collar-strengthening increased the shear and flexural capacity of the column along with the overall stiffness of the column, which greatly reduced the lateral deformation. The columns showed no residual deformation but some cracks in the jacket. The ESF of the RC collar-strengthened column was 338 kip (1505 kN). In the FE modeling, the authors did not consider any mechanical connection/connector for the RC collar and thus no separation was reported. Although this research is based on impact force on building columns and the magnitude of the impact force is significantly lower compared to bridge piers, the behavior of RC axial members strengthened with RC collar subjected to impact force is still relevant to the current study.

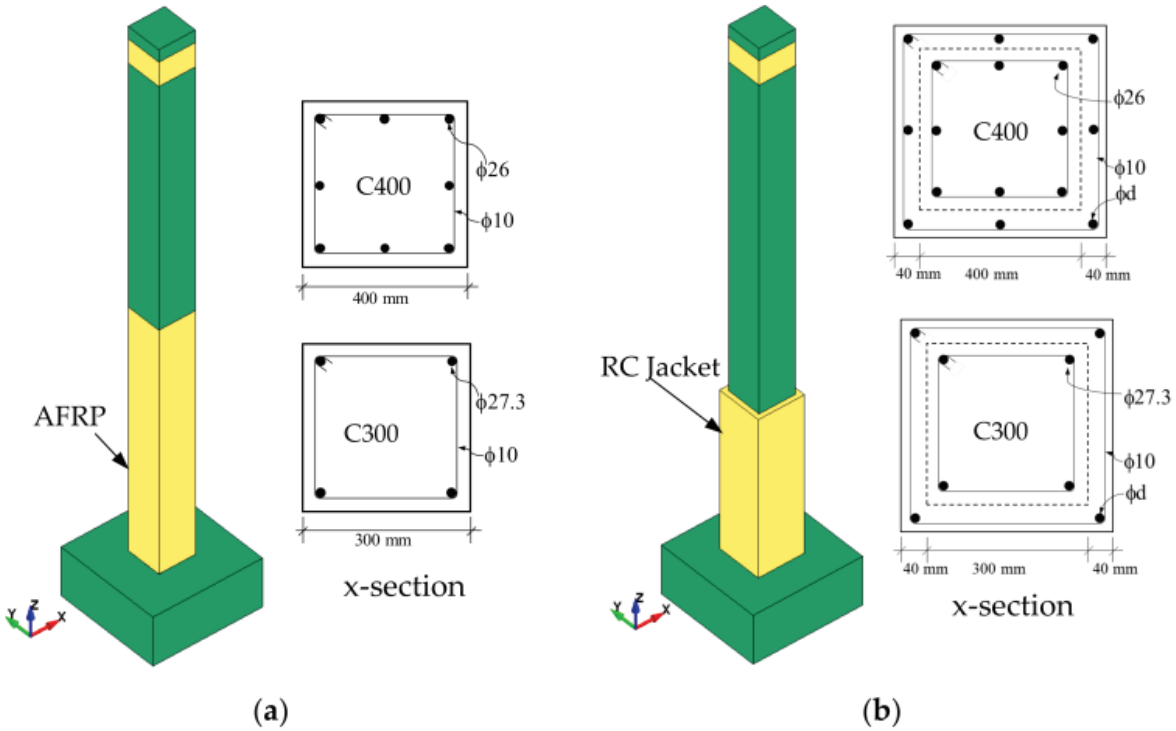

Figure 2-18 RC building column strengthening by: (a) AFRP wrap; (b) RC collar (Fuhaid et al., 2022)

2.3.2 UHPC collar-strengthening and code recommendations

UHPC has been experimentally verified to possess many excellent mechanical properties and energy absorption capacity. Due to its very dense and compact matrix, it also exhibit superior durability in comparison with ordinary concrete. Owing to these excellent properties in strength and durability, UHPC has been employed to improve the static capacity (e.g., shear strength, bending strengths) of RC beams and slabs in recent studies. Adding UHPC layers was demonstrated as capable of improving the static performance of RC members. In addition to static performances,

dynamic performances (e.g., impact and blast) of UHPC members were also studied. The followings are the examples of performance of UHPC collar on RC column against impact loading:

Fan et al. (2018) also developed high-resolution FE models implemented in LS-DYNA to investigate the performance of UHPC-strengthened pier columns (full-length UHPC collar) subjected to vehicle impacts (using FE model of a 16,000 lb Ford F800 single unit truck or SUT). With the validation of the drop impact test results in Fan et al. (2019), this study followed the same models of RC and UHPC-strengthened columns (with varying UHPC collar thickness from 4-12 inch or 100-300 mm). A typical three-span overpass bridge with multiple column bents was finely modeled, including the superstructure. Figure 2-19 shows the detailing of the RC pier (total diameter of 24 inch or 600 mm including UHPC collar) and UHPC collar (4 inch or 100 mm thickness) strengthened pier where they kept the same diameter for the unstrengthened and strengthened piers. They used a corrugated steel duct (thickness = 0.06 inch or 1.6 mm) to improve the bond between the outer UHPC layer and the inner normal concrete core during FE modeling (Figure 2-19). However, no guideline or specification was followed in the detailing of the UHPC collar FE models. They reported that the damage extents in the RC columns were more severe than those of the UHPC-strengthened columns for the same collision events. Slight damage occurred in the RC column only when the initial impact speed was just 12.4 mph (20 km/h), whereas the UHPC-strengthened column exhibited obvious damage when the impact speed exceeded 37.2 mph (60 km/h). The severe damage and the large displacement were observed for the RC column at the impact speed of 43.5 mph (70 km/h). On the contrary, only slight or moderate damage was exhibited in the UHPC-strengthened column (Figure 2-21). The impact resistance of UHPC-strengthened columns was up to 1,792 kip (7,970 kN) for an impact velocity of 62 mph (100 km/h) compared to 1,553 kip (6,910 kN) for unstrengthened columns (Figure 2-20), but the ESF was not as per the AASHTO LRFD (AASHTO, 2012a) specification minimum requirement. Undoubtedly, the impact resistance of a bridge column was greatly improved due to the presence of the UHPC collar.

Fan et al. (2018) concluded that, compared to the conventional RC column, the impact-induced displacements and damage severity can be dramatically reduced (at least 50% reductions in displacement) due to the presence of the UHPC collar. On the other hand, the impact force was not obviously increased when the UHPC-strengthened column was used. This is attributed to the fact the impact force is mainly dependent upon the resistance of the colliding vehicle rather than the collided column. Therefore, the UHPC-based enhancement was demonstrated as being an effective measure for improving the impact-resistant performance of bridge structures with a multi-column bent. Further FE analysis in their study reveals that the residual capacity of the UHPC-strengthened column increases with the thickness of UHPC collar and the UHPC strength. Compared to the impact speed and the thickness of UHPC collar, the UHPC strength had a limited influence on the impact-induced response. In addition, the influence of the UHPC thickness on residual capacity was dependent upon initial impact speed. The residual capacities increased with increasing the thickness of UHPC collar when the initial impact speed was not very high. This was because the impact damage was low and most of the UHPC at the bottom retains the high axial load-carrying capacity after a vehicle impact (see Figure 2-21b). The increase in the UHPC area due to the increase in UHPC thickness was significantly beneficial for improving the residual axial capacity. On the contrary, if the impact velocity is 62 mph (100 km/h), the residual capacity cannot be effectively enhanced by thickening UHPC collar. In this case, severe shear damages (see Figure 2-21b) always occurred at the bottom for all thicknesses of UHPC collar as the impact force at the lower part of pier caused higher shear force near the bottom support and the impact energy was very high at the bottom compared with dissipating energy of the UHPC-strengthened column. As a result, the failure

occurred at the bottom. Accordingly, the effective UHPC area, which is good for improving residual axial capacity, cannot be increased with the thickness of UHPC collar, as the higher impact speed was shown to have a greater influence on the residual capacity than the thickness of UHPC collar. Adding a corrugated steel duct out of the normal concrete as given in this study may not be practical in existing bridge piers, but it can be followed in a new construction.

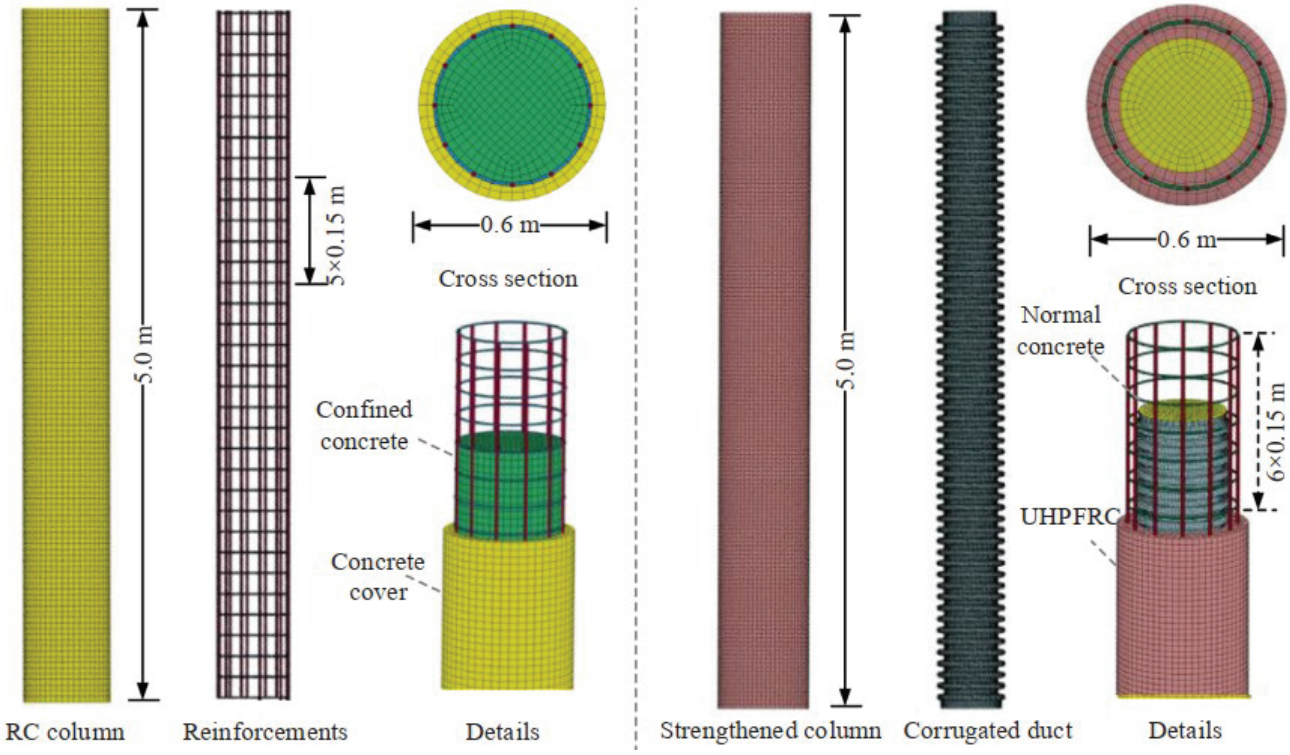

Figure 2-19 Detailing of overpass bridge RC pier and UHPC collar-strengthened pier in the high-resolution FE model (Fan et al., 2018)

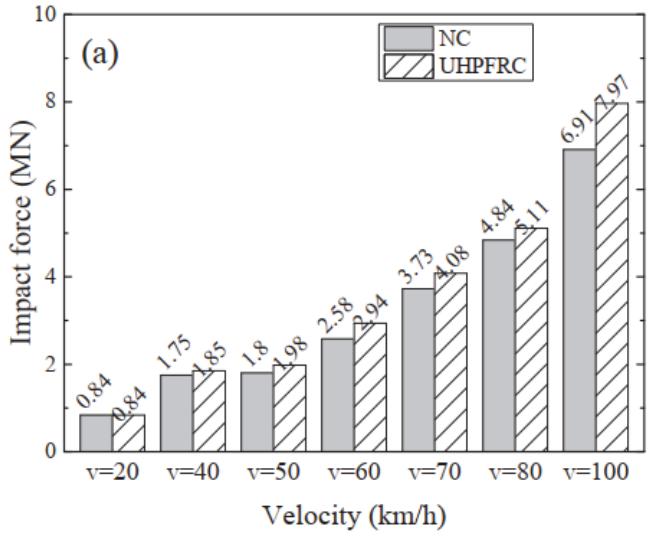

Figure 2-20 Peak impact force responses for different collision scenarios; here UHPFRC refers to UHPC (Fan et al., 2018)

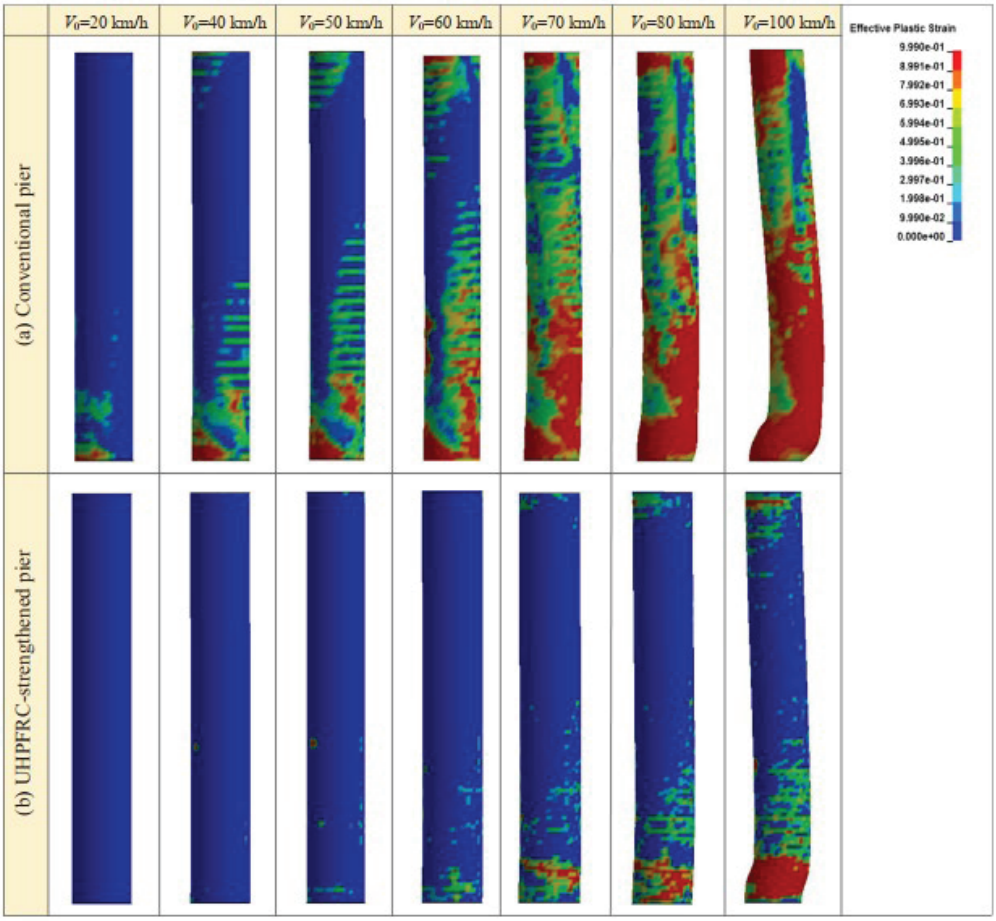

Figure 2-21 Comparison of impact-induced damage between RC column and UHPC-strengthened column; here UHPFRC refers to UHPC (Fan et al., 2018)

Fan et al. (2019) studied drop-hammer impact tests (Figure 2-22a) on three types of partially UHPC-strengthened RC columns (8 inch or 200 mm dia circular cross-section and a 86.6 inch or 2200 mm length, see Figures 22b, 22c) to determine appropriate configurations for impact strength improvement. The maximum thickness of the applied UHPC collar was 2 inch (50 mm). Figure 2-23 shows the fabrication detailing of the UHPC collar. The weight of the drop hammer was 1253 pounds and the impact velocity was 12 and 15 mph (19.5 and 24.5 km/h). They also proposed a finite element modeling method implemented in LS-DYNA and validated against experimental data of the impact tests to evaluate the impact-resistant performance of UHPC columns and UHPC-strengthened RC columns (Figure 2-24). The peak impact force of the UHPC collar-strengthened column was up to 223 kip (991 kN) compared to the unstrengthened column up to 156 kip (695 kN). However, in the case of the full section UHPC RC column, the peak impact force was 292 kip (1299 kN), but none of the impact load conformed to the AASHTO LRFD (AASHTO, 2012a) specification minimum requirement. They observed that brittle shear (or punching) failure occurred in the nonstrengthened RC portion between the midspan UHPC collar and the end UHPC collar and the peak impact force increased substantially in this column. The magnitude of peak impact force influences the occurrence of shear failure. Accordingly, the increase in peak impact force means an increase in the shear demand. Although the UHPC collar possesses a good shear bearing capacity, the RC portions failed due to the limitation of shear bearing capacity.

Overall, these experiments revealed that the strengthening method of adding UHPC collars at both ends had the best potential in improving the impact performance. This method not only offers significant decreases in impact-induced damage and displacement but also does not result in a noticeable increase in the impact force. The method of adding a UHPC collar in the contact zone is less desirable than the above option, but still acceptable. However, the strengthening scheme of adding UHPC collars in both the contact zone and the two ends should be prohibited because brittle failure is prone to happen. On the other hand, the strengthening technique with a two-end UHPC collar was more feasible in engineering practice than that with a UHPC collar in the contact zone. For example, it is often difficult to accurately predict the contact location when an aberrant vessel hits bridge columns because the water level and the detailed vessel structures are variable. As a result, it is impractical to apply the strengthening scheme with a contact-zone UHPC collar in this case. These phenomena were also observed in the FRP strengthening schemes as well (Al-Bukhaiti et al., 2021). However, it may not be a concern for vehicular impact consisting of specific contact zones.

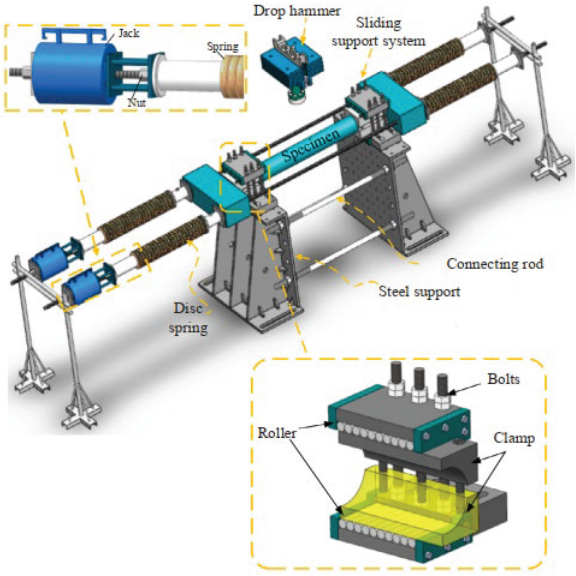

(a)

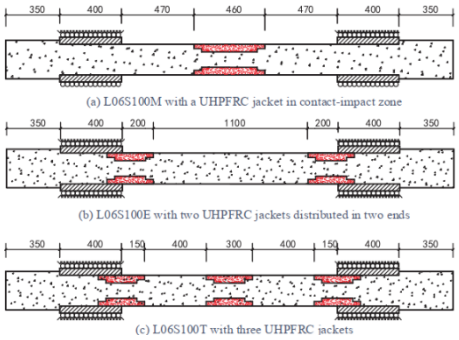

(b)

(c)

Figure 2-22 (a) Drop hammer impact test setup; (b) three different types of the UHPC-strengthened column (unit: mm); (c) pre-embedded UHPC collar (Fan et al., 2019)

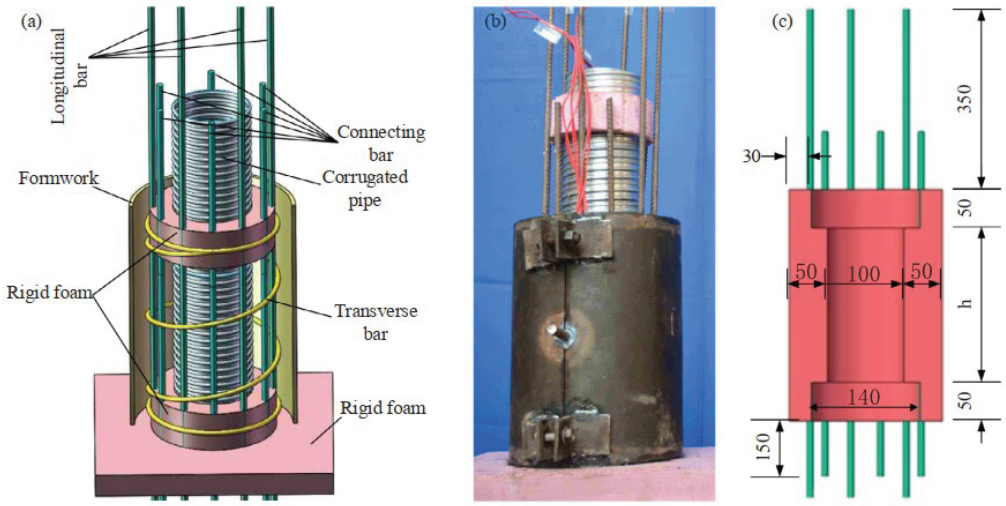

Figure 2-23 Details of UHPC collar: (a) formwork; (b) picture of fabrication; (c) dimensions (unit: mm) (Fan et al., 2019)

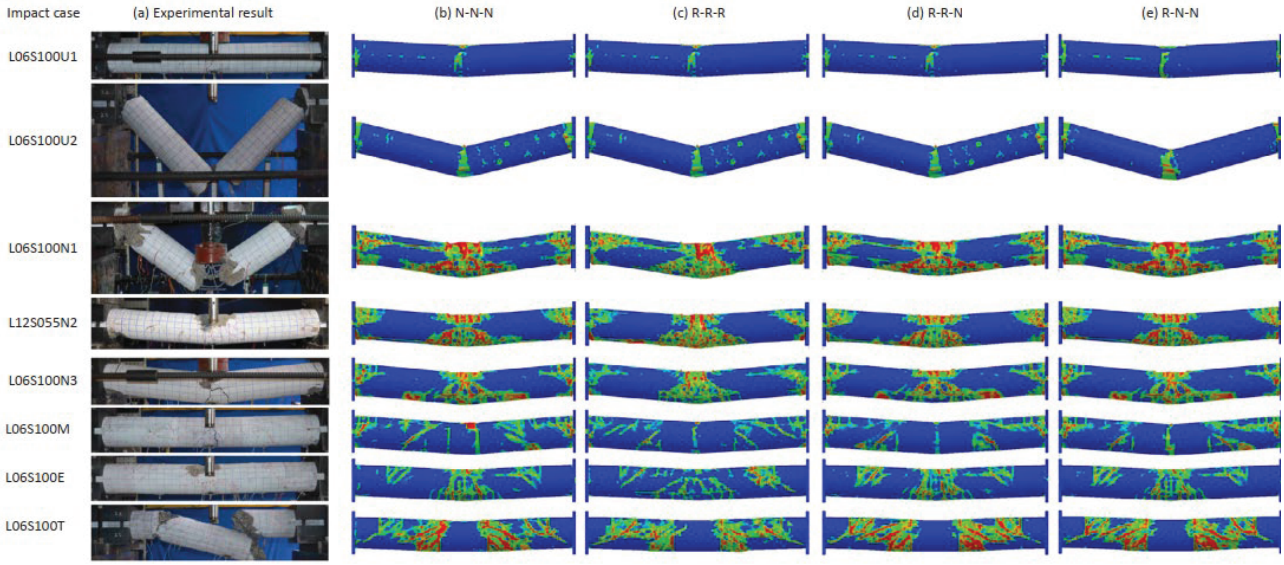

Figure 2-24 Experimental and FE failure modes (Fan et al., 2019)

2.3.3 FRP wrap strengthening and code recommendations

The use of fiber-reinforced polymer (FRP) composites to repair damaged bridge components is a viable option that requires less highway closure time Only limited studies reported using FRP wraps for strengthening of bridge piers against vehicular impact. However, the method has been extensively studied and implemented as a popular strengthening method for reinforcing concrete buildings due to its ease of installation, rapid curing epoxies, conformity, high tensile strength, corrosion resistance, and lightweight density. The relevant findings, common practice, and specifications are briefly reviewed here.

The AASHTO Guide Specifications for Design of Bonded FRP Systems for Repair and Strengthening of Concrete Bridge Elements, First Edition (AASHTO, 2012b), hereafter referred to as AASHTO FRP), was developed based on two National Cooperative Highway Research Program (NCHRP) reports: NCHRP Report 655, 2010 "Recommended guide specification for the design of externally bonded FRP systems for repair and strengthening of concrete bridge elements" (NCHRP, 2010) and NCHRP Report 678, 2011 "Design of FRP systems for strengthening concrete girders in shear" (NCHRP, 2011). As per the strengthening schemes recommended in NCHRP Report 655 (NCHRP, 2010), the RC bridge elements shall be strengthened with externally bonded FRP reinforcement using one of the following methods, which were included in AASHTO FRP (AASHTO, 2012b): (a) Side bonding, (b) U-jacketing (wrap), (c) U-jacketing (wrap) combined with anchorage, and (d) Complete wrapping (Figure 2-25). As per the AASHTO FRP (AASHTO, 2012b), the side bonding is the least effective FRP shear reinforcement scheme due to premature debonding under shear loading and should be avoided if possible. FRP U-jacketing (wrap) is the most common externally bonded shear strengthening method for RC beams and girders. The key drawback of this system is the possibility of premature debonding of the FRP, which may reduce its effectiveness. Regardless of this drawback, the system is quite popular in practice, due to its simplicity. FRP U-jacketing combined with anchorage aims to increase the effectiveness of FRP by anchoring the fibers, preferably, in the compression zone. Properly designed anchors may result in the fibers reaching their tensile capacity, permitting the jacket to behave as if it were completely wrapped. Finally, the complete wrapping should be applied for axial members such as bridge piers and building columns. Complete wrapping of the cross-section is the most effective scheme and is commonly used in strengthening columns to enhance axial capacity where there is sufficient access for such application (NCHRP, 2011).

As the bridge pier is subjected to large shear force due to vehicular impact, the complete FRP wrap strengthening at transverse direction may increase the shear resistance along with axial capacity of RC axial member similarly as beams or girders. As per AASHTO FRP (AASHTO, 2012b), the shear strengthening of RC members using FRP reinforcement may be provided by bonding the external reinforcement (typically in the form of sheets) with the principal fiber direction as parallel as practically possible to that of maximum principal tensile stresses, so that the effectiveness of FRP is maximized. The most common case of structural members subjected to lateral loads (perpendicular to the member axis) are columns under seismic forces. It is normally more practical to attach the external FRP reinforcement with the principal fiber direction perpendicular to the member axis.

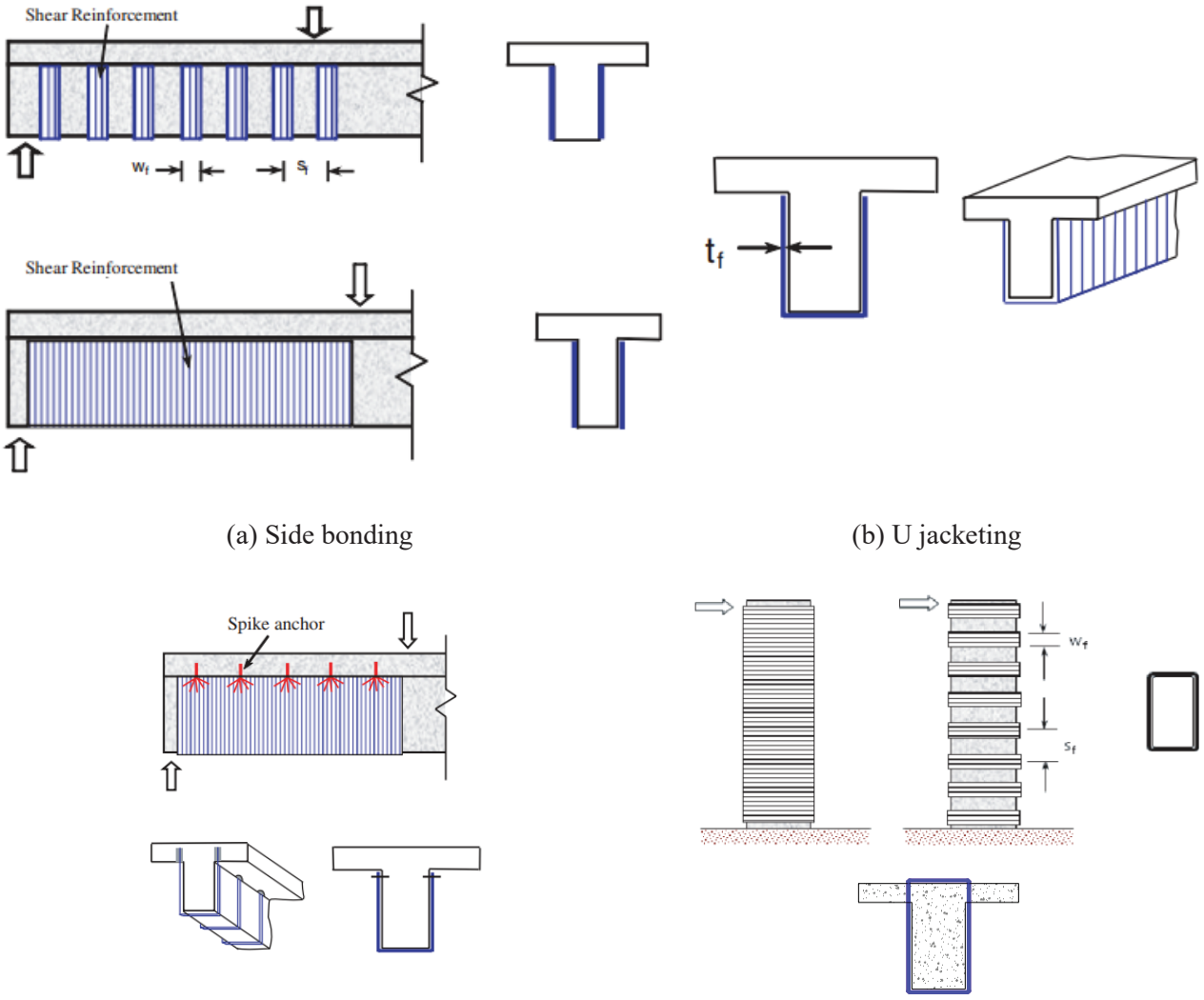

(a) Side bonding

(b) U jacketing

(c) Jacketing with anchorages

(d) Complete wrapping (column and beam)

Figure 2-25 Shear strengthening scheme of bridge element as per NCHRP Report 655 (NCHRP, 2010)

There is no information available in the AASHTO FRP (AASHTO, 2012b) on the delamination or debonding of FRP wrap under impact loading or damage due to sharp metal fragments during vehicular impact, however, it mentioned about this issue for FRP-strengthened RC beams or girder under shear and flexure. As per the AASHTO FRP (AASHTO, 2012b), the end-termination (delamination or debonding) of an externally bonded reinforcement system, when subjected to combined shear and flexure, may separate in the form of debonding in three different modes: (a) critical diagonal crack debonding with or without concrete cover separation, (b) concrete cover separation, and (c) plate-end interfacial debonding. The critical diagonal crack debonding may occur where the FRP end is located in a zone of high shear force and the amount of steel shear reinforcement is limited. In such a case a major diagonal shear crack forms and intersects the FRP, and then propagates towards the end. This failure mode is suppressed if the shear strength of the strengthened member remains higher than the flexural strength. Complete wrapping may reduce the probability of debonding or delamination which can be observed on the review of existing literature later on in this section. The AASHTO FRP (AASHTO, 2012b) does not provide adequate guideline

regarding FRP wrap application method for axial members. However, ACI 440.2R: Guide for the design and construction of externally bonded FRP systems for strengthening concrete structures (ACI, 2017), hereafter referred to as ACI 440.2R-17, provides information about strengthening axial member (RC column of building) to enhance axial and bending capacity by enhancing P-M interaction behavior. It also provides design examples for shear strengthening of axial member (non-circular RC column of building) but not due to impact load.

Liu, T et al. (2022) conducted an experimental investigation and FE modeling on the effectiveness of wrapping FRP composites (CFRP wraps consisted of the epoxy resin adhesive and unidirectional carbon fiber sheets with a nominal thickness of 0.007 inch or 0.167 mm) around full-scale RC pier columns (13 inch or 330 mm in diameter and 67 inch or 1700 mm in height) to improve their resistance against vehicular collision. However, no guideline or specification was followed in the FRP application, and no information was provided about any debonding prevention method. They employed the nonlinear FE program LS-DYNA to simulate the FRP composites-wrapped RC pier columns against vehicle collisions. A pendulum-type test truck equipped with an instrumental rigid hammer was used with a velocity and mass of 10-75 mph (16-120 km/h) and 3483 lbs (1582 kg). The maximum ESF was 2360 kip (10500 kN), which conformed to AASHTO LRFD (AASHTO, 2012a) specification minimum requirement. All the columns showed shear failure and no flexural failure or FRP rupture was observed.

Isaac et al. (2011) investigated the behavior of square RC columns (5.5 inch x 5.5 inch or 140 mm x 140 mm) strengthened with transverse fiber reinforced polymer (FRP) wrapping (complete wrapping at transverse direction to the axis of the column) under impact loads with equivalent unwrapped columns. However, they did not follow any guideline or recommendation for FRP wrap application and did not provide detailed information about the application design. They conducted eleven tests where the impact velocity (6 and 7.5 mph or 9.3 and 12 km/h), impact mass of 1638 lbs (743 kg), and the point of load application varied. The impact velocity was varied by altering the drop height. They reported that the peak displacements of columns strengthened with FRP were up to 39% lower than those of specimens not wrapped with FRP for comparable impacts, and this reduction in the peak displacement of wrapped specimens was most likely attributable to the higher failure strains of confined concrete (Figure 2-26). The FRP wraps provide substantially greater ductility to the section and significantly more energy is dissipated through the crushing of the concrete. In all cases, the specimens deformed in a flexural manner and no shear failures of RC column were observed, and the CFRP was not observed to rupture.

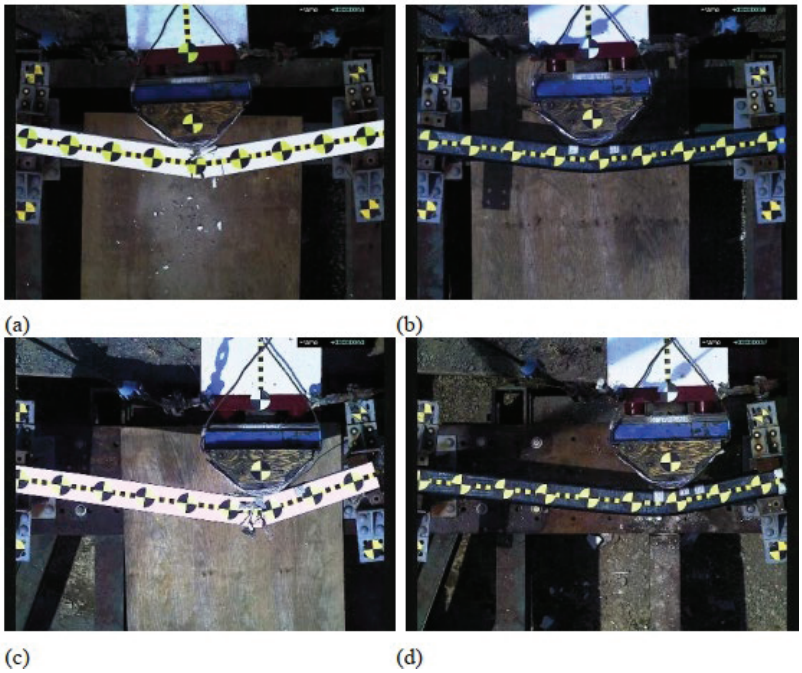

Figure 2-26 Typical photos for specimen peak displacement: (a) and (b) unstrengthened and strengthened specimens, respectively, with impact load at midspan; (c) and (d) unstrengthened and strengthened specimens, respectively, with impact load at 470 mm (18.5 inch) from midspan (Isaac et al., 2011)

Sha and Hao (2015) conducted pendulum impact tests on scaled CFRP-strengthened and unstrengthened pier models (3 inch or 78 mm dia) to investigate the effect of CFRP strengthening technique on the pier column subjected to barge impact. They applied complete wrapping of FRP composite following the manufacturer's procedure to avoid debonding, however, the procedure is not clearly mentioned in the study. Moreover, they did not follow any guideline or recommendation about FRP application and preventing debonding other than the manufacturer's manual. They recorded and compared the impact force and pier response without and with CFRP strengthening which are 2697 kip (12000 kN) and 3372 kip (15000 kN) respectively, which conformed to the AASHTO LRFD (AASHTO, 2012a) specification minimum requirement. The unstrengthened pier column suffered from concrete crushing at the impact location and spalling at the two ends under impact loads. It experienced a flexural failure with large damages at the impact location and the two ends of the column. However, the CFRP-strengthened pier experienced a direct shear failure at the ends. No concrete crushing and spalling damage were found in the pier column after peeling of the CFRP wrap. They also developed numerical models of the CFRP-strengthened and unstrengthened circular piers (with a diameter of 110 inch or 2.8 m and height of 82.7 ft or 25.2 m) using LS-DYNA and calibrated them with the scaled laboratory test results considering an impact velocity up to 2.5 mph (4 km/h). With the validated model, parametric calculations are carried out to simulate full-scale barge impacting on bridge piers with or without CFRP strengthening. The simulation results indicated that the CFRP wrap successfully confined and protected the concrete pier. It was also found that increasing CFRP thickness led to a slight decrease in the peak impact force. They reported that a thicker layer of CFRP composite resulted in a relatively softer impact between the composite and the barge since the out-of-plane stiffness of the CFRP was low.

Mohammed and Parvin (2020) investigated the response of as-built and carbon fiber reinforced polymers (CFRP)-strengthened RC bridge piers struck with lightweight and medium-

weight vehicles at a city speed limit of 35 mph (56 km/h), a highway speed limit of 62 mph (100 km/h), and a police chase speed of 93 mph (150 km/h). They developed a nonlinear FE model in LS-DYNA and simulated vehicle pier collisions, however, they did not follow any guideline or recommendation in the FRP modeling to prevent debonding. The CFRP wrap layers were applied up to 6 ft (1.83 m) height of the pier to cover the collision spot for a wide range of vehicle sizes. The maximum ESF from the FE simulation based dynamic analysis was found to be 2697 kip (12,000 kN), which conformed to the AASHTO LRFD (AASHTO, 2012a) specification minimum requirement. The damage level was associated with the amount of internal strain energy of the RC pier. Compared to the as-built RC pier, the internal energy demand was reduced by approximately 6.7% in the CFRP-strengthened RC bridge pier reinforced with 4, 8, and 12 layers (0.15, 0.3, and 0.45 inch or 4 mm, 8 mm, and 12 mm thickness respectively) of CFRP wrap for a city speed limit of 35 mph (56 km/h). For a highway speed limit of 62 mph (100 km/h), these reductions were 16.1%, 26.3%, and 30.9% in piers strengthened with 4, 8, and 12 layers of wrap, respectively. In the case of a police chase speed of 93 mph (150 km/h), the internal energy demand was reduced by 0.4%, 10.1%, and 15.8% for the bridge piers strengthened with 4, 8, and 12 layers of CFRP wrap, respectively. No global deformation of the pier was observed for all analyses, but localized concrete damage was observed at the location of impact. CFRP wrap layers helped to reduce and evenly distribute the effect of impact load and minimized the damage at the point of impact compared to the as-built RC pier.

Al-Bukhaiti et al. (2021) studied the effectiveness of the use of CFRP shear-reinforcement to increase the impact resistance of CFRP confined RC square elements under the lateral impact loads coming from a train. In this work, using three CFRP RC specimens, an unequal lateral impact test was carried out. The authors followed ACI 440.2R: Guide for the design and construction of externally bonded FRP systems for strengthening concrete structures (ACI, 2002), hereafter referred to as ACI 440.2R-02, and the Chinese code (GB50010, 2010) design guide for externally applied FRP systems for strengthening RC structures as reference documentation. The impact test was carried out on a DHR-9401 drop hammer (143 lb or 65 kg of weight with a total mass of 595 lb or 270 kg) impact tester and the ESF was up to 112 kip (500 kN). These were scaled specimens and the applied load was lower compared to the AASHTO LRFD (AASHTO, 2012a). However, the failure behavior should be noted in this study. The authors evaluated two methods of CFRP wrap installation, e.g., in first method, the fibers of CFRP wrap was placed along the longitudinal direction (prepared two specimens, one with one CFRP wrap layer and the other with six CFRP layers) with respect to the specimen. In the second method, the fibers of CFRP wrap were places along the transverse direction with respect to the specimen (Figure 2-26a). In this method, they also applied extra three layers of CFRP wrap (defined as partial CFRP layer) in transverse direction at the location of impact load to stiffen to impact location (Figure 2-26b). For the first method, one layer of CFRP wrap with fibers along longitudinal direction failed in shear mode (Figures 27a). The specimen with six layers of CFRP wrap along the longitudinal direction was found effective to resist shear fracture (Figures 27c). In the case of second method, the specimen with fibers along transverse direction failed strangely in flexure mode along with CFRP wrap fracture and rebar buckling (Figure 2-27b). The authors did not clearly explain the reason for such failure. But, observing the CFRP wrap applied in the second method, it may be conclude that, the extra 3 layers of CFRP wrap (partial CFRP layer, in total 4 layers at the impact location) at the location of impact load probably make that part of the specimen highly stiff. This caused a higher stress concentrations during the impact load event compared to the ends of the CFRP 4 layers, thus there occurred brittle fracture (characterized by flexure mode, see Figure 2-27b).

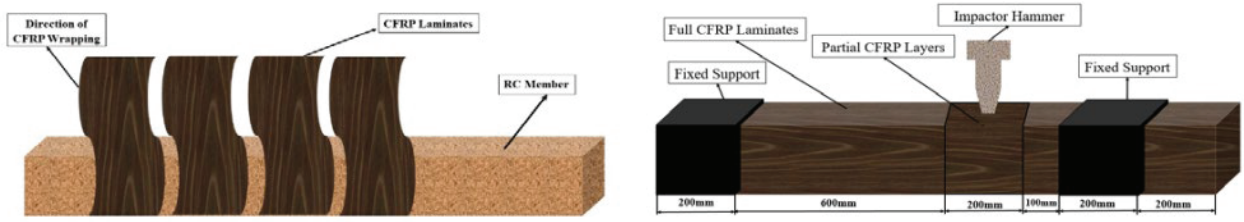

(a) (b)

Figure 2-27 The schematic diagram of FRP application at transverse direction: (a) CFRP wrapping direction; (b) Partial CFRP Layers wrapping (Al-Bukhaiti et al., 2021)

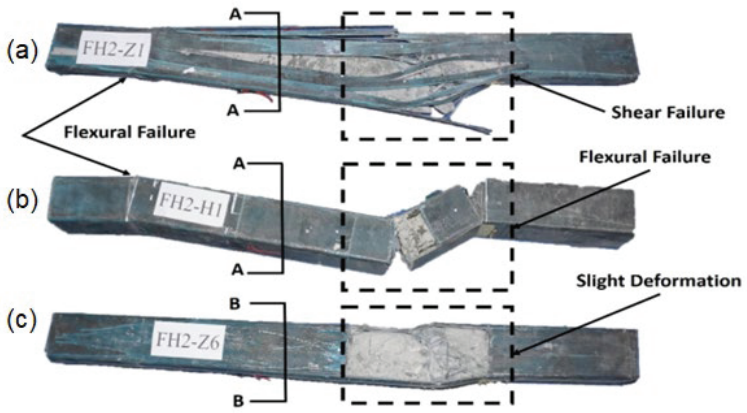

Figure 2-28 Failure modes after the end of the impact scenario for all elements (Al-Bukhaiti et al., 2021)

Li et al. (2022b) investigated the effectiveness of CFRP shear-strengthening on vehicular impact resistance of double-column RC bridge pier (10 inch or 250 mm dia circular and 10.2 inch x 15 inch or 260 mm x 380 mm rectangular with 67 inch or 1700 mm clear span) experimentally and employing FE simulation. The lateral impact force was applied at 16 inch (400 mm) from the base and the maximum ESF was recorded at 168 kip (747 kN), which did not conform to the AASHTO LRFD (AASHTO, 2012a) specification minimum requirement. They performed impact tests on unstrengthened pier, CFRP wrap strengthened of damaged pier, and CFRP-strengthened intact RC bridge piers with three consecutive impact loads. They applied four layers of epoxy saturated CFRP are used to wrap the pier, the thickness of each layer is 0.007 inch or 0.167 mm (Figure 2-29a), and the fiber orientation was zero degree-angle in reference to the pier circumferential direction according to the Chinese code for strengthening design of concrete structure (GB 50367, 2013). To obtain a good bonding effect between CFRP and concrete, the concrete surface was smoothed by the polishing machine as well as cleaned to remove the dust and loosened aggregates before wrapping. They reported that three failure modes occurred after the consecutive impacts, i.e., shear, shear-flexural and flexural modes. For the unstrengthened pier specimen, the well-marked shear crack remained at the shear span suffered the severe shear failure, showing the poor consecutive impact resistance (Figure 2-29b). For the strengthened damaged pier, initially a few minor horizontal cracks appeared on the concrete and outer CFRP layer at the back of the impact location; several wide and evenly spaced horizontal cracks formed on the concrete and outer CFRP layer on the rear surface of the impact location after the third impact (Figure 2-29b). In the case of strengthened intact piers, several horizontal cracks were observed under all the impacts, while the core concrete was still kept intact in the impact region (Figure 2-29b). Also, the strengthened intact pier sustained flexural

failure compared with bare and strengthened slight-damaged piers. Finally, they reported that the CFRP strengthening can effectively enhance the consecutive impact resistance of intact piers, avoiding the brittle failure happening.

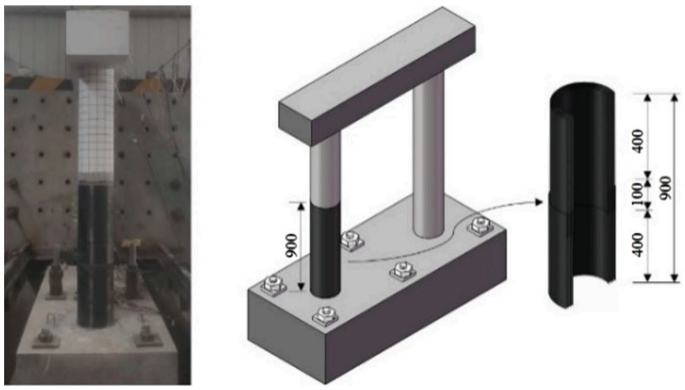

(a)

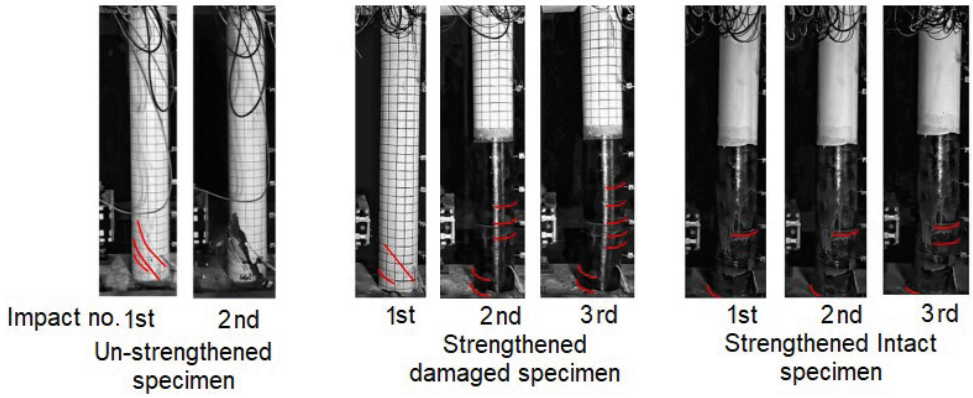

(b)

Figure 2-29 (a) Configuration of CFRP wrapped bridge pier specimen (units: mm); (b) failure modes of the unstrengthened and strengthened specimens after multiple impacts (Li et al., 2022b)

2.3.4 Other strengthening methods

There exists several other repair and strengthening systems that have been proposed and studied in the literature. Although these methods are less commonly used, a brief literature review of these methods is provided here for reference.

Liu, X et al. (2022) proposed a hybrid strengthening technology, namely FRP grid-reinforced UHPC composite strengthening technology to investigate the anti-collision performance of RC columns (10 inch x 10 inch or 250 mm x 250 mm). The composite reinforcement layer used in this reinforcement technology was composed of an FRP grid and UHPC layer (thickness 0.8 inch or 20 mm) and the FRP grid was embedded into UHPC as the reinforcement material. Initially, a layer of UHPC with a thickness of approximately 0.4 inch (10 mm) was applied on the pier surface. Then, starting from a side of the pier, the FRP grid was evenly wrapped onto the specimen surface. After that, the grid was covered with 0.4 inch (10 mm) thick UHPC mix. Finally, the surface was leveled using a spatula. The composite reinforcement layer used in this reinforcement technology is

composed of FRP grid and UHPC: FRP grid are embedded into UHPC as the reinforcement material, which effectively improves the mechanical performance of the UHPC. In addition to increasing the cross-sectional area of the main beam as the reinforcement material, the UHPC, as an interface binder, effectively overcomes the shortcomings of the bonding reinforced composite reinforcement technology. Defects, such as composite grid peeling, caused by epoxy resin aging and concrete cracking are avoided. This method effectively improved the mechanical performance of the UHPC by omitting the defects, such as composite grid peeling, caused by epoxy resin aging, concrete cracking, and debonding of FRP composite. They conducted an experimental study on the anti-collision performance of an FRP grid reinforced UHPC composite layer strengthened RC column (F-U-RC column) and an ordinary RC column (see Figure 2-30a-d) via impact test. When the impact velocities are 8, 9, and 9.6 mph (13.3, 14.7, and 15.5 km/h), the peak impact forces are 180, 203, and 213 kip (799.8, 901.2, and 946.6 kN), respectively. The authors also developed a numerical model using LS-DYNA and simulated a parametric study on the performance of the strengthening system (Figure 2-31). Under vehicle impact loading by numerical simulation, both the RC column and F-U-RC column exhibited shear failure, however, the failure mode of the F-U-RC column only produced cracks, and there was no large area spalling like that of the RC column (Figure 2-31). Table 2-5 provides a summary of the studies on the impact responses of strengthened RC bridge piers due to vehicular collisions.

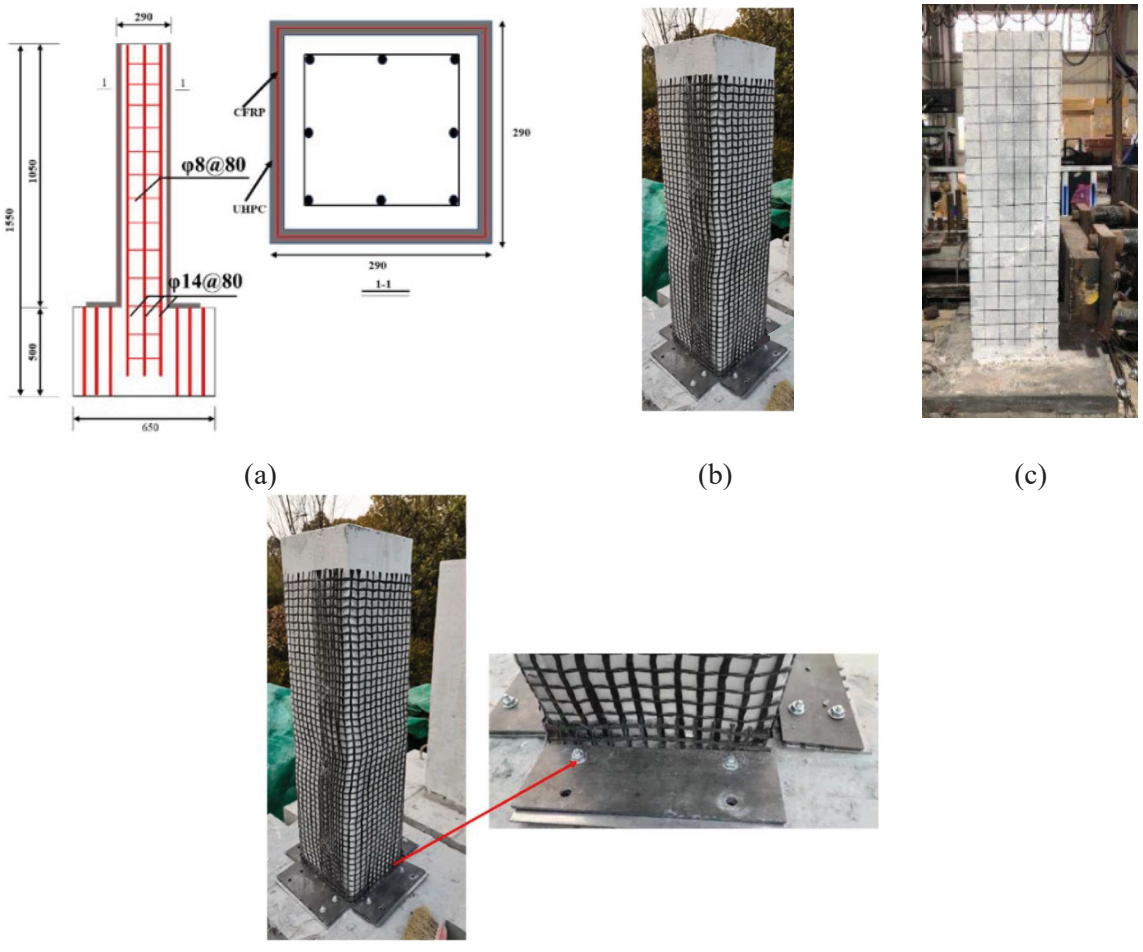

(a) (b) (c)

(d)

Figure 2-30 (a) Detailing of F-U-RC column; (b) F-U-RC column wrapped with FRP grid; (c) F-U-RC specimen after UHPC collar application; (d) FRP grip bottom (Liu, X et al., 2022)

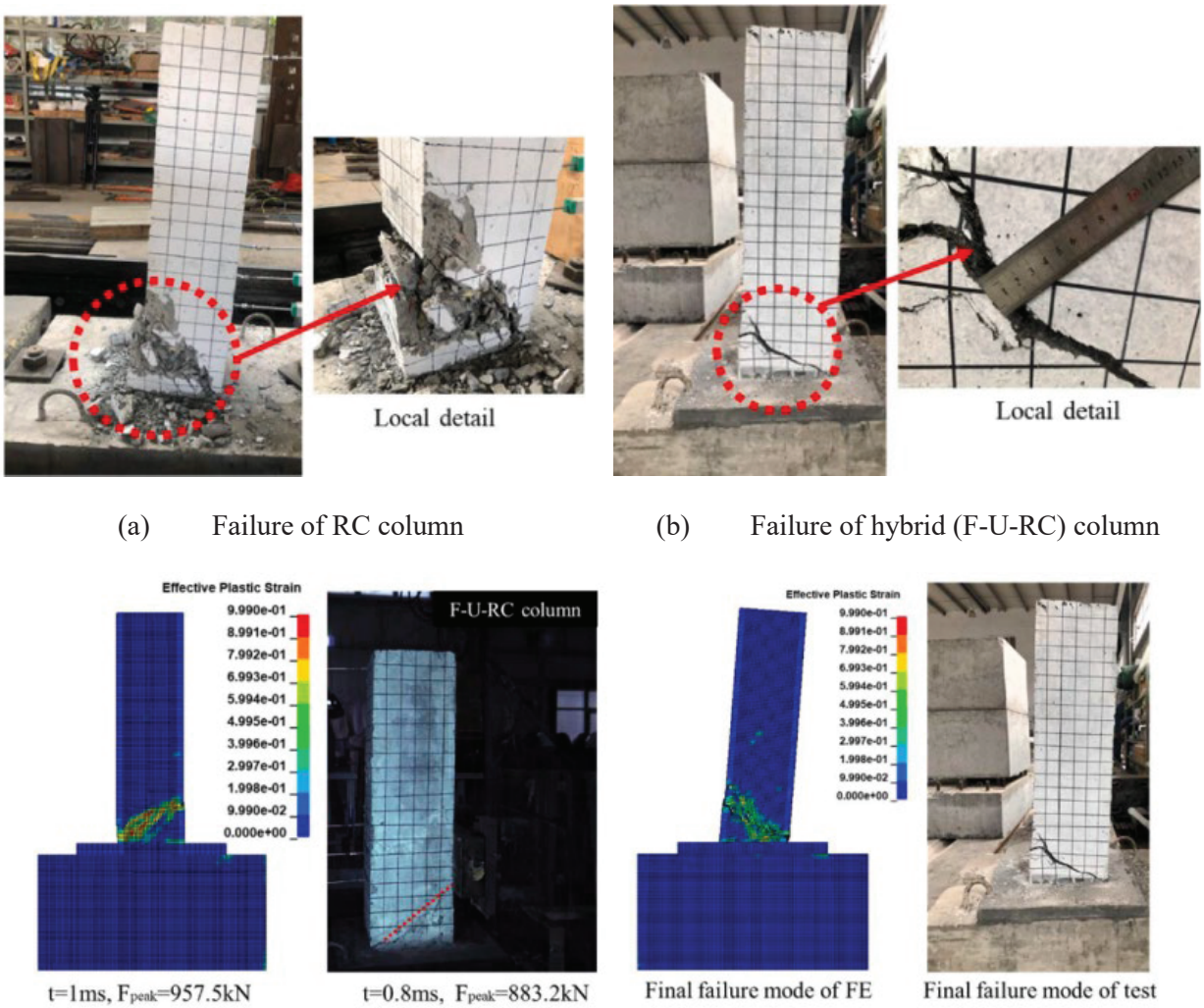

(a) Failure of RC column (b) Failure of hybrid (F-U-RC) column

(c) validation of failure mode of the F-U-RC column with the numerical model

Figure 2-31 Failure modes of experimental test and numerical model (Liu, X et al., 2022)

Takahashi et al. (1994) were the first to mention titanium's application in civil engineering and construction. The corrosion resistance of titanium alloys makes them ideal for marine environments due to their corrosion resistance. In their view, titanium is the ideal metallic material for construction because of its light weight, flexibility, and slight dimensional change when heated. Aside from being as strong as carbon steel, it is nonmagnetic, nontoxic, does not easily ionize, and does not pollute the environment, making it an even better alternative for underwater and marine construction.

Near-surface mounting (NSM) of supplemental reinforcing bars has emerged as a common retrofit method for strengthening RC structures. In this method, bars are bonded with an adhesive within grooves that are cut into the surface of the member. The most common reinforcing material used in the NSM application is fiber reinforced polymer (FRP). FRP materials are elastic until fracture thus providing no ductility. In addition, they can debond or delaminate prematurely limiting the effectiveness of the strengthening action. For this reason, new titanium alloy bars (TiABs) were developed as a potential alternative for FRP bars in NSM applications. TiABs have well-defined material properties including high strength, low stiffness, and negligible inelastic strain hardening

compared to conventional reinforcing steel. They are lightweight (which make them easy to work with in construction), fully impervious to conventional sources of corrosion (long-term exposure to the environment is not a concern), and have a coefficient of thermal expansion that is closer to concrete than reinforcing steel. The high cost of TiABs is a concern, however small diameter bars can be used because of the high strength and durability and simplified details allow for economical installation (Higgins et al., 2020).

The AASHTO Guide for Design and Construction of Near-Surface Mounted Titanium Alloy Bars for Strengthening Concrete Structures (AASHTO, 2020b), here after referred to as AASHTO NSM-TiABs, provides design and construction recommendations for strengthening existing RC structures with titanium alloy bars with 6 percent aluminum and 4 percent vanadium alloying elements (TiABs) using the near-surface mounted (NSM) construction method. The overall approach and organization of this guide are based on those presented in ACI 440.2R-17 (ACI, 2017). Recommendations are provided for shear and flexural strengthening of girders. The recommendations are supported by experimental and analytical research as well as field experiences (Higgins et al., 2017) that have demonstrated the application of TiABs for strengthening full-scale specimens typical of bridge girders by Oregon Department of Transportation (ODOT) at the O.H. Hinsdale Wave Research Laboratory at Oregon State University (OSU). The available experimental evidence includes the influences of combined high-cycle fatigue and environmental durability on the structural performance of NSM-TiAB-strengthened girders. TiABs are not sensitive to environmental deterioration such as corrosion. Their use near the concrete surface will not be adversely affected by environmental degradation. Long-term durability of applications with TiABs will be controlled by the concrete substrate and bonding materials. This guide does not address seismic strengthening applications.

This guide applies only to the application of NSM-TiABs for strengthening existing RC structures for flexure and shear. The methods require the use of standard 90-degree hooks at both ends of the bars to provide anchorage. The methods are not applicable to straight-bar applications without hooks at the ends. The methods include interactions of flexure on shear strength. The methods are applicable to concrete substrates that are able to effectively transmit bond stresses along the length of the bars and that can anchor the hooks. The minimum required concrete compressive strength is 3 ksi. The bond of TiABs along the NSM length provides crack control and limits deflections. At ultimate strength, significant cracking of the concrete, distress around the bonded regions, and debonding of the TiABs are anticipated. These methods are applicable to design with TiABs when the load effects are established using conventional elastic structural analysis with the load distribution factors prescribed in AASHTO LRFD (AASHTO, 2020a). This guide mentioned that the using this guide for TiAB based strengthening design in combination with advanced structural analysis methods requires additional caution. Figure 2-32 shows shear and flexural strengthening configuration for TiAB as per AASHTO NSM-TiABs (AASHTO, 2020b).

Research using TiABs for strengthening RC structures was first reported in 2013 (Higgins, 2013). However, a large body of knowledge has been developed over the past quarter century using NSM-FRP and NSM-metallics. Relevant literature for NSM-FRP is reported in ACI 440.2R-17 (ACI, 2017). Much of the bond behavior and models for NSM-FRP are relevant to NSM-TiAB applications. Research on the development and application of NSM-TiABs for strengthening RC structures has been reported by Higgins (2013, 2016); Higgins et al. (2014, 2015a, 2015b, 2015c, 2016, 2017, 2020); Knudtsen and Higgins (2017); and Vavra and Higgins (2017). Key details of these studies are reported subsequently.

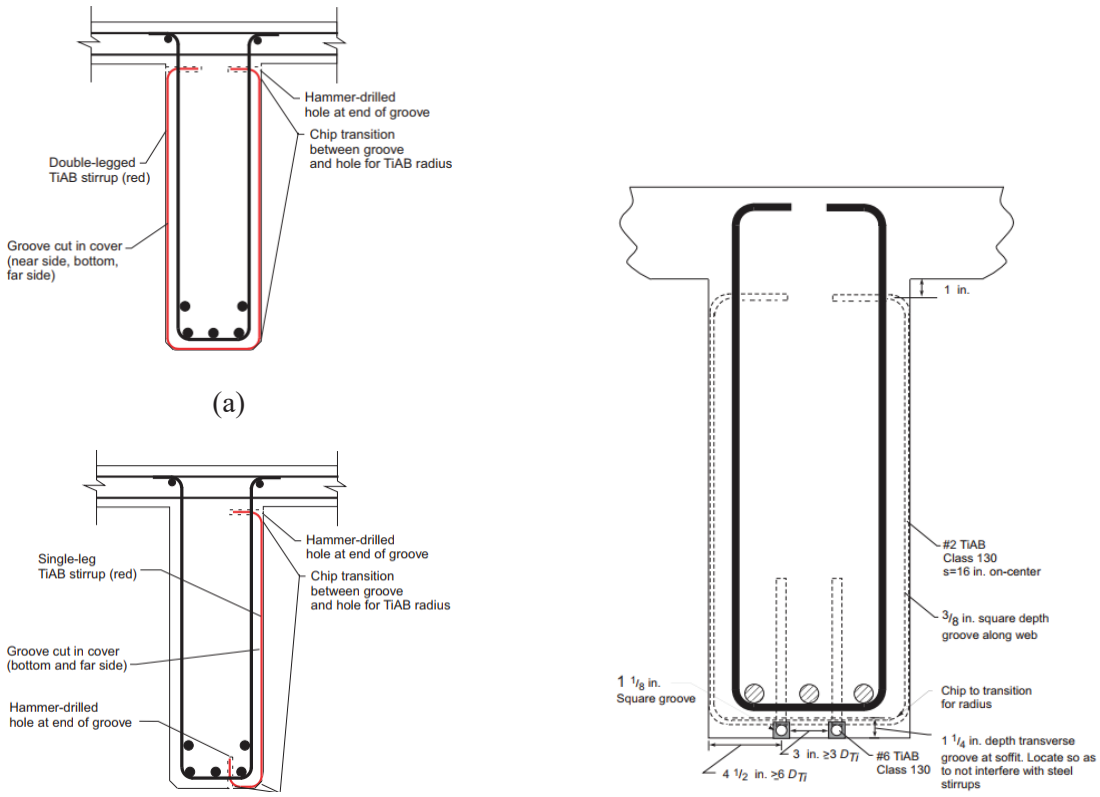

Figure 2-32 Shear and flexural strengthening configuration for TiAB: (a) continuous stirrup; (b) stirrup with single leg; (c) shear stirrup and flexural rebar together with specifications (AASHTO, 2020b)

Higgins et al. (2015a) reported results of experimental tests on full-scale RC deck girders containing poorly detailed flexural reinforcing steel representative of mid-twentieth century (1950s) design and construction practice. NSM-TiABs were used to strengthen the specimens. The beams were 48-in. (1.22-m) tall and 26-ft (7.92-m) long. The TiABs were 0.625 in. (15.9 mm) diameter and had 90-degree hooks at each end for anchorage. The beams were tested to failure under four-point bending. The authors also tested three replica beams for an in-service bridge to demonstrate design proof-of concept prior to installation of NSM-TiABs on the bridge. TiABs were shown to effectively increase strength and to shift nonductile diagonal-tension failures to ductile flexural failure.

Vavra and Higgins (2017) tested full-scale RC deck girders similar to those in Higgins et al. (2015a). One of the specimens was constructed with a flexural anchorage deficiency and strengthened with NSM-TiABs. The specimen was then subjected to simultaneous application of high cycle fatigue loading and freeze–thaw cycle exposure prior to testing to failure. Results demonstrated that exposure to high-cycle fatigue (equivalent to over 50 years of service-level loading) and 200 freeze–thaw cycles (equivalent to between 59 and 83 years of exposure for the Pacific Northwest) had no considerable effect on the service-level behavior or ultimate strength. NSM-TiAB bond specimens were tested using 15.9 mm and 6.4 mm (5/8 in and 1/4 in) diameter TiABs. The specimens were inverted half-beam pullout specimens. Straight-bond length and hooked ends were investigated. Hooked ends were able to achieve much higher bond strength than straight-bar anchorages.

Knudtsen and Higgins (2017) tested full-scale RC girders strengthened in shear with TiABs. The specimens were designed to simulate 1950s-era bridge girders in materials, proportions, and construction. Two specimens were subjected to simultaneous freeze–thaw and fatigue cycles before being tested to failure. NSM-TiABs provided significant increases in the shear strength of the specimens compared to similar unstrengthened specimens. The bond between the titanium and concrete was observed to provide strains in TiABs twice that of the adjacent steel stirrups. Figure 2-33 (a, b and c) shows typical stirrup and hook detail, Figure 2-33 (d and e) shows groove cutting and TiAB installation process, and Figure 2-33 (f) shows diagonal crack in NSM-TiAB strengthened girder at end of test.

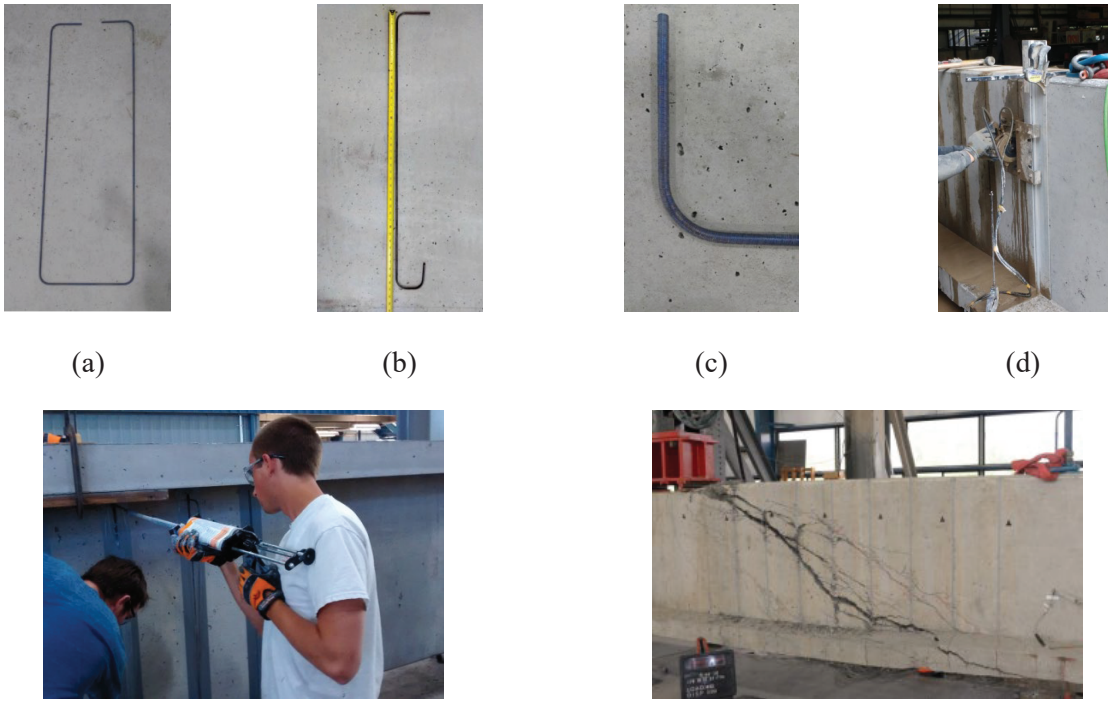

(a) (b) (c) (d)

(e) (f)

Figure 2-33 TiAB-strengthened RC girder: (a) Double leg titanium stirrup; (b) single leg titanium stirrup; (c) hook detail; (d) groove cutting process with aluminum saw guide; (e) titanium installation process; (f) diagonal crack at end of test in NSM-TiAB strengthened girder (Knudtsen and Higgins, 2017)

Vavra and Higgins (2017) also tested the use of TiABs in externally unbonded conditions. Although the unbonded specimens increased in strength and ductility, the external unbonded technique resulted in relatively low stiffness and large crack widths. The use of unbonded TiABs was recommended only for effective short-term or temporary repair of structures.

Higgins et al. (2020) conducted laboratory experiments with full-scale specimens using titanium alloy bars (TiABs) to investigate their potential for seismic retrofitting of seismically deficient RC columns. The specimens were designed to have vintage details and proportions that are widely recognized as being seismically deficient. The structural behaviors of 14 full-scale column specimens were investigated to study the effect of the proposed seismic retrofit on their cyclic performance. The program consisted of design, construction, and reverse cyclic lateral loading of column specimens under constant axial load. The main test variables were the column height, lateral loading direction, height of the retrofit shell, presence and absence of vertical ligaments, hook angle

of vertical ligaments, type of materials used for vertical ligaments, and the foundation details and restraints. The specimens were grouped based on the height of the column stubs: 12-ft (3657-mm) high considered tall columns and 8-ft (2438-mm) high considered short columns. The proposed seismic retrofit using TiABs consisted of two parts and aimed to compensate for the common inadequate flexural and transverse reinforcing steel details that are observed in vintage RC columns. Vertical TiABs were embedded into epoxy-filled drilled holes in the footings and columns to provide an alternative flexural tension load path and self-centering or restoring mechanism to the column and the column was then wrapped in plastic sheathing to debond (to be able to capture the relative movement at the interface due to lateral loading and to remove the shell after the test to evaluate the damage in the original column) the concrete infill from the column faces (Figure 2-34a). A spiral TiAB-reinforced concrete shell was added to provide confinement to the column core and bracing of the vertical TiABs that were unbonded along their length (Figure 2-34b). The spiral TiAB-reinforced shell was formed without concrete cover (Figure 2-34c). Splitting cracks on the retrofit shell along the column corners followed by flexural crack and uplifting of TiAB-concrete shell were observed in short columns (Figures 2-35a and 2-35b). In the case of long columns, similar cracks were observed in addition to some diagonal and horizontal cracks in the shell (Figures 2-35c and 2-35d). Cracks also spread to the footings. The study concluded that the control specimens without TiABs exhibited non-ductile response with no displacement ductility, limited energy dissipation, and overall poor performance. The TiAB-strengthened specimens exhibited greatly improved energy dissipation and higher viscous damping, and the spiral TiAB-reinforced shell provided excellent confinement and delayed bond failure of the reinforcing steel splice. After removal of the shell, only limited cracking was observed along the column height. Column damage was concentrated at the interface of the column and footing. The study also suggested that for retrofit designs that only use a shell (including steel plate, CFRP, etc.), sliding failures should be prevented. For the present retrofit, a second spiral could be added over the bottom of the column (a height equal to the column dimension) that anchors on the opposite face of the column from the first spiral. Alternatively, some additional dowel reinforcement could be considered. Unstrengthened columns are not likely to slide because the columns fail due to bond slip before the concrete can be crushed and reduced to powder at the interface.

(a) (b) (c)

Figure 2-34 (a) Column wrapped in plastic sheathing and TiAB ligaments (vertical rods) are installed; (b) TiAB spiral wrapped around column; (c) completed TiAB seismic retrofit details for short columns (Higgins et al., 2020).

(a) (b) (c) (d)

Figure 2-35 (a) short column failure; (b) short column after removal of TiAB spiral-concrete shell; (c) long column failure; (d) column after removal of TiAB spiral-concrete shell (Higgins et al., 2020)

Table 2-4 Summary of the studies on the impact responses of strengthened RC piers due to vehicle collisions

Studies	Test methods	Vehicle	Protection on bridge piers	ESF kN (kip)	Failure modes
Fuhaid et al., (2022)	FE	Ford van, Ford Explorer	RC collar, AFRP wrap	1450 kN (326 kip)	Shear failure for unstrengthened column, no significant damage for RC collar, large deformation for AFRP-strengthened column
Liu, T et al., (2022)	PT+FE	Truck	CFRP	10500 kN (2360 kip)	Shear failure
Isaac et al., (2011)	PT	Trucks	CFRP	NA	Flexure, no CFRP rupture
Sha and Hao (2015)	PT+FE	Berge	CFRP	15000 kN (3372 kip)	Flexural failure of the unstrengthened column, direct shear failure at the ends of the strengthened column
Mohammed and Parvin (2020)	FT+FE	Chevrolet C2500 pickup, Ford F800	CFRP-strengthened	12000 kN (2697 kip)	CFRP sheets puncture, localized concrete damage
Al-Bukhaiti et al., (2021)	DT	Train/trucks	CFRP	500 kN (112 kip)	CFRP failure, flexure mode
Li et al., (2022b)	HT+FE	Truck model	Unstrengthened and CFRP-strengthened	747 kN (168 kip)	Shear failure of unstrengthened pier and flexure mode of failure for CFRP-strengthened pier
Fan et al., (2018)	FT+FE	Ford F800 SUT	UHPC-strengthened column	7970 kN (1792 kip)	Slight damage exhibited in UHPC-strengthened column
Liu, X et al., (2022)	HT+FE	Truck	Hybrid (CFRP grid + UHPC)	Up to 946.6 kN, (213 kip)	Shear failure

Note: FT = Full scale crash tests, PT = Pendulum impact tests, FE = FE simulation, DT = Drop-hammer impact tests, HT = Horizontal impact test.

There has been extensive research conducted regarding the repairing and strengthening of bridge piers against static and seismic loadings, however the studies regarding strengthening bridge piers against lateral impacts caused by vehicular collisions are still very limited. FRP wraps and RC collars are highly researched methods of repair and strengthening of axial members. A number of

advanced cementitious composites, especially UHPCs are now being used as UHPC collar-strengthening for RC piers in order to their improved performance. After reviewing the above literature, the following points can be summarized:

- RC collars are the method of strengthening bridge piers which are currently allowed by FDOT Structures Manual (FDOT, 2024). While other methods have been implemented or demonstrated by different researchers and projects which is not currently accepted by the manual. However, the manual provides only a limited information regarding the requirements for RC collar for bonding with the existing pier. Moreover, these requirements are not yet verified experimentally or by FE simulation based dynamic analysis. On the other hand, AASHTO LRFD (AASHTO, 2020a) do not provide any guideline for RC collar-strengthening design, detailing or requirements to prevent delamination for bridge piers against vehicular impact.

- There was only one study available on RC collar-strengthening of columns under vehicular impact load. The researchers reported that the RC collar-strengthening increased the shear and impact load capacity of the column by up to 60% and 54%, respectively, compared to an unstrengthened column. This enhancement also significantly reduced the lateral deformation, with the columns showing no residual deformation but rather some cracks in the jacket. The ESF of the RC collar-strengthened column was 338 kip (1505 kN). The recorded maximum ESF was 326 kip (1450 kN) for an RC collar-strengthened pier (19 inch x 19 inch or 480 mm x 480 mm section) with a vehicle weighing 4971 lbs (2254 kg) traveling at 37 mph (60 km/h).

- In the case of UHPC collar-strengthening, the impact resistance capacity increased significantly compared to unstrengthened columns. Only slight or moderate damage was exhibited in the UHPC collar-strengthened columns compared to unstrengthened column under impact load. Only a few shear cracks were developed in the UHPC collar-strengthened columns with no concrete spalling. However, UHPC collar-strengthened column and RC collar-strengthened columns showed similar performance in reducing deformation due to impact load.

- In the case of strengthened columns or bridge piers, the FRP wrap confinement showed better resisting the shear failure compared to unstrengthened pier and also showed a reduction of impact force. In most of the cases, the FRP wrap did not show any debonding failure, however, local puncture or tearing was observed at the location of the impact. CFRP strengthening can effectively enhance the resistance of intact piers against consecutive impact loading and prevent brittle failure. The AASHTO FRP (AASHTO, 2012), FDOT Structures Manual (FDOT, 2024), or ACI 440.2R-17 (ACI, 2017) have limited information regarding the application of FRP, however, no solid information is available regarding the specification of construction procedure and design for large shear stress developed due to impact load as well as the requirements (e.g., FRP wrap method, number of wraps, lapping for vertical and horizontal extension) to avoid debonding or delamination of FRP wraps during impact load event. However, in the available literature no FRP debonding was reported in the case of complete wrapping method. Yet in most cases the ESF of the FRP wrap strengthened pier was found not conformed to AASHTO LRFD (AASHTO, 2012) specified minimum requirement. However, ACI 440.2R-17 (ACI, 2017) provides information about strengthening axial member (RC column of building) to enhance axial and bending capacity by enhancing P-M interaction behavior. It also provides design example for shear strengthening of axial member (non-circular RC column of building) but not due to impact load.

- Several other strengthening methods, including hybrid strengthening systems, or even steel collar, shape memory alloys, strain-hardening cementitious composites, near surface mounted reinforcing bars, etc. have been studied for strengthening of RC members, but have not been well

studied for impact force and required a detailed study to evaluate the performance against vehicular collision.

- After reviewing the literature, it is observed that the impact force increases with increasing vehicle speed. For example, the vehicle impact force was found to increase from 189 kip (840 kN) to 1553 kip (6910 kN) as the vehicle speed increased from 12.4 mph (20 km/h) to 62 mph (100 km/h).

2.4. Summary

This report provides pertinent information on the behavior of RC bridge pier due to impact load from a vehicular collision. The following conclusions are drawn from above discussion:

- **Behavior of unstrengthened RC bridge pier under impact load:**

1. The vehicular collision can be divided into four important phases, e.g., (a) initial peak impact force phase (0–50 ms): At the impact position of the affected pier, no evident damage or displacement occurred since the vehicle's front's stiffness was much lower than the RC piers, (b) impact force of development phase (50–150 ms): At the impact site, concrete started to spall at the impact location. (c) maximum peak impact force phase (150–200 ms): Shear failure happened at the point of collision, (d) impact force of attenuation phase (200–300 ms): the pier's shear and axial bearing capacities were reduced, and residual horizontal displacement and vertical settlement occurs.

2. The researchers employed different method to apply the impact force experimentally on the bridge pier specimens, e.g., full scale crash tests, pendulum impact tests, drop-hammer impact tests, horizontal impact test. Very few literature were found where the authors were able to create the ESF by applying the impact force using these methods as per the AASHTO LRFD (AASHTO, 2012) specification minimum requirement (2669 kN or 600 kip) due to lack of adequate testing facilities.

3. From the literature, most of the unstrengthened RC bridge piers showed shear failure due to impact loading. In most cases, the columns failed due to shear failure initially and subsequently by flexural failure leading to collapse. The observed failure modes can be categorized as shear or shear flexural types of failures depending on the test variables. In some cases, excessive shear forces were generated at the contra-flexure points located close to the supports. These observations may be cited as a potential reason for the failure of the column. It is also recommended to avoid the lapping joint of steel reinforcement on the pier and applying adequate transverse reinforcement to avoid complete separation of pier from the structure.

4. There are several failure modes of unstrengthened RC bridge piers subjected to a vehicle collision, i.e., flexural cracks, shear failure, punching shear failure, and total collapse. The failure modes vary dramatically under different loading circumstances. Moreover, when the vehicle speed rises, a significant diagonal shear fracture develops on the column top's negative side due to the large bending moment and shear force. It is obvious that as vehicle velocity increases, the damage to the bridge column varies significantly, from minor local concrete damage at the impact region to the total collapse of pier.

5. Again, there exists a complex relationship between the cross-sectional dimensions of piers on the impact force. If the cross-sectional size of piers increases that increases the deforming area of the vehicle, and hence decreases the residual kinetic energy of the vehicle

when the cargo hits. Therefore, the peak impact force on a rigid pier caused by cargo impact decreases as the cross-sectional size of the pier increases. On the other hand, increasing the cross-sectional dimension of the RC pier would enhance its stiffness and impact load-bearing capacity, which might lead to a higher response in the impact force history.

6. Regarding RC piers with normal sizes (e.g., with a diameter larger than 762 mm or 30 inch) subjected to vehicular impact, FE simulation results showed that the gravity loads from the superstructure, boundary conditions of the superstructure as well as the characteristics of the foundation have little effect on the engine-induced peak of impact force.

7. After reviewing the literature, it is observed that the impact force increases with increasing vehicle speed. For example, FE analyses showed that the vehicle impact force was found to increase from 189 kip (840 kN) to 1553 kip (6910 kN) as the vehicle speed increased from 12 mph (20 km/h) to 62 mph (100 km/h).

8. The influence of vehicle type on the impact force is also complicated. The larger and heavier vehicles may not necessarily produce larger impact force. It was observed from the FE simulations that, despite being heavier and larger than the single-unit truck, a tractor-trailer collision induced a smaller second peak of impact force in the impact-time history response. This is because the distance between the trailer and the front of the truck is longer, resulting in larger energy consumption of the truck body so that its cargo would hardly collide with the pier.

- **Behavior of strengthened RC bridge pier under impact load:**

1. RC collars are the method of strengthening bridge piers which are currently allowed by FDOT Structures Manual (FDOT, 2024). While other methods have been implemented or demonstrated by different researchers and projects which is not currently accepted by FDOT Structures Manual (FDOT, 2024). However, the FDOT Structures Manual (FDOT, 2024) provides only a limited information regarding the requirements for RC collar for bonding with the existing pier. Moreover, these requirements are not yet verified experimentally or by FE simulation. On the other hand, AASHTO LRFD (AASHTO, 2020a) do not provide any guideline for RC collar-strengthening design, detailing or requirements to prevent delamination for bridge piers against vehicular impact. However, ACI 440.2R-17 (ACI, 2017) provides information about strengthening axial member (RC column of building) to enhance axial and bending capacity by enhancing P-M interaction behavior. It also provide design example for shear strengthening of axial member (non-circular RC column of building) but not due to impact load.

2. There was only one study available on RC collar-strengthening of columns under vehicular impact load. The researchers reported that the RC collar-strengthening increased the shear and impact load capacity of the column by up to 60% and 54%, respectively, compared to an unstrengthened column. This enhancement also significantly reduced the lateral deformation, with the columns showing no residual deformation but some cracks in the jacket. The ESF of the RC collar-strengthened column was 338 kip (1505 kN). The recorded maximum ESF was 326 kip (1450 kN) for an RC collar-strengthened pier (19 inch x 19 inch or 480 mm x 480 mm section) with a vehicle weighing 4971 lbs (2254 kg) traveling at 37 mph (60 km/h).

3. In the case of UHPC collar-strengthening, the impact resistance capacity increased significantly compared to unstrengthened columns. Only slight or moderate damage was exhibited in the UHPC collar-strengthened columns compared to unstrengthened column under impact load. Only a few shear cracks were developed in the UHPC collar-strengthened columns

with no concrete spalling. However, UHPC collar-strengthened column and RC collar-strengthened columns showed similar performance in reducing deformation due to impact load.

4. Compared to the impact speed and the thickness of UHPC collar, the UHPC strength had a limited influence on the impact-induced response. In addition, the influence of the UHPC thickness on residual capacity was dependent upon initial impact speed. The residual capacities increased with increasing the thickness of UHPC collar when the initial impact speed was not very high. This was because the impact damage was low and most of the UHPC at the bottom retains the high axial load-carrying capacity after a vehicle impact. The increase in the UHPC area due to the increase in the UHPC thickness was significantly beneficial for improving the residual axial capacity. On the contrary, if the impact velocity is 62 mph (100 km/h), the residual capacity cannot be effectively enhanced by thickening the UHPC collar. In this case, severe shear damages always occurred at the bottom for all thicknesses of UHPC collar as the impact force at the lower part of pier caused higher shear force near the bottom support and the impact energy was very high at the bottom compared with dissipating energy of the UHPC-strengthened column. As a result the failure occurred at the bottom

5. In the case of strengthened columns or bridge piers, the FRP wrap confined bridge columns exhibited better shear resistance and reduced impact force. In most of the cases, the FRP wrap did not show any debonding failure, however, local puncture or tearing was observed at the location of the impact. In the case of consecutive impact loading, CFRP strengthening can effectively enhance the consecutive impact resistance of intact piers, avoiding the brittle failure happening.

6. Under vehicle impact loading experimentally and numerical simulation, the hybrid strengthening method using FRP grid-and UHPC collar showed promising result compared to unstrengthened specimen. Both the RC column and FRP grid-and UHPC collar-strengthened column exhibited shear failure, however, the failure mode of the hybrid-strengthening method column only produced shear cracks, and there was no large area spalling like that of the RC column

- **Importance of dynamic analysis and dynamic FE simulation of unstrengthened and strengthened RC bridge pier:**

1. All the methods discussed in this study to calculate the ESF for designing bridge piers that are subject to vehicle collisions have some limitations. The stiffness-based method introduced by Chopra (2011) only considers the elastic response of the structure. In reality, the majority of the kinetic energy of the impacting vehicle is absorbed by plastic deformation of the vehicle. The remaining kinetic energy is then absorbed through plastic deformation of the pier. The method recommended by the Eurocode 1 (BSI 2006a) considers plastic deformation in the structural components exposed to the kinetic energy of the vehicle; however, it fails to account for the inertial forces that play a large role in the load-resisting mechanisms of a structure undergoing dynamic loads. Lastly, the ESF obtained by filtering the contact force-time history data using moving averages accounts for the structural properties of the pier. However, it requires access to the time history of the contact forces during the crash, which is hard to achieve considering the cost and accuracy associated with conducting such tests or FE simulations.

2. The pier that undergoes the dynamic collision load experiences much larger displacements and damage levels. The ESF recommended by AASHTO LRFD (AASHTO, 2020a) was only able to produce the same displacements and contact forces as a dynamic

collision for a truck traveling less than 30 mph (50 km/h). At higher vehicle speeds, the static analysis greatly underestimates the displacement and force demand experienced by a bridge pier in a collision. As per the current AASHTO LRFD (AASHTO, 2020a) design provision, the ESF is based on a single vehicle traveling at 50 mph (80 km/h). On the other hand, as potential impact conditions are dependent on local traffic conditions, piers may be overdesigned in areas with generally low vehicle speeds and under-designed in areas with high vehicle velocities and a high volume of heavy commercial vehicles. Therefore, a FE simulation-based dynamic analysis is necessary along with ESF based design to ensure safety and economy.

3. Moreover, it is observed that the prescribed ESF of AASHTO LRFD (AASHTO, 2020a) is only comparable to the actual dynamic impact load applied by a truck moving at speeds less than 30 mph (48.3 km/h). Thus, the prescribed ESF significantly underestimates the actual impact event. This proves that only ESF-based design and strengthening of RC bridge piers should be avoided and also reflects the necessity of FE-based dynamic analysis.

4. The FE nonlinear modeling based dynamic analysis using LS-DYNA showed promising results to simulate the behavior of strengthened and unstrengthened RC bridge piers. The researchers showed good agreement in prediction of impact force and displacement, validation of failure modes and dynamic behavior of bridge piers due to the collision between the FE models of bridge pier and heavy vehicle with various mass and impact speed using the nonlinear FE modeling platform of LS-DYNA.

5. In the available studies, most of the researchers did not apply the impact force experimentally to develop ESF as per the AASHTO LRFD (AASHTO, 2012a) specification minimum requirement due to lack of adequate testing facilities, however, they successfully simulated dynamic response via the FE models in LS-DYNA and were able to validate the behavior of unstrengthened and strengthened piers.

Based on our review, we also identified the following research gaps that require further investigation:

1. Although the FDOT Structures Manual (FDOT, 2024) allows the use of RC collar to strengthen bridge piers against lateral impact and prescribed detailing requirements to ensure bonding between the collar and existing piers, they are not yet verified experimentally or by FE simulation. It is necessary to conduct further experimental study and FE simulation on design parameters and structural performance to verify the performance of RC collar and these detailing requirements with mechanical connection and without mechanical connection between existing concrete column and concrete collar.

2. Although FRP wraps and UHPC collars have been studied for strengthening of bridge piers against lateral impact, there is no guide specifications on the design and construction of such strengthening methods. Due to the absence of proper guidance from available standards and literature, to achieve the confident on performance-based design, extensive experimental and numerical analyses are required to understand the behavior of these strengthening schemes under dynamic impact loading, and to determine the influence of different design parameters.

3. Moreover, there are not sufficient studies available on the improvement of the bonding of the strengthening materials (RC collar, UHPC collar, FRP wrap etc.) due to actual vehicular impact. There is still a demand for further development of FE modeling for proper interface between the strengthening materials and the existing RC bridge pier to simulate the deboning or delamination which can help to improve and predict the performance of the strengthening

method. More experimental investigations also need to be performed to validate FE results to contribute to the codes and guidelines in the future for performance based design of strengthening for impact load.

4. Very few literature verified the performance of different strengthening methods under full scale crash test, or the impact force required by AASHTO LRFD (AASHTO, 2012a). Thus, more experimental investigation is required to fully understand and evaluate the behavior of unstrengthened and strengthened bridge pier under impact due to realistic vehicular collision.

5. There are other strengthening methods that showed promises in strengthening RC members, which are not well studied for impact force and required a detailed study to evaluate the performance against vehicular collision, e.g., steel collar, near-surface mounted titanium alloy bars (NSM-TiABs) for strengthening RC bridge piers, using shape memory alloy (SMA) rebar, etc. Although AASHTO NSM-TiABs (AASHTO, 2020a) and few recent studies showed the design procedure strengthening RC girder for flexure and shear, and promising results using titanium rebar for strengthening RC columns for lateral load (seismic load), further research is recommended in order to examine the performance under impact loading.

CHAPTER 3 ANALYSIS PLANNING AND VARIABLE MATRIX

Based on the literature review from chapter 1 and the meeting with the PM and other FDOT engineers, the parameters to investigate via FE modeling are shown in Table 3-1. In the variable matrix, an 80-kip (36,287-kg) tractor-semitrailer was considered as impact vehicle following the AASHTO LRFD (AASHTO, 2020a). The impact speed was 50 mph (80.47 km/h) as per AASHTO LRFD (AASHTO, 2020a). The horizontal impact angle was 0°. A total of five pier models were developed, including (i) baseline pier (no strengthening), (ii) RC collar-strengthened pier without dowel bars, (iii) RC collar-strengthened pier along with dowel bars, (iv) FRP-strengthened pier, and (v) UHPC-strengthened pier. The baseline pier was circular in shape, and the diameter and length was 30 in (762 mm) and 16 ft (4.88 m), respectively. These dimensions were selected to represent the existing piers that needed to be strengthened in Florida. Currently, the FDOT Structures Manual (FDOT, 2024) requires post-installed anchor systems (e.g., adhesive-bonded dowel bars) to attach new construction to structurally sound concrete to prevent debonding of the strengthening system. However, due to the construction cost and time, there was an interest in removing this requirement if it is not necessary. Therefore, in the current study, we modeled and analyzed RC collar-strengthening both with and without dowel bars to determine the necessity of using dowel bars in such a strengthening method.

Due to the lack of experimental data, the developed FE model for the five pier models cannot be fully validated. As future research, the PIs recommend experimental testing for validation. In the meantime, in this research, sensitivity studies were conducted on selected parameters, which will aid decision-making by FDOT in the future. The sensitivity analysis was to determine the effects of changing model parameters on the results of the model. For example, the thickness of the FRP wrap or UHPC layer and transverse reinforcement ratio can be changed to see how they influence the impact response. Therefore, the number of FE simulations was greater than five. Additional parameters were included in the sensitivity study as needed, depending on the outcome of the initial sensitivity study.

Table 3-1 Parameters to investigate

Parameters	Cases	Number of variation
Vehicle	80-kip (36287.39-kg) tractor-semitrailer	1
Impact speed	50 mph (80.47 kph)	1
Impact angle (horizontal)	0°	1
Strengthening method	1. baseline (no strengthening) 2. RC collar-strengthened without dowel bar 3. RC collar-strengthened with dowel bars 4. FRP-strengthened 5. UHPC-strengthened	5
Pier shape	Circular	1
Pier diameter	30 in (762 mm)	1
Pier length	16 ft (4.88 m)	1

CHAPTER 4 HAND CALCULATION

Hand calculations were performed to provide a set of preliminary strengthening plans that will be investigated in later FE simulation. The strengthening plans were targeted to provide sufficient capacity for the strengthened pier to resist a 600-kip (2668.93-kN) equivalent static force, as specified in AASHTO LRFD (AASHTO, 2020a) and FDOT Structures Manual (FDOT, 2024). The hand calculations of four piers were performed, including a baseline pier that needed to be strengthened and three piers strengthened with RC collar, FRP wraps, and UHPC collar, respectively.

The baseline pier was designed to represent the existing piers that needed to be strengthened in Florida, and its capacity was calculated according to AASHTO LRFD (AASHTO, 2020a). The RC collar-strengthened pier was designed according to FDOT Structures Manual (FDOT, 2024), and its capacity was checked according to the AASHTO LRFD (AASHTO, 2020a). The design and calculation of the FRP-strengthened pier was performed following the recommendations from ACI 440.2R-17 (ACI, 2017). The design and calculation of the UHPC-strengthened pier was done according to AASHTO Guide Specification for Structural Design with UHPC (AASHTO, 2021), hereafter referred as AASHTO UHPC Design Guide. The design details of these four piers are given in Figure 4-1, and details of the calculations are presented in the following sections, from section 4.1 to section 4.4.

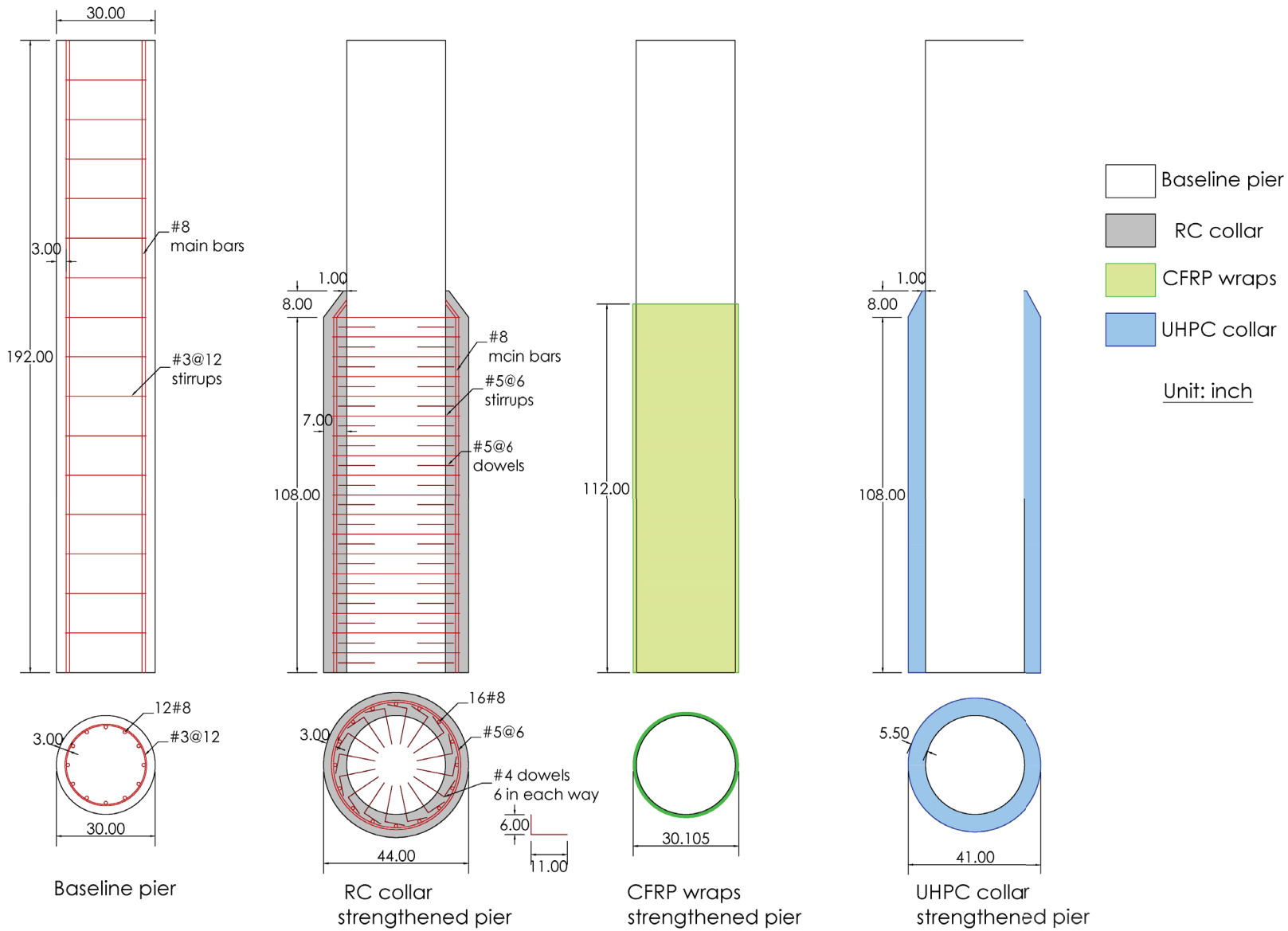

Figure 4-1 Design details of baseline pier, RC collar-strengthened pier, FRP wrap-strengthened pier, and UHPC collar-strengthened pier

4.1 Baseline RC Pier

The baseline pier is circular in shape with a diameter of 30 in. (762 mm) and a height of 16 ft (4.88 m). The design compressive strength of concrete is 3.4 ksi (23.44 MPa), which was taken as the minimum value for Class II concrete as specified in FDOT Structures Manual (FDOT, 2024). Grade 40 steel is used as reinforcement. The longitudinal reinforcement consists of twelve #8 bars, corresponding to a reinforcement ratio of 1.33%. The stirrups are #3 bars with a spacing of 12 in (304.8 mm).

Shear capacity calculation as per AASHTO LRFD (AASHTO, 2020a)

$f_c' = 3.4\ ksi$ (Compressive strength of concrete)

$f_y = 40\ ksi$ (Yield strength of steel reinforcements)

$D = 30\ in$ (Diameter of the pier)

$c_c = 3\ in$ (Clear cover of steel reinforcement)

$d_l = 1\ in$ (Diameter of the longitudinal reinforcement)

$d_s = 0.375\ in$ (Diameter of stirrups)

$D_r = D - 2c_c - 2d_s - d_l = 22.25\ in$ (Diameter of the longitudinal reinforcement circle)

$A_v = 0.22\ in^2$ (Area of the two-leg stirrups)

$s = 12\ in$ (Stirrups spacing)

$b_v = D = 30\ in$ (Effective width for shear)

$d_v = 0.9d_e = 0.9(D/2 + D_r/\pi) = 19.87\ in$ (Effective depth for shear)

$\beta = 2.0$ (Article 5.7.3.4.1)

$\theta = 45°$ (Article 5.7.3.4.1)

$\lambda = 1.0$ (Article 5.4.2.8)

$\phi = 1.0$ (Article 1.3.2.1)

$V_c = 0.0316\beta\lambda {f_c'}^{0.5} b_v d_v = 69.47\ kip$ (Eq. 5.7.3.3-3)

$V_s = \frac{A_v f_y d_v cot\theta}{s} = 14.74\ kip$ (Eq.5.7.3.3-4)

$V_n = 2(V_c + V_s) = 168.42\ kip$ (Nominal shear strength of two failure planes)

$V_u = 600kip > \phi V_n = 168.42\ kip$

According to above calculations, the baseline pier is unable to resist the 600-kip (2668.93-kN) equivalent static force required by AASHTO LRFD (AASHTO, 2020a). Therefore, the baseline pier needs to be strengthened.

4.2 RC Collar-strengthened Pier

The RC collar is circular in shape and has a thickness of 6 in. (152.4 mm). The diameter of the pier at the strengthened section is 44 in (1117.6 mm). The design compressive strength of concrete is 3.4 ksi (23.44 MPa). Grade 60 steel is used as reinforcement. The longitudinal reinforcement are 16 #8 bars, and the stirrups are #5 bars with a spacing of 6 in (152.4 mm). According to the Article 3.6.5 of AASHTO LRFD (AASHTO, 2020a), the equivalent static force is assumed to act at a distance of 5 ft (1.52 m) above the ground. Considering the 45-degree shear failure plane, the RC collar should at least have a height of 5ft+44 in=104 in (2641.6 mm). The height of the RC collar is taken as the next multiple of the spacing of stirrups, which is 108 in (2743.2 mm). The additional 8 in (203.2 mm) of concrete at the end of the RC collar is an adaptation of the RC collar design from the Campbell Drive Interchange Improvements project.

Shear capacity calculation as per AASHTO LRFD (AASHTO, 2020a)

$f_c = 3.4\ ksi$ (Compressive strength of concrete)

$f_y = 60\ ksi$ (Yield strength of steel reinforcement)

$D = 44\ in$ (Diameter of the strengthened section)

$c_c = 3\ in$ (Clear cover of steel reinforcement)

$d_l = 1\ in$ (Diameter of the longitudinal reinforcement)

$d_s = 0.625\ in$ (Diameter of stirrups)

$D_r = D - 2c_c - 2d_s - d_l = 35.75\ in$ (Diameter of the longitudinal reinforcement circle of the strengthened section)

$A_v = 0.62\ in^2$ (Area of the two-leg stirrups)

$s = 6\ in$ (Stirrups spacing)

$b_v = D = 44\ in$ (Effective width for shear)

$d_v = 0.9d_e = 0.9(D/2 + D_r/\pi) = 30.04\ in$ (Effective depth for shear)

$\beta = 2.0$ (Article 5.7.3.4.1)

$\theta = 45°$ (Article 5.7.3.4.1)

$\lambda = 1.0$ (Article 5.4.2.8)

$\phi = 1.0$ (Article 1.3.2.1)

$V_c = 0.0316\beta\lambda f_c'^{0.5} b_v d_v = 154.03\ kip$ (Eq. 5.7.3.3-3)

$V_s = \frac{A_v f_y d_v cot\theta}{s} = 186.25\ kip$ (Eq. 5.7.3.3-4)

$V_n = 2(V_c + V_s) = 680.56\ kip$ (Nominal shear strength of two failure planes)

$V_u = 600\ kip < \phi V_n = 680.56\ kip$

According to above calculations, the RC collar-strengthened pier is able to resist the 600-kip (2668.93-kN) equivalent static force. Therefore, the design of the RC collar is satisfactory. According to the FDOT Structures Manual (FDOT, 2024), a grid of mechanical connections should be provided when using RC collars to strengthen existing piers. Thus, A grid of dowels between the

RC collar and the original pier at a horizontal and vertical spacing of 6 in (152.4 mm) is designed, as shown in Figure 6. The details of the dowel bars also follow the design of RC collar dowel bars from the Campbell Drive Interchange Improvements project. According to the FDOT Structures Manual (FDOT, 2024) Article 7.3.6, the following measures should also be taken when constructing the RC collar:

- Show the existing concrete cover removed to reveal the vertical bars inside the stirrups or spirals;
- Use a Shrinkage Reducing Admixture for the collar concrete;
- Roughen the existing concrete interface surface to a minimum amplitude of 1/4 in (6.35 mm);
- The existing concrete interface surface shall have a Saturated Surface Dry condition when placing the concrete collar.

4.3 FRP Strengthened Pier

The HM-60 Unidirectional Carbon Fiber Sheet provided by Horse Construction Co., Ltd (https://www.horseen.com) is used for design calculation. Details of the CFFP sheet properties from the manufacturer's website are given in Appendix A.

Shear capacity calculation as per ACI 440.2R-17

$f_{fu}^{*} = 598.05\ ksi$ (Ultimate tensile strength of the FRP as reported by manufacturer)

$\varepsilon_{fu}^{*} = 0.0169$ (Ultimate rupture strain of the FRP as reported by manufacturer)

$E_f = 33671.96\ ksi$ (Tensile modulus of elasticity of the FRP as reported by manufacturer)

$c_E = 0.85$ (Experimental reduction factor as per table 9.4)

$\varepsilon_{fu} = c_E \varepsilon_{fu}^{*} = 0.0144$ (Design rupture strain of the FRP)

$\varepsilon_{fe} = \min(0.004, 0.75\varepsilon_{fu}) = 0.004$ (Effective strain of FRP attained at failure, Eq. 11.4.1.1)

$t_f = 0.01311\ in$ (Thickness of one layer of FRP as reported by manufacturer)

$w_f = s_f$ (For continuously applied FRP, the width of FRP wraps w_f equals to the center-to-center spacing s_f of FRP wraps)

$n = 4$ (Number of FRP layers applied)

$A_{fv} = \frac{\pi}{2} n t_f w_f$ (Eq. 11.4c)

$D = 30\ in$ (Diameter of the baseline pier)

$d_{fv} = 0.8D = 24\ in$ (Article 11.4)

$V_f = \frac{A_{fv} f_{fe} d_{fv}}{s_f} = 266.25\ kip$ (Eq. 11.4a)

$V_c = 69.47\ kip$ (Nominal shear strength provided by concrete)

$V_s = 14.74\ kip$ (Nominal shear strength provided by stirrups)

$\psi_f = 0.95$ (Additional reduction factor for FRP as shear reinforcement, table 11.3)

$V_n = 2(V_c + V_s + \psi_f V_f) = 674.30kip$

$\phi = 1.0$

$V_u = 600\ kip < \phi V_n = 674.30\ kip$

According to the above calculations using the FRP properties provided from the company's website, the baseline pier strengthened with four layers of FRP sheets is able to resist the 600-kip (2668.93-kN) equivalent static force. The diameter of the strengthened section is 30.105 in (764.67 mm).The FRP wraps, with the fiber oriented perpendicular to the longitudinal axis of the pier, will be installed continuously up to a height of 108 in (2743.2 mm), so it can be compared with other strengthening methods. Before installing the FRP wraps, ACI 440.2R-17 (ACI, 2017) recommends preparing the pier surface so it is free of unsound materials, and the localized out-of-plane variations of the pier surface should not exceed 1/32 in (0.79 mm). However, it also requires that the specific requirements be consulted with the manufacturing company.

4.4 UHPC Collar-strengthened Pier

The design strengths of the UHPC are taken as the minimum values from the Appendix A1 of the AASHTO UHPC Design Guide (AASHTO, 2021). Currently, there aren't any design code provisions that could be used to calculate the shear strength of circular concrete-UHPC sections or circular hollow sections, so the method proposed by Queiroz Junior et al. (2016) was used to convert the UHPC collar to an equivalent solid section first, and then the shear strength of this equivalent solid section was calculated according to the AASHTO UHPC Design Guide (AASHTO, 2021). The method proposed by Queiroz Junior et al. (2016) is validated against a data base where the ratio between the thickness of the solid part to the overall depth of the section ranges from 0.125 to 0.33, which is consistent with the UHPC collar-strengthened section here.

Shear capacity contribution of the UHPC collar as per AASHTO UHPC Design Guide (AASHTO, 2021)

$f'_{u,c} = 18\ ksi$ (Compressive strength of UHPC)

$f_{u,t,loc} = 0.75\ ksi$ (Crack localization stress of UHPC)

$t = 5.5in$ (UHPC collar thickness)

$b_{u,v} = 2t = 11\ in$ (Equivalent width of the UHPC collar according to Queiroz Junior et al., (2016))

$d_{u,v} = 0.8(D + 2t) = 32.8\ in$ (Equivalent depth of the UHPC collar according to Queiroz Junior et al., (2016))

$\gamma = 0.85$ (Factor accounting for the variability of UHPC tensile strength, article 1.4.2.5.4)

$\theta = 45°$

$V_{uhpc} = \gamma f_{u,t,loc} b_{u,v} d_{u,v} cot\theta = 230.01kip$ (Eq. 1.7.3.3-3)

$V_c = 69.47\ kip$ (Nominal shear strength provided by concrete)

$V_s = 14.74\ kip$ (Nominal shear strength provided by stirrups)

$V_n = 2(V_c + V_s + V_{uhpc}) = 628.44\ kip$

$\phi = 1.0$

$V_u = 600\ kip < \phi V_n = 628.44\ kip$

According to the above calculations, the baseline pier strengthened with a 5.5-in (139.70-mm) thick UHPC collar is able to resist the 600-kip (2668.93-kN) equivalent static force. The diameter of the strengthened section is 41 in (1041.4 mm). Considering the equivalent static force acting at a distance of 5 ft (1.52 m) above the ground and the 45-degree shear failure plane, the height of the UHPC collar should be at least 101 in. Thus, the height of the UHPC collar is taken as the same as that of the RC collars. The end details of the UHPC collar also followed the RC collar design from the Campbell Drive Interchange Improvements project. AASHTO UHPC Design Guide (AASHTO, 2021) does not provide recommendations for the construction of UHPC collars, so the requirements for the construction of RC collars from the FDOT Structures Manual (FDOT, 2024) are adopted:

- Show the existing concrete cover removed to reveal the vertical bars inside the stirrups or spirals;
- Roughen the existing concrete interface surface to a minimum amplitude of 1/4 in (6.35 mm);
- The existing concrete interface surface shall have a Saturated Surface Dry condition when placing the concrete collar.

CHAPTER 5 CALIBRATION ANALYSIS

In FE analysis, the validation and calibration of material constitutive models and modeling techniques are crucial for achieving accurate and reliable simulation results. These models, which predict material behavior under various stresses, must be calibrated against empirical data to enhance the precision of the simulations. In this chapter, the vehicle model, which is a tractor-trailer, was first validated against a full-scale collision test. Then the material models—RC, UHPC, and FRP—and modeling techniques were calibrated against published experiments.

5.1 Validation of Tractor-trailer Model

5.1.1 Full-scale tractor-trailer and bridge pier collision test

The full-scale tractor-trailer and steel pier collision tests performed by Buth et al. (2011) formed the basis for the 600-kip (2669-kN) equivalent static force in current AASHTO LRFD (AASHTO, 2020a). Therefore, the TEST NO. 429730-2 in their study was used to verify the FE tractor-semitrailer model. The time history of the impact force of the vehicle on pier was selected as the validating data. In this test, a 2001 Freightliner FLD tractor with a 1983 Utility van trailer was used, as shown in Figure 5-1(a). The total gross static weight of this vehicle was 79,640 lb (36,124 kg). The steel bridge pier had a 36-in (914.4-mm) diameter and a 14-ft (4.27-m) height, and it was firmly supported so it can be treated as a rigid column with fixed boundary. The impact speed of the tractor on pier was 48.4 mph (77.89 km/h).

5.1.2 FE modelling of the collision test with LS-DYNA

The original LS-DYNA model of tractor-semitrailer was developed by Miele et al. (2010), and the model was downloaded from the official website of Oak Ridge National Laboratory. This website documents their work on the development and optimization of FE models of semitrailer trucks for simulation of crash events involving roadside safety hardware such as bridge rails and median barriers. The site contains interactive manuals and documentation for the developed models. The research team of Battelle Memorial Institute, Oak Ridge National Laboratory (ORNL) and the University of Tennessee at Knoxville (UTK) was sponsored by National Transportation Research Center Inc. (NTRCI). The developed tractor-semitrailer vehicle FEM models are currently the most advanced publicly available models of this vehicle class in terms of physical function, geometric detail, and material property accuracy. The ORNL researchers reported that the models have been extensively debugged and used for hundreds of simulations for different speeds and impact angles and have been shown to be reasonably accurate. This website was developed with a goal to make these models widely available to the engineering community for design and development of roadside safety hardware and for an overall improvement of public safety. However, possibly due to the version issue, the FE model could not be used as-is but instead needed to be modified in this research. The modifications include adjusting some material models, remeshing of some components, modification of the connection between various parts, adding or removing mass to key components to better match the real truck used in the test by Buth et al. (2011).

In our FE simulation, the tractor was based on the Tractor Sleeper Model Version 100308 from ORNL's website, and the semitrailer was based on the Semitrailer Model Version 100805 with a length of 48 ft (14.63 m), as shown in Figure 5-1. The FE model of tractor-semitrailer consists of

55,321 solid elements, 304,029 shell elements, and 629 beam elements, and its static weight is 80,000 lb (36,287kg). The pier model has the same geometric configuration as the pier in the test. Rigid material is used to model the column, and the boundary condition was considered as fixed at the top and the bottom. The impact speed of the tractor on pier was 48.34 mph (77.8 km/h), which is at the same magnitude as the experimental work conducted by Buth et al. (2011). The contact between the tractor-trailer and the pier was modeled by AUTOMATIC_SURFACE_TO_SURFACE.

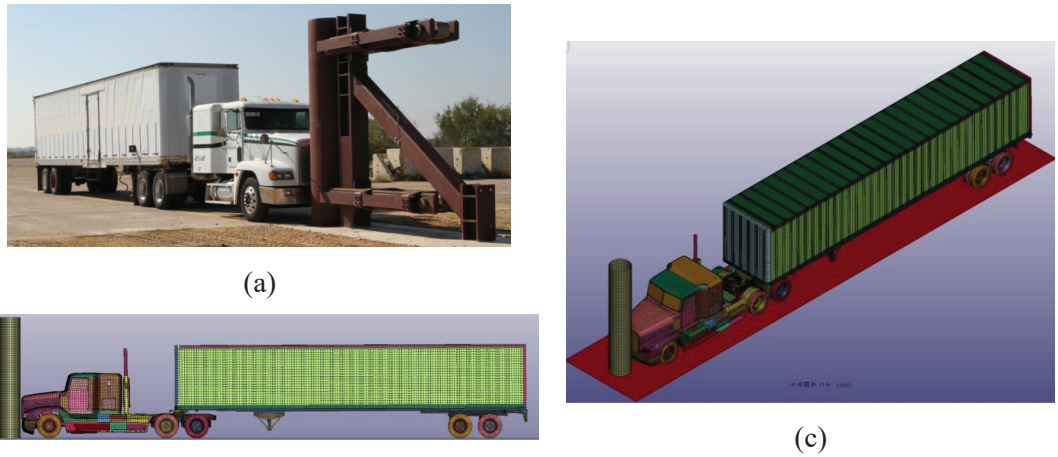

(a)

(b)

(c)

Figure 5-1 (a) tractor-trailer used in the full-scale test by Buth et al., (2011); (b) side view of the FE model of tractor-trailer; (c) isometric view of the FE model of tractor-trailer

5.1.3 Comparison of the experiment and FE modelling results

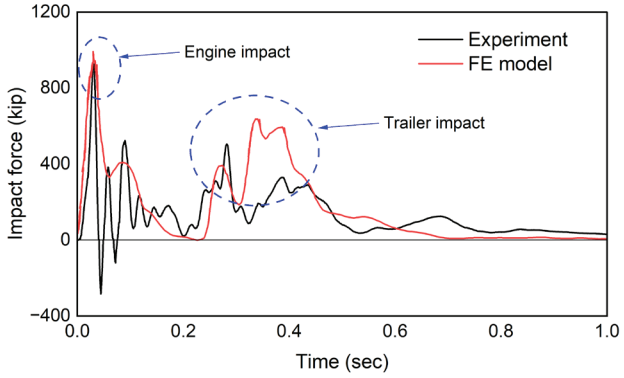

Figure 5-2 Comparison of the impact force–time histories of the experiment and the FE simulation

The comparison between the experimental and FE simulation results are shown in Figure 5-2 and Figure 5-3. As can be seen from Figure 5-2, time histories of the impact force of both the experiment and the FE simulation can be divided into two phases. The first phase was the interaction of tractor frame and engine with the pier, and the simulation results agreed well with the experiment results. The second phase, from 0.23 sec to about 0.50 sec, was the interaction between the trailer and the pier. During this phase, the trailer first interacted with the pier through the crushed cab of the tractor, corresponding to the peak at about 0.26 sec, then the tractor failed structurally and the trailer interacted more directly with the pier, causing the peak at about 0.38 sec. The differences between the experiment and simulation results at this phase could be explained by the complexity of cargo, which was difficult to replicate exactly in the FE model. Nevertheless, it could be said that the FE

model was able to simulate the impact of a tractor-trailer on a pier properly in terms of peak values and durations. The crashing sequence comparison of the experiment and FE simulation is displayed in Figure 5-3, and good agreement can be found between the experiment and the simulation. The comparison between the experiment and simulation results confirmed the validity of the FE tractor-trailer model. Therefore, this FE tractor-trailer model will be used for later modeling of vehicle-pier collisions.

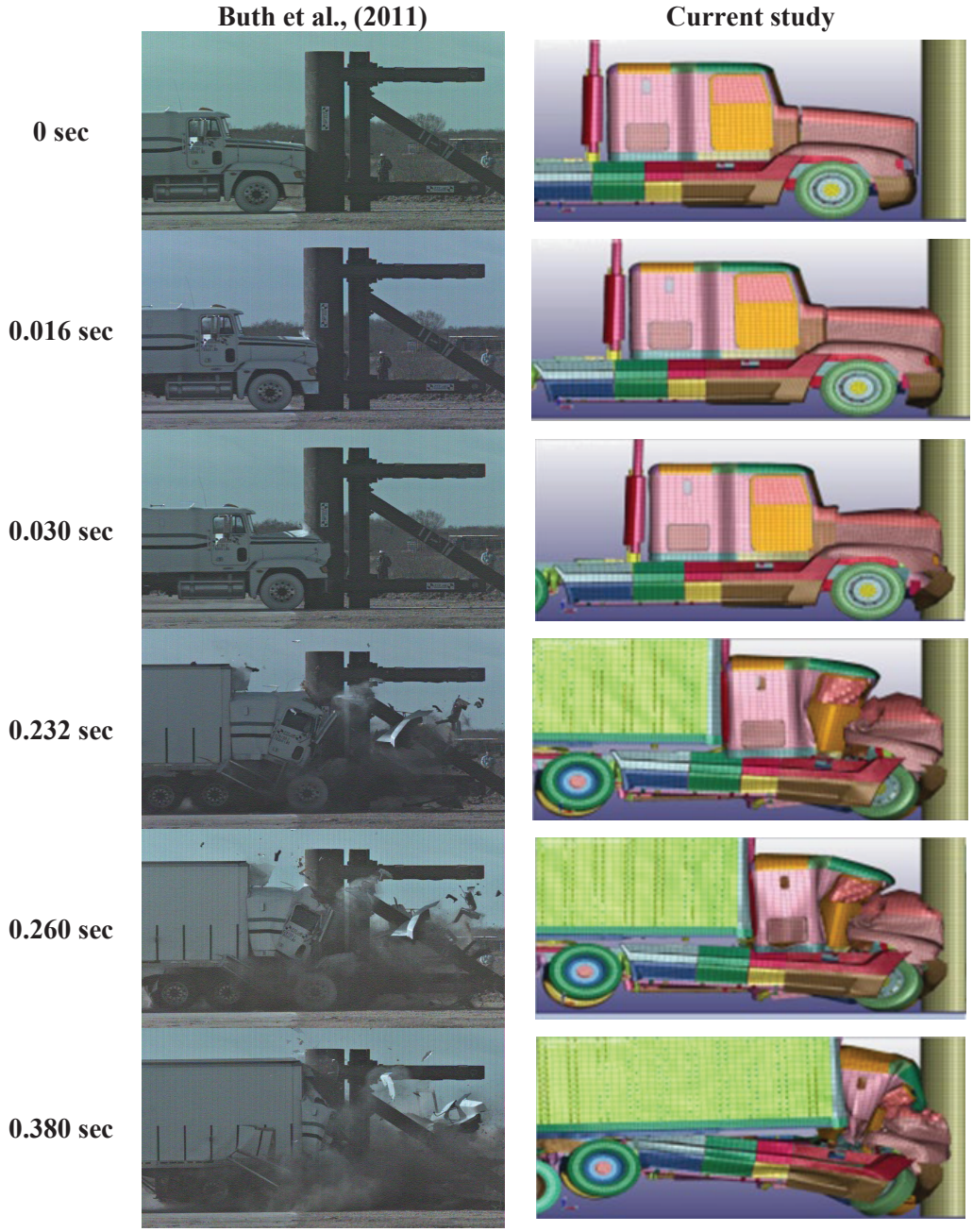

Figure 5-3 Comparison of crashing sequence of the experiment and FE simulation

5.2 Validation of RC Material Models and Modeling Techniques

5.2.1 Low-velocity impact RC beam test

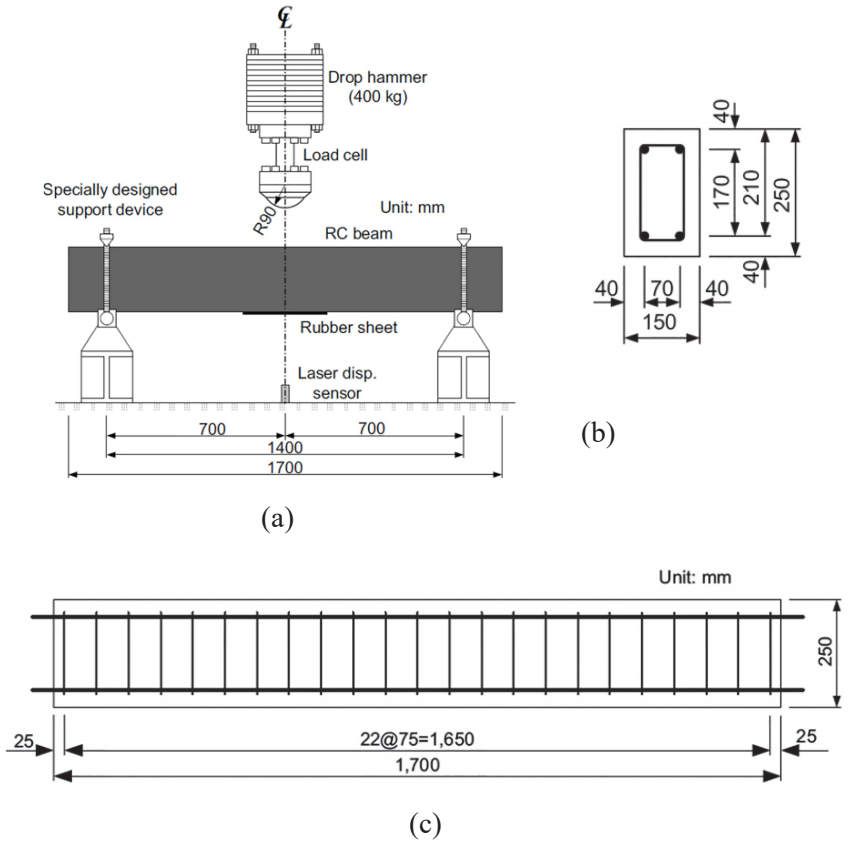

Figure 5-4 Test setup and geometry and rebar detailing of the RC beam specimens: (a) test setup; (b) cross-section view and side view (Fujikake et al., 2009)

During a vehicle collision, the RC piers are subjected to low-velocity lateral impact loading and usually exhibit flexural or shear failure. Therefore, the drop-hammer RC beam test performed by Fujikake et al. (2009) was selected as the modeling experiment. The damage pattern and the time histories of the midspan displacement and impact force were used as the validating data. The beam configuration and the experiment setup are illustrated in Figure 5-4. The beams were 9.84 in. (250 mm) in depth, 5.91 in (150 mm) in width, and 66.93 in (1700 mm) in total length. The distance between the supports, which allowed the beam to rotate freely at the support points while preventing out-of-plane displacement, was 55.12 in (1400 mm). An 881.85 lb (400 kg) hammer was dropped freely onto the top surface of the beam (at midspan) from a height of 2.94 ft (1.2 m). The striking head of the drop hammer had a hemispherical tip with a radius of 3.54 in (90 mm).

5.2.2 FE modelling of drop-hammer RC beam test with LS-DYNA

The continuous surface cap model for concrete, 159-CSCM_CONCRETE, was used to model the behavior of concrete under impact loading. By inputting an unconfined compressive strength of concrete and a maximum aggregate size, this model was able to generate other parameters automatically. For this simulation, the unconfined compressive strength of concrete and the maximum aggregate size were taken from the experiment, which were 6,091.58 psi (42 MPa)

and 0.39 in (10 mm), respectively. The 003-PLASTIC_KINEMATIC model was used to model steel reinforcements. The input yield stresses were 60,625.8 psi (418 MPa) and 42,786.1 psi (295 MPa) for flexural and shear reinforcement, respectively, and these values were also taken from the experiment.

Solid elements were used to model the concrete beam; beam elements were used to model the steel reinforcements; and rigid shell elements were used to model the support and drop hammer. The bond between the steel reinforcement and concrete elements was modelled using a constraint-based coupling feature LAGRANGE_IN_SOLID in LS-DYNA. This feature provides a constraint-based coupling between steel reinforcement and concrete, enabling the steel reinforcement beam elements to move with Lagrangian concrete solid elements. Unlike traditional node-haring methods, this keyword allows the concrete and steel reinforcement elements to be meshed independently. The contact between the drop hammer and concrete beam and the contact between concrete beam and supports were modeled by the AUTOMATIC_SURFACE_TO_SURFACE contact type.

5.2.3 Comparison of the experiment and FE modelling results

The comparison between FE modelling results and experiment results is shown in Figure 5-5. As can be seen from Figure 5-5(b) and (c), the damage pattern (effective plastic strain) from the FE analysis agrees well with the experiment; both are characterized by crushing at the loading point and multiple flexural and shear cracks. There are some differences between the displacement and impact force responses of FE modelling and experimental results, as shown in Figure 5-5(d) and (e); this could be caused by not considering the bond-slip relations between concrete and steel and the confinement of stirrups on concrete. Nevertheless, the peak values and impact durations agree well, so it can be said that the FE model is able to properly simulate the behavior of RC beams under lateral impact loading. Therefore, these material models, element types, and constraining types between steel reinforcements and concrete will be used for modelling bridge piers under vehicle collision.

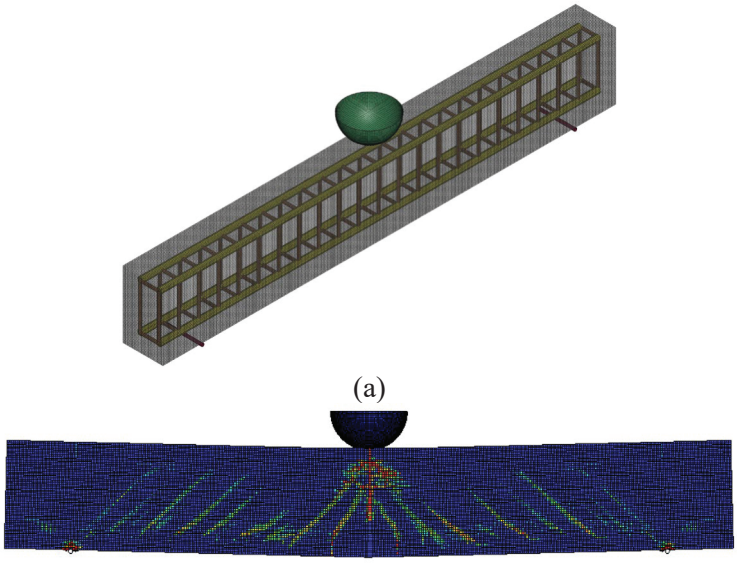

(a)

(b)

Figure 5-5 FE modelling results of the drop-hammer beam test: (a) overview of the FE model; (b) concrete damage pattern of the FE model

(c)

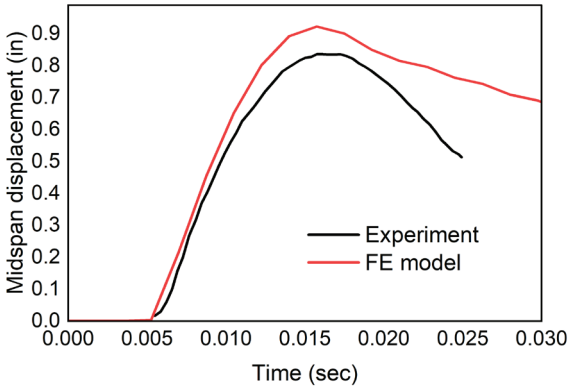

(d)

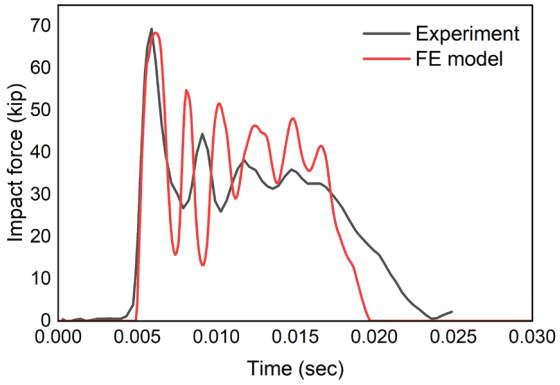

(e)

Figure 5-5 FE modelling results of the drop-hammer beam test: (c) concrete damage pattern of the test by Fujikake et al. (2009); (d) time histories of the midspan displacement; (e) impact force histories

5.3 Calibration of UHPC Model

5.3.1. MAT159: continuous surface cap model

Continuous surface cap model (CSCM) has been proved to be suitable for simulating the behavior of concrete under low velocity impact loading. Considering the similar mechanical properties of UHPC and concrete, some studies (Guo et al., 2018; Jia et al., 2021) extended the CSCM into simulating UHPC. In CSCM, the failure criterion is defined by the failure and hardening surface, which is a function of three stress invariants and the cap hardening parameter R, as shown in Figure 5-6. In the tensile and low confining pressure region, the concrete strength is governed by the shear surface. For greater confining pressure, isotropic hardening cap is included.

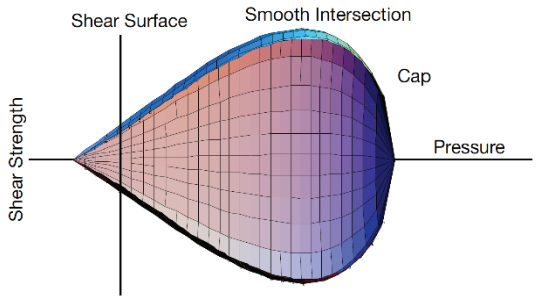

Figure 5-6 CSCM failure surface (Murray, 2007)

For concrete with strength ranging from 2.9-8.4 ksi (20-58 MPa), LS-DYNA provides the option (MAT_CSCM_Concrete) for generating all parameters automatically based on two inputs: uniaxial compressive strength and maximum aggregate size. For UHPC, these parameters need to be calibrated and input manually. There are a total of 44 parameters, as listed in Table 5-1, which account for the failure and hardening surface, strain-softening behavior, modulus reduction due to damage, and strain rate effect.

In the elastic domain, the material response is governed by Hooke's Law, which depends on two constants: the bulk modulus *K* and the shear modulus *G*. According to the linear elasticity theory, these two constants can be calculated as:

$$K = \frac{E}{3(1-2\nu)} \quad (5\text{-}1)$$

$$G = \frac{E}{2(1+\nu)} \quad (5\text{-}2)$$

where *E* is the elastic modulus and it can be estimated based on the uniaxial compressive strength of UHPC f_c': $E = 3837{f_c'}^{0.5}$ (in MPa) (Graybeal, 2006). *v* is the Poisson's ratio of UHPC and can be taken as 0.2 for this study (Russell et al., 2013).

To determine the yield surface, Guo et al. (2018) derived a series of equations using regression analysis based on the test data of Williams et al. (2009). These equations are as follows:

$$\alpha = -2.381 \times 10^{-5} f_c'^2 + 0.8064 f_c' + 21.78 \text{ (MPa)} \quad (5\text{-}3)$$

$$\lambda = 8.333 \times 10^{-5} f_c'^2 + 0.7168 f_c' + 18.8 \text{ (MPa)} \quad (5\text{-}4)$$

$$\beta = 5.381 \times 10^{-8} f_c'^2 - 3.187 \times 10^{-5} f_c' + 6.926 \times 10^{-3} \text{ (Mpa}^{-1}\text{)} \quad (5\text{-}5)$$

$$\theta = -2.381 \times 10^{-7} f_c'^2 + 1.357 \times 10^{-4} f_c' + 0.1306 \text{ (MPa)} \quad (5\text{-}6)$$

$$\alpha_1 = 1, \lambda_1 = 0.4226, \theta_1 = 0 \quad (5\text{-}7)$$

$$\alpha_2 = 1, \lambda_2 = 0.5, \theta_2 = 0 \quad (5\text{-}8)$$

$$\beta_1 = \beta_2 = 4.689 \times 10^{-8} f_c'^2 - 2.258 \times 10^{-5} f_c' + 3.476 \times 10^{-3} \text{ (Mpa}^{-1}\text{)} \quad (5\text{-}9)$$

$$X_D = 0.0204 f_c'^2 - 1.232 f_c' + 104.87 \text{ (MPa)} \quad (5\text{-}10)$$

$$R = (X_D - f_c')/(f_c'/\sqrt{3}) \quad (5\text{-}11)$$

$$W = 4.257 \times 10^{-3} \quad (5\text{-}12)$$

$$D_1 = 2.825 \times 10^{-10} \text{ (MPa}^{-1}\text{)} \quad (5\text{-}13)$$

$$D_2 = 3.352 \times 10^{-6} \text{ (MPa}^{-2}\text{)} \quad (5\text{-}14)$$

In CSCM, a viscoplastic formulation is implemented to the yield surface to model the strength increase with increasing strain rate. Fujikake et al. (2002) and Fujikake et al. (2006) investigated the rate effects of UHPC under direct tension and compression with experiments. Based on these tests results, Guo et al. (2018) proposed the following equations to calculate the input parameters for rate effects in CSCM:

$$\eta_{0t} = 0.7912 f_t'/E \quad (5\text{-}15)$$

$$N_t = 0.7087 \quad (5\text{-}16)$$

$$\eta_{0c} = 1.311 f_c'/E \quad (5\text{-}17)$$

$$N_c = 0.7817 \quad (5\text{-}18)$$

where f_t' is the uniaxial tensile strength of UHPC, and can be estimated as $f_t' = 8.3{f_c'}^{0.5}/\sqrt{145}$ (MPa) (Graybeal, 2006).

With equations(5-1)-(5-18), the elastic constants, input parameters for yield surface, and input parameters for rate effects can be determined based wholly on f_c'. An example of this for UHPC with a compressive strength of 18.9 ksi (130 MPa) is listed in Table 5-1. Parameters related to damage formulation, including ductile shape softening parameter *B*, duction softening parameter *D*, fracture energy in compression G_{fc}, tension G_{ft}, and shear G_{fs} can be calibrated based on material tests under static loading. The calibration process and the validation of this model was discussed in section 5.3.2.

Table 5-1 CSCM for UHPC with a compressive strength of 18.9 ksi (130 MPa)

Parameter	**Description**	**Value**
G (MPa)	Shear modulus	1.823E+4
K (MPa)	Bulk modulus	2.431E+4
α (MPa)	Tri-axial compression surface constant term	1.262E+2
θ	Tri-axial compression surface linear term	0.1267
λ (MPa)	Tri-axial compression surface nonlinear term	1.134E+2
β (MPa^{-1})	Tri-axial compression surface exponent	3.692E-3
N_H	Kinematic hardening initiation	1 (default)
C_H	Kinematic hardening rate	0 (default)
α_1	Torsion surface constant term	1
θ_1	Torsion surface linear term	0
λ_1	Torsion surface nonlinear term	0.4226
β_1 (MPa^{-1})	Torsion surface exponent	1.333E-3
α_2	Tri-axial extension surface constant term	1
θ_2	Tri-axial extension surface linear term	0
λ_2	Tri-axial extension surface nonlinear term	0.5
β_2 (MPa^{-1})	Tri-axial extension surface exponent	1.333E-3
R	Cap aspect ratio	2.125
X_D (MPa)	Cap initial location	2.895E+2
W	Maximum plastic volume compaction	4.257E-3
D_1 (MPa^{-1})	Linear shape parameter	2.825E-10
D_2 (MPa^{-2})	Quadratic shape parameter	3.352E-6
B	Ductile shape softening parameter	1E+2 (default)
G_{fc} (MPa*mm)	Fracture energy in uniaxial stress	20
D	Brittle shape softening parameter	3000

Table 5-1 CSCM for UHPC with a compressive strength of 18.9 ksi (130 MPa)

Parameter	Description	Value
G_{ft} (MPa*mm)	Fracture energy in uniaxial tension	5
G_{fs} (MPa*mm)	Fracture energy in pure shear stress	5
PWRC	Shear-to-compression transition parameter	5 (default)
PWRT	Shear-to-tension transition parameter	1 (default)
PMOD	Modify moderate pressure softening parameter	0 (default)
η_{0c}	Rate effects parameter for uniaxial compressive stress	3.896E-3
N_c	Rate effects power for uniaxial compressive stress	0.7817
η_{0t}	Rate effects parameter for uniaxial tensile stress	1.421E-4
N_t	Rate effects power for uniaxial tensile stress	0.7807
OVERC (MPa)	Maximum overstress allowed in compression	0 (default)
OVERT (MPa)	Maximum overstress allowed in tension	8
SRATE	Ratio of effective shear stress to tensile stress fluidity parameters	1 (default)
REPOW	Power which increases fracture energy with rate effects	1 (default)
ρ (kg/m^3)	Mass density	2.6E+3
INCRE	Maximum strain increment for subincrementation	0
IRATE	Rate effects options	1
ERODE	Control the erosion of elements	0
RECOV	Control the recovery of elastic modulus	0 (default)
ITRETRC	Cap retraction option	0 (default)
PRED	Pre-existing damage	0

5.3.2. Calibration of CSCM for UHPC

The four-point bending test on a UHPC prism conducted by Wei et al. (2021) was chosen to calibrate the UHPC model. The test setup and specimen details are displayed in Figure 5-7(a). The UHPC used in the test has a compressive strength of 130 MPa (18.9 ksi). The UHPC prism has a cross-section of 3.9 in × 3.9 in (100 mm × 100 mm) and a length of 15.7 in (400 mm). Load was applied through a hydraulic machine in two stages: first, it was controlled by force up to 2.2 kip (10 kN); then, it was controlled by deflection up to failure. The corresponding FE model in LS-DYNA is displayed in Figure 5-7(b). UHPC was modeled with constant stress solid elements with a mesh size of 0.2 in (5 mm). Support and loading rods are modeled with Belytschko-Tsay shell elements using rigid material. The bottom support rods are fixed (constrained from rotation and displacement), while for the top loading rods, only vertical displacement was allowed. The contact between rods and UHPC beam was achieved by Automatic_surface_to_surface contact type with a coefficient of friction of 0.4. By default, LS-DYNA employs an explicit solver, which is not suitable for static loading. For this simulation, the implicit solver was activated.

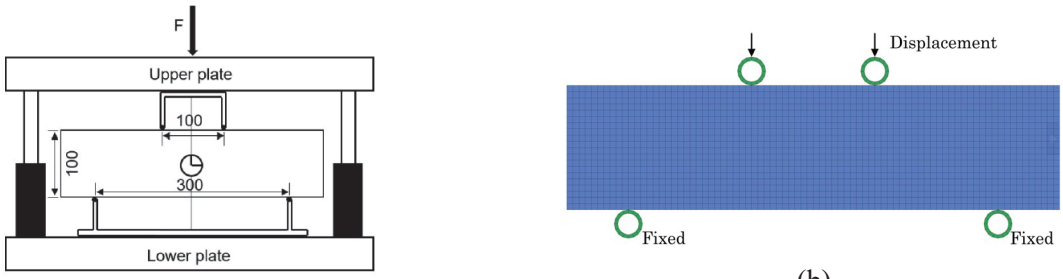

(a) (b)

Figure 5-7 Four-point bending test: (a) test by Wei et al. (2021); (b) FE model

There are five parameters that need to be calibrated: B, D, G_{fc}, G_{ft}, and G_{fs}. Parameter B affects the compression softening behavior after the maximum compressive strength, but it has a limited influence on the behavior of structures. Therefore, the default value recommended by the model developer (Murray, 2007) was adopted. Additionally, following the recommendation of the model developer (Murray, 2007), G_{fs} is set equal to G_{ft}. The model was then calibrated by adjusting the values for D, G_{fc}, and G_{ft}. To further facilitate the calibration process, the value of G_{fc} is assumed to be four times the value of G_{ft}, which is similar to the assumption made by Wei et al. (2023). After multiple trials, it was found that a D value of 3000 and a G_{ft} value of 5 produced the closest result to the test result, as shown in Figure 5-8. The corresponding G_{fc} value was 20 and G_{fs} value was 5.

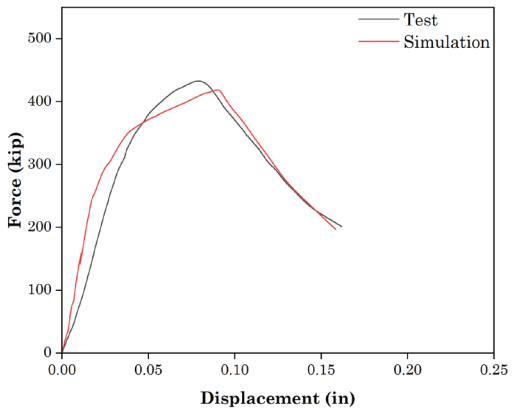

Figure 5-8 Four-point bending test results

5.3.3 Validation of UHPC material model

To check the validity of the UHPC model, the drop hammer impact test on a UHPC beam from the same study by Wei et al. (2021) was simulated. The test setup and specimen details are shown in Figure 5-9. The total mass of the drop hammer system was 1,412 lb (641 kg), and the indenter was sphere-shaped with a radius of 3.9 in (100 mm). The drop hammer was released from a height of 1.1 ft (1 m) above the beam, producing an impact speed of 4.8 ft/s (4.43 m/s). Specimen L1.5S-a was selected as it had a UHPC compressive strength of 18.9 ksi (130 MPa), which was from the same batch as that used in the four-point bending test.

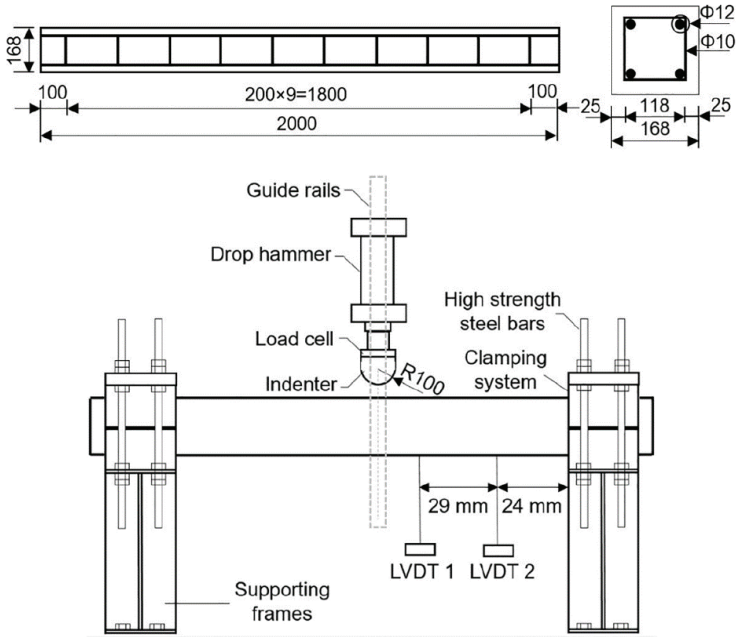

Figure 5-9 Drop hammer test setup and specimen details (unit: mm) (Wei et al., 2021)

The FE model corresponding to the drop hammer impact test on the UHPC beam is presented in Figure 5-10. Constant stress solid elements with a mesh size of 0.2 in (5 mm) were used to model the UHPC beam. The material model for UHPC is specified in Table 5-1. For modeling the longitudinal reinforcement, Hughes-Liu beam elements were used, and the MAT_Plastic_Kinematic model was employed with input parameters listed in Table 5-2. The yield strength and elastic modulus were the same as reported in the actual test, while the strain rate parameters *SRC* and *SRP* were adopted from studies by Guo et al. (2018) and Fan et al., (2019), which specifically dealt with low-velocity impact loading. The drop hammer and the support were modelled with constant stress solid elements using elastic material with a modulus of 2902.8 ksi (20,000 MPa). In the actual test, the specimen was placed on clamping devices to achieve a fully fixed boundary condition. The clamping devices were positioned on fixed steel girders at the bottom and were secured at top by steel plates connected to the bottom steel girders through steel bars. In the FE model, supports with the same dimension were created, and the Automatic_surface_to_surface contact type with a coefficient of friction of 0.4 was used to define the contact between UHPC beam and supports. The interaction between UHPC and steel reinforcement is modelled with Lagrange_in_solid constraint, which constrains the beam elements (steel reinforcement) to move with solid elements (UHPC) at the same velocity and acceleration. The hammer-beam contact and beam-support contact are modelled with the Automatic_surface_to_surface contact type, which is a common treatment in impact simulations (Guo et al., 2018; Fan et al., 2019; Gholipour et al., 2022).

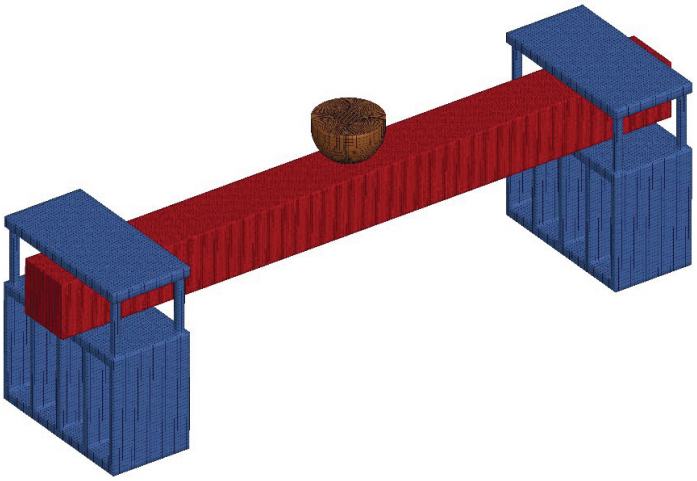

Figure 5-10 FE model of drop hammer impact test

Table 5-2 Input parameters for steel reinforcement material model

Parameter	Description	Value
ρ (kg/m^3)	Mass density	7.8E+3
E (MPa)	Young's modulus	2E+5
ν	Poisson's ratio	0.3
σ_y (MPa)	Yield stress	500 for longitudinal bars 300 for stirrups
SRC (ms^{-1})	Strain rate parameter C for the Cowper Symonds strain rate model.	7.274E+7
SRP	Strain rate parameter P for the Cowper Symonds strain rate model.	11.2
FS	Effective plastic strain for eroding elements	0.25

The comparison of the impact histories and deflection histories of the test and simulation results is displayed in Figure 5-11. The maximum impact force from the simulation is 137.1 kip (610 kN), which is 93% of that from the test. The maximum deflection from the test is 1.7 in (43 mm), which is about 96% of that from the test. It can be said that the model can reasonably predict the peak impact and deflection of the UHPC beam. The simulation results showed a shorter impact duration than that of the test, and the residual deflection from the simulation is slightly larger than the test results. These may be due to the Lagrange_in_solid constraint used to model the interaction between steel bars and UHPC, which is not identical to the actual bond-slip relations between steel bars and UHPC and consequently affects the post-peak dynamic response of reinforced UHPC beams. It may also be caused by the inaccuracies in the material model, as some parameters were determined without comprehensive material testing. Nevertheless, for the response that this study cares about the most, which is the ultimate strength of the UHPC structure under impact loading, the model gives a satisfactory prediction.

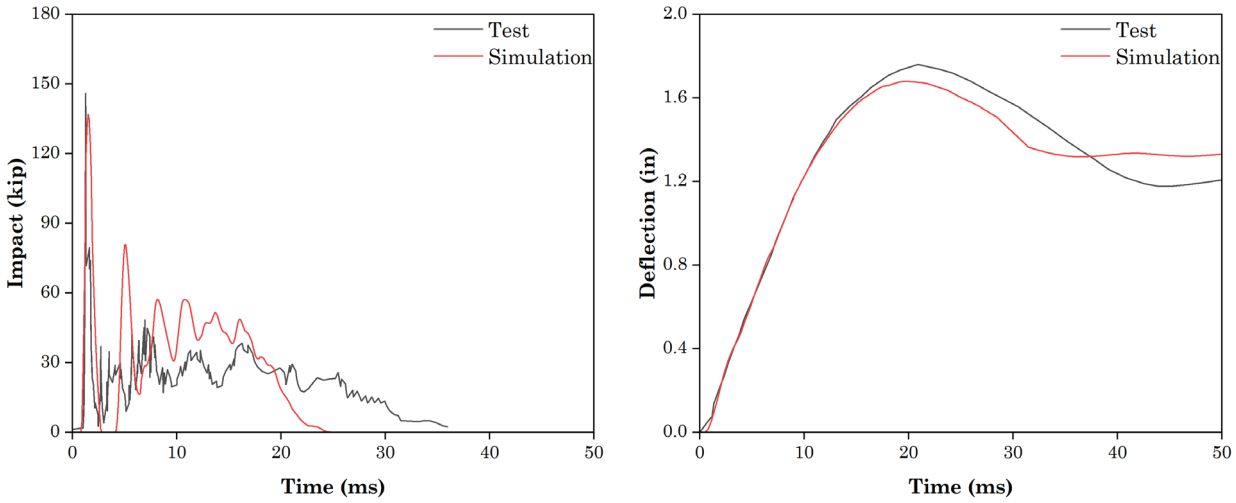

(a) (b)

Figure 5-11 Drop hammer impact test results: (a) Impact histories; (b) Deflection histories

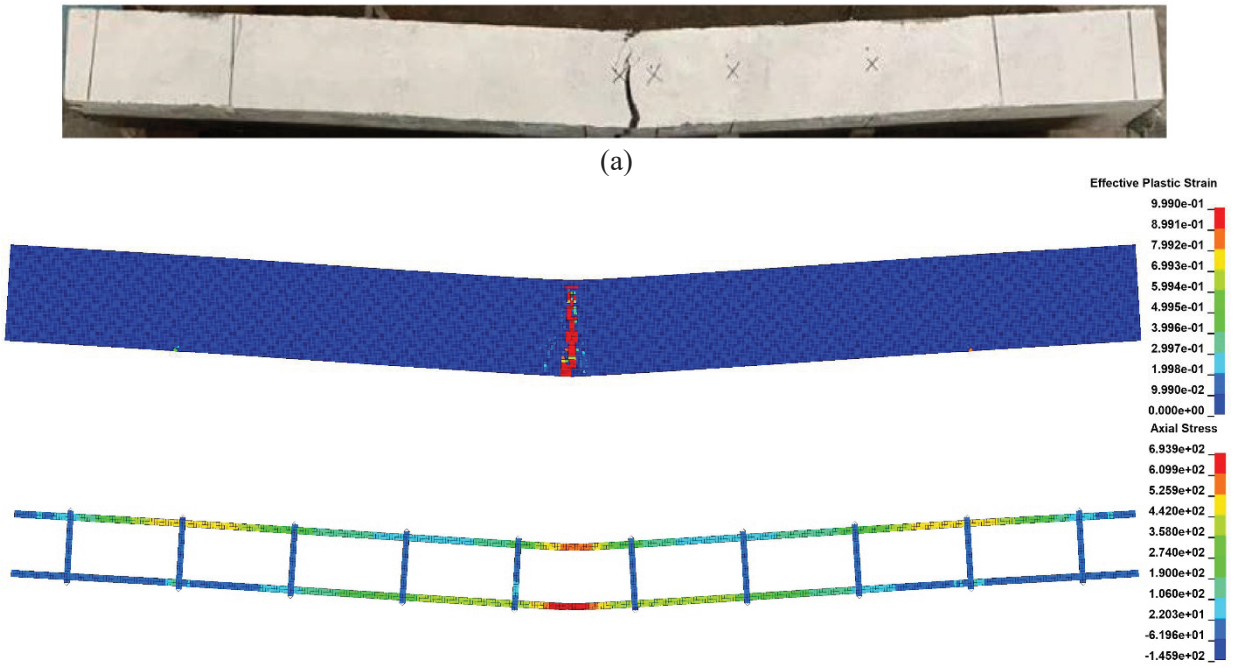

(a)

(b)

Figure 5-12 Damage patterns after the test: (a) test by Wei et al. (2021); (b) FE simulation (unit: MPa)

Figure 5-12 presents a comparison of the damage patterns between the simulation and experimental results. The simulation produced the same damage pattern as observed in the test, characterized by a flexural crack at the impact section. The axial stress of steel reinforcement from the simulation shows that yielding of steel reinforcement occurred at the cracked section, and the stress distribution and deformed shape of steel reinforcement are consistent with loading setup of the beam. These confirm that the steel reinforcement was developed and the Lagrange_in_solid constraint was effective. Based on these comparisons, it can be said that the overall simulation results agree well with the test results, and the calibrated UHPC material model is able to predict the UHPC behavior under impact loading.

5.4 Calibration of FRP Model

5.4.1 MAT54: enhanced composite damage model

MAT54 is a built-in material model in LS-DYNA designed specifically for orthotropic materials, such as FRP. It has been successfully used in impact simulations (Heimbs et al., 2009; Ma et al., 2019). In this model, the material is linearly elastic until the failure surface is reached. Upon reaching the failure surface, the material becomes damaged, and the elastic properties in the failure direction are set to zero. The failure surface is determined by the Chang-Chang failure criteria (Chang et al., 1987), which includes the following types of failure modes:

Tensile failure in longitudinal direction,

$$e_f^2 = (\sigma_{aa}/X_t)^2 + \beta(\sigma_{ab}/S_c)^2 - 1, \quad \begin{matrix} e_f^2 \geq 0 \Rightarrow failed \\ e_f^2 \leq 0 \Rightarrow elastic \end{matrix} \quad (5\text{-}19)$$

Compressive failure in longitudinal direction,

$$e_f^2 = (\sigma_{aa}/X_c)^2 - 1, \quad \begin{matrix} e_f^2 \geq 0 \Rightarrow failed \\ e_f^2 \leq 0 \Rightarrow elastic \end{matrix} \quad (5\text{-}20)$$

Tensile failure in transverse direction,

$$e_f^2 = (\sigma_{aa}/Y_t)^2 + \beta(\sigma_{ab}/S_c)^2 - 1, \quad \begin{matrix} e_f^2 \geq 0 \Rightarrow failed \\ e_f^2 \leq 0 \Rightarrow elastic \end{matrix} \quad (5\text{-}21)$$

Compressive failure in transverse direction,

$$e_f^2 = (\sigma_{aa}/Y_c)^2 - 1, \quad \begin{matrix} e_f^2 \geq 0 \Rightarrow failed \\ e_f^2 \leq 0 \Rightarrow elastic \end{matrix} \quad (5\text{-}22)$$

Matrix shear failure,

$$e_m^2 = (\sigma_{ab}/S_c)^2 - 1, \quad \begin{matrix} e_m^2 \geq 0 \Rightarrow failed \\ e_m^2 \leq 0 \Rightarrow elastic \end{matrix} \quad (5\text{-}23)$$

where Xt and Yt are the tensile strengths of the composite in longitudinal and transverse directions, respectively, and Xc and Yc are the compressive strengths in longitudinal and transverse directions, respectively. Sc is the matrix shear strength. β is the weighting factor for shear in tensile failure mode. Xt, Yt, Xc, Yc and Sc can be obtained through material tests, whereas β can only be determined by trial and error.

5.4.2 Validation using lateral impact tests

To validate the use of MAT54 for modelling FRP, the lateral impact tests on FRP-strengthened circular RC columns performed by Xu et al. (2020) are modelled. The test setup and specimen details are shown in Figure 5-13. The steel impact truck has a total mass of 3848 lb (1582 kg), including a flat rectangular hammer at the front. The truck is connected to a drop mass through a steel wire. By releasing the drop mass, the truck will accelerate and collide with the column at a height of 15.7 in (400 mm) from the ground. By adjusting the weight and releasing height of the drop mass, the impact speed can be adjusted.

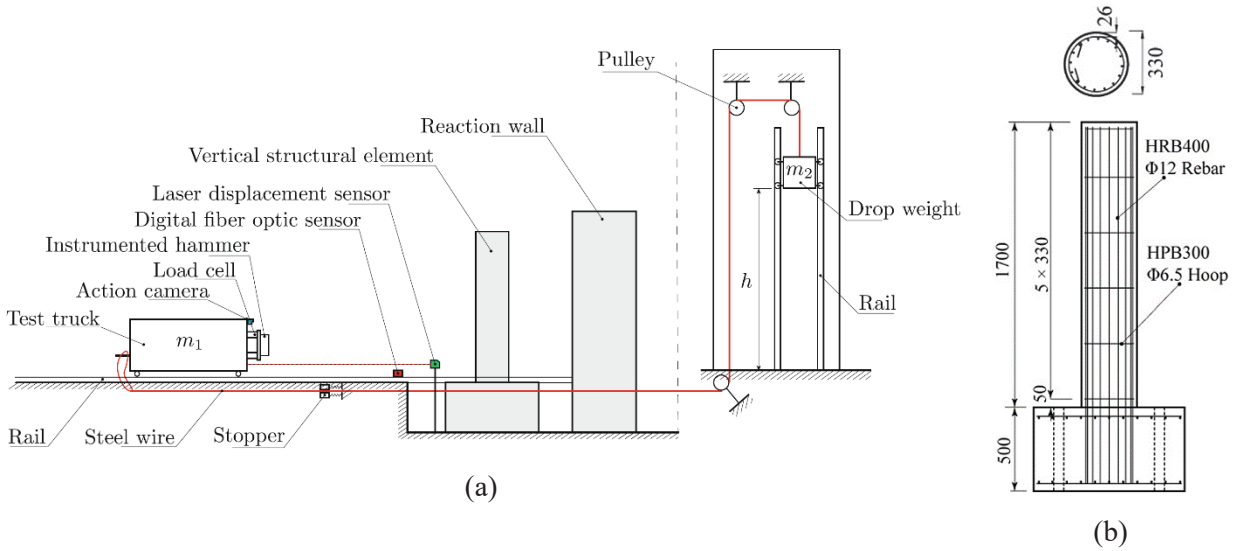

Figure 5-13 (a) Lateral impact test setup; (b) specimen details (unit: mm) (Xu et al., 2020)

Among the six specimens tested by Xu et al. (2020), two were selected for analysis: specimen C3H0, a reference RC column, and specimen C3H2, which is strengthened with FRP wraps. The impact speed for both specimens is 15.1 ft/s (4.6 m/s). Both specimens have a diameter of 13 in (330 mm) and a height of 66.9 in (1700 mm). The longitudinal reinforcement comprises 16 steel bars with a diameter of 0.47 in (12 mm) and a yield strength of 68.3 ksi (471 MPa). For the transverse reinforcement, 0.26-in (6.5-mm) diameter steel ties at a spacing of 13 in (330 mm) were used, with a yield strength of 61.9 ksi (427 MPa). The concrete strength is 4.4 ksi (30 MPa) for C3H0 and 4.6 ksi (32 MPa) for C3H2. C3H2 is strengthened with 2 layers of woven-based FRP fabric up to a height of 35.4 in (900 mm) from the bottom. The FRP material properties are given in Table 5-3.

Table 5-3 FRP material properties (Nanjing Hitech Composites 2021)

Area density (g/m^2)	**Thickness (mm)**	**Tensile strength (MPa)**	**Tensile modulus (MPa)**	**Matrix shear strength (MPa)**	**Shear modulus (MPa)**
296	0.17	3494	240000	20	5240

Table 5-4 Input parameters for FRP material model

Parameter	Description	Value
ρ (kg/m^3)	Mass density	1741
E_a (MPa)	Young' modulus in longitudinal direction	240000
E_b (MPa)	Young's modulus in transverse direction	240000
G_{ab} (MPa)	Shear modulus	5240
X_c (MPa)	Compressive strength in longitudinal direction	2000
X_t (MPa)	Tensile strength in longitudinal direction	3494
Y_c (MPa)	Compressive strength in transverse direction	2000
Y_t (MPa)	Tensile strength in transverse direction	3494
S_c (MPa)	Matrix shear strength	20
β	Weighting factor for shear in tensile failure mode	0

Figure 5-14 shows the FE model of the lateral impact tests. Concrete and the impact truck were modeled with constant stress solid elements. Steel reinforcement was modelled with Hughes-Liu beam elements. FRP was modelled with Belytschko-Tsay shell elements. The material model for concrete was generated using the MAT_CSCM_Concrete option by inputting compressive strength and maximum aggregate size. Elastic material with a modulus of 2900 ksi (20,000 MPa) was used for the truck and the hammer. The input parameters for the FRP material model are listed in Table 5-4. Most of the input values were the same as the material properties in Table 5-3. The compressive strength was not documented in the experimental study, thus it was approximated as 60% of the tensile strength, according to Ueda et al. (2011). It should be noted that FRP wraps primarily bear tensile stress in the circumferential direction, and the compressive strength of FRP has little influence on the response of the structure. Considering the woven-based pattern of the FRP fabric, where the fibers in the longitudinal and transverse directions were close to independent, β was set to 0. Besides the parameters listed in Table 5-4, there are other optional parameters in MAT54 that can be used to define more complex failure behaviors. For instance, a strain-based failure criterion can be established by inputting maximum failure strains in tension and compression. There are also non-physical parameters that characterize the behavior after failure initiation, such as parameters for determining the minimum stress limit after stress maximum, softening factors, and strength reduction factors. These non-physical parameters cannot be determined through material tests; instead, they are usually determined by trial and error. For the purposes of this study, only the parameters in Table 5-4, which define the strength-based Chang-Chang failure criterion, were used as input. The remaining parameters were set to zero by default, so these options were not activated. The material model for steel reinforcement was MAT_Plastic_Kinematic, whose input parameters were taken from the tests and listed in Table 5-5. The interaction between the steel reinforcement and concrete was modeled using the Lagrange_in_solid constraint, and the truck-column contact was modeled using the Automatic_surface_to_surface contact type. The bonding between FRP and concrete was achieved through node sharing. This modeling technique was justified by the observation that no debonding was observed during the impact tests conducted by Xu et al. (2020) and Li et al. (2022b).

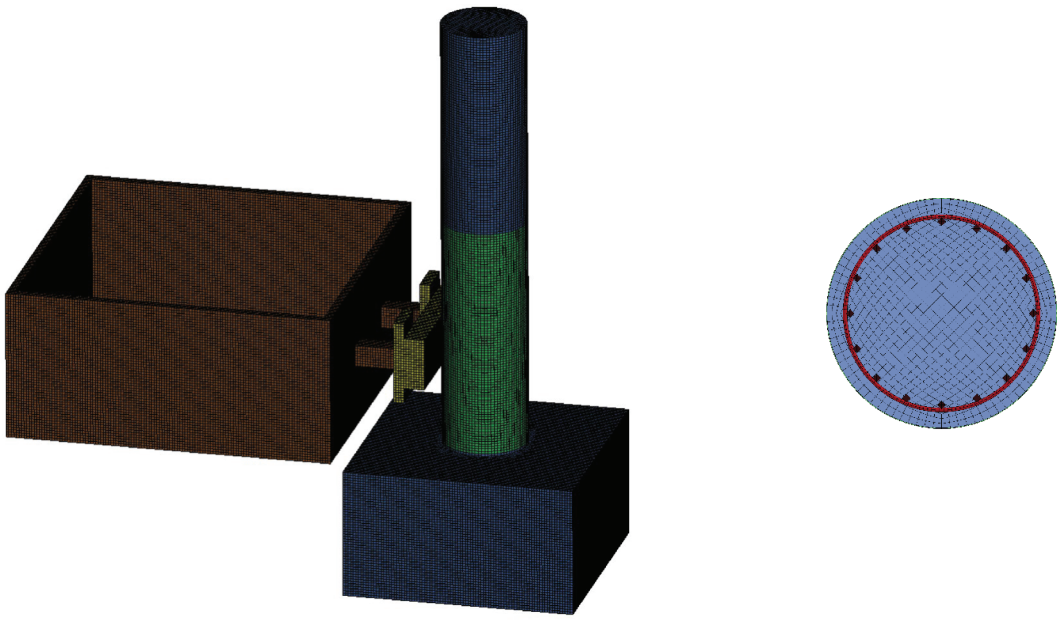

Figure 5-14 FE model of lateral impact tests

Table 5-5 Input parameters for steel reinforcement material model

Parameter	Description	Value (longitudinal)	Value (transverse)
ρ (kg/m^3)	Mass density	7.8E+3	7.8E+3
E (MPa)	Young's modulus	1.94E+5	2.04E+5
ν	Poisson's ratio	0.3	0.3
σ_y (MPa)	Yield stress	471	427
ETAN (MPa)	Tangent modulus	556	224
SRC (ms^{-1})	Strain rate parameter C for the Cowper Symonds strain rate model.	7.274E+7	7.274E+7
SRP	Strain rate parameter P for the Cowper Symonds strain rate model.	11.2	11.2
FS	Effective plastic strain for eroding elements	0.25	0.25

5.4.3 Comparison of FE and experiment results

Figure 5-15 displays the impact histories of FE simulation and experimental results. Generally, there is good agreement between the two. However, some differences between the simulation and experiment responses can be observed after the initial impact peak. These disparities were due to the complexities of dynamic problems, making it impractical to replicate the experiment responses exactly. When comparing the responses of C3H0 and C3H2, it can be found that FRP strengthening did not increase the peak impact force, but it improved the energy dissipation capacity of the column. This can be explained by the damage evolution of these two columns, as depicted in Figure 5-16 and Figure 5-17. In C3H0, the damage primarily concentrated at a single diagonal crack, resulting in shear failure. Whereas in C3H2, the FRP wraps restricted the progression of the shear crack, and damage was distributed over a longer length of section that was strengthened with FRP. As a result, the impact force in C3H2 remained at a higher level for a longer duration after the initial peak, allowing the column to absorb more energy. In contrast to the shear failure of C3H0, C3H2 eventually failed at the base by separating from the ground foundation. These observations from the FE simulation are consistent with those of the experiment. Therefore, it can be said that the calibrated MAT54 material model is able to simulate the response of FRP under impact loading.

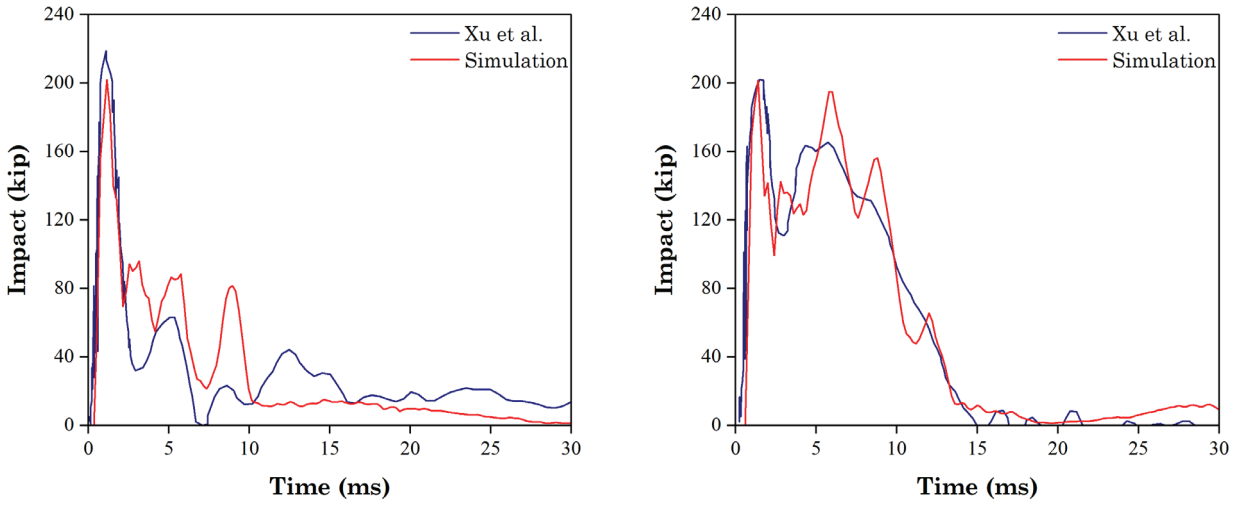

(a) (b)

Figure 5-15 Impact histories: (a) C3H0: RC column; (b) C3H2: strengthened with FRP wraps

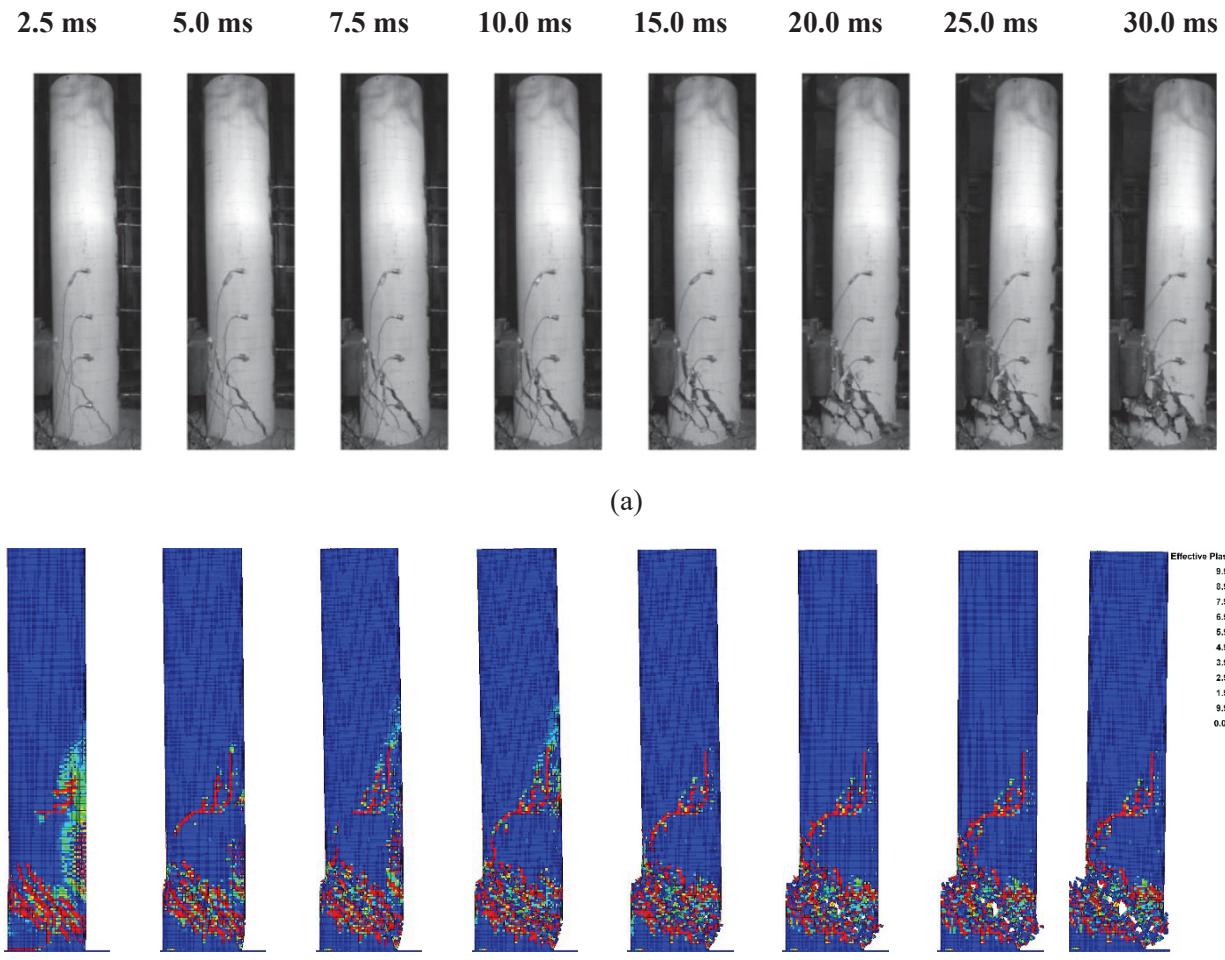

Figure 5-16 Damage evolution of C3H0: (a) test by Xu et al. (2020); (b) FE simulation

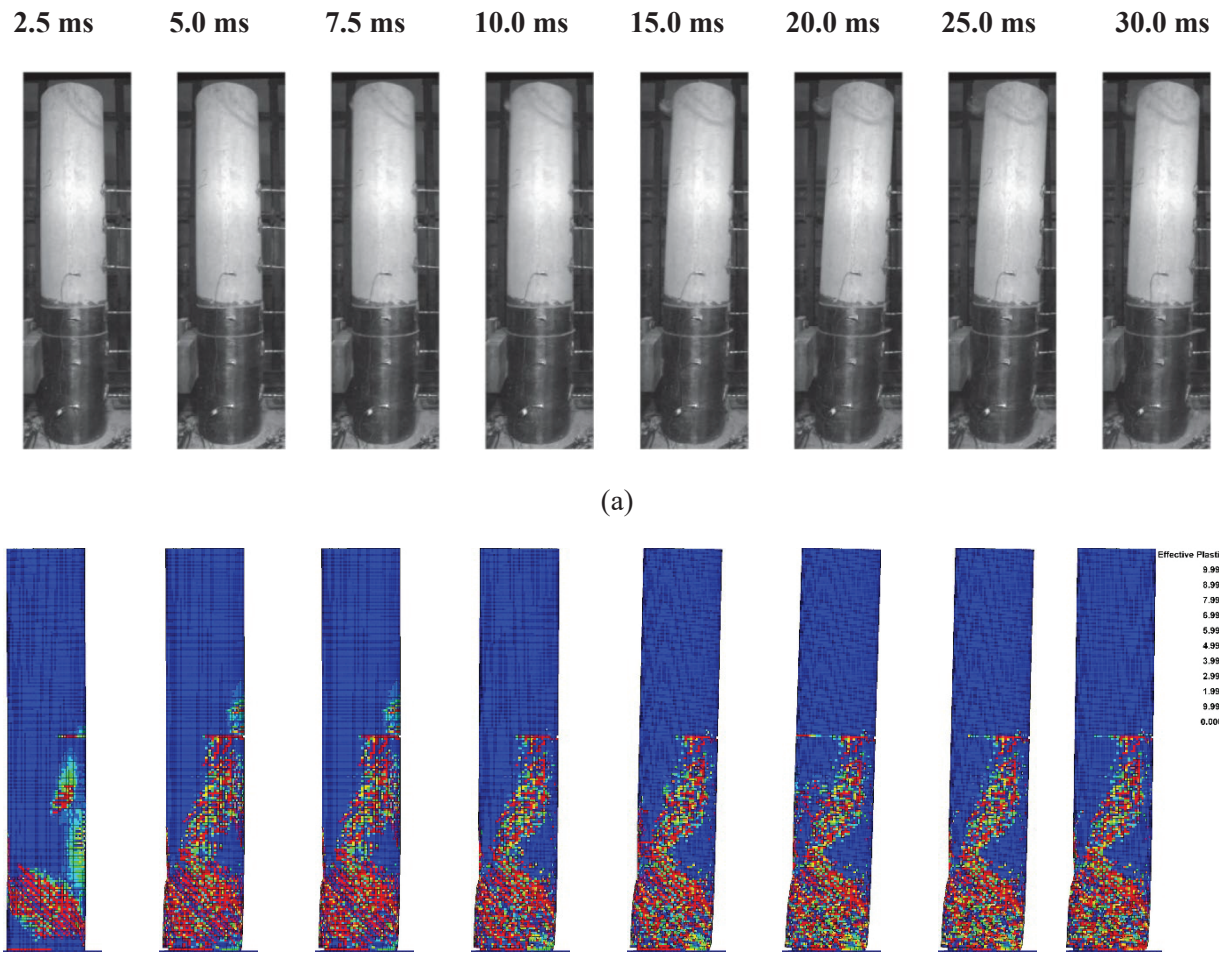

Figure 5-17 Damage evolution of C3H2: (a) test by Xu et al. (2020); (b) FE simulation

CHAPTER 6 FE SIMULATION OF VEHICLE COLLISION WITH PIERS

In the previous chapters, we validated the vehicle FE model and calibrated the material models for concrete, steel bars, UHPC, and FRP. In this chapter, we applied the previously validated models to perform FE analysis of vehicle collisions with piers with different strengthening designs. Besides the analysis matrix presented in chapter 3, we also conducted additional analysis to evaluate the influences of various parameters. Based on the results, the effectiveness of various strengthening methods was evaluated and compared.

6.1 FE Simulation Overview

6.1.1 Analysis matrix

The analysis matrix for all simulations is listed in Table 6-1. While the designs of all RC collar-strengthened piers were the same, we examined four different interface conditions between the existing pier (the baseline pier inside the collar in strengthened cases) and the RC collar to understand the effects of interface strength and dowel bars. For UHPC collar-strengthened piers, U-1 followed the design in chapter 4; five other piers were created to investigate the influence of collar thickness, collar height, and collar reinforcement. For FRP wrap strengthening, C-1 corresponded to the design in chapter 4; three other piers were created to investigate the effect of changing FRP wrap thicknesses and height. Details of the models are provided in later sections.

Table 6-1 Summary of analysis matrix

Pier Type	Case	Strength of strengthening material (ksi)	Strengthening details		Model details
			Thickness (in)	Height (in)	
baseline	baseline	-	-	-	-
RC collar-strengthened	RC-1	3.4	7	108	- Perfect bonding
	RC-2				- Interface model and 6-in-spacing dowel bars
	RC-3				- Interface model and 12-in-spacing dowel bars
	RC-4				- Interface model only
UHPC collar-strengthened	U-1	18	5.5	108	- Interface model - Without collar reinforcement
	U-2		5.0	108	
	U-3		5.0	94	
	U-4		5.0	80	
	U-5		4.5	108	
	RU-5			108	- Interface model - With collar reinforcement

Table 6-1 Summary of analysis matrix

Pier Type	Case	Strength of strengthening material (ksi)	Strengthening details		Model details
			Thickness (in)	Height (in)	
FRP wrap strengthened	C-1	598	0.053	108	- Interface model
	C-2			150	
	C-3			192 (full height)	
	C-4		0.1	108	

6.1.2 Collision simulation setup

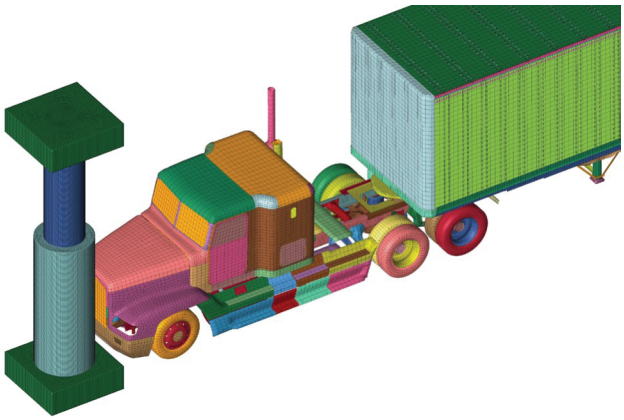

Figure 6-1 Collision simulation setup

The collision simulation setup is depicted in Figure 6-1. The vehicle, a tractor-trailer previously validated in chapter 5, had a weight of 80,000 lb (36,287 kg) and a speed of 48.34 mph (21.6 m/sec). The pier at the bottom was connected to a 20 in × 20 in × 60 in (508 mm × 508 mm × 1524 mm) concrete footing, which was constrained from displacement and rotation at its bottom. At the top, the pier was also connected to a fixed concrete block with the same dimensions as the bottom footing. The axial force caused by the weight of superstructure was not considered in this model. While the study by Liu et al. (2017) showed that axial force had a positive effect on RC columns with relatively small displacement (1.3 in (33 mm), 2.4% of column length) and had a negative effect on RC columns with large displacement (not qualified since the column failed completely), it should be noted that simply applying a constant axial force, as in Liu et al.'s study (2017), is not accurate for representing the axial force caused by the weight of superstructure. This is because the axial force would redistribute among the multiple piers under the same bent during a collision. On the other hand, the study by Abdelkarim and ElGawady (2017) showed that superstructure weight had a negligible effect on the peak impact force during collision. Therefore, a fixed boundary condition at top was adopted as a simplified way to simulate the constraint from pier bent. Similar boundary conditions were adopted by Abdelkarim and ElGawady (2017), Agrawal et al. (2018), and Cao et al. (2019) to study RC piers under vehicle collisions. The centerline of the vehicle was aligned with the centerline of the pier. Contact between the vehicle and piers were defined by the Automatic_surface_to_surface contact type in LS-DYNA, which was used for previous validations.

6.2 Baseline Pier

6.2.1 Modelling details of baseline pier

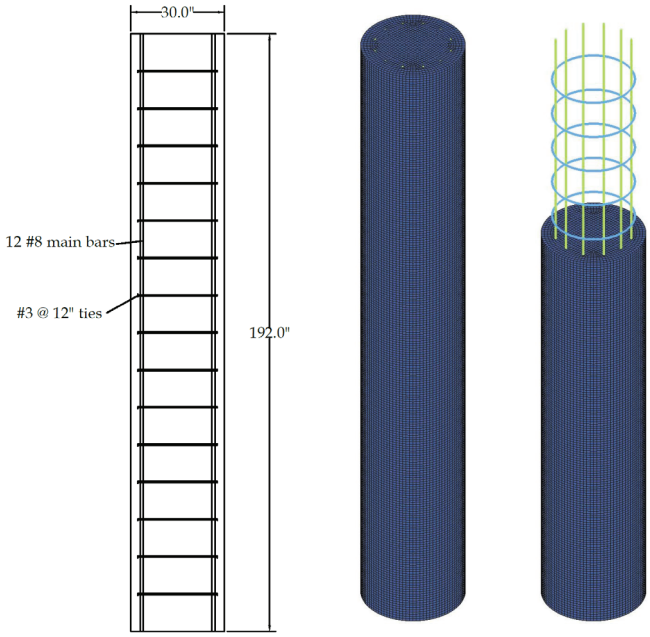

Figure 6-2 Design and FE model of baseline pier

The design and FE model of the baseline pier was created following the design in chapter 4, as shown in Figure 6-2. Concrete was modelled with solid elements, and the material model for concrete was CSCM_Concrete with a compressive strength of 3.4 ksi (23.4 MPa). Steel reinforcement was modelled with beam elements, and the material model was plastic kinematic model with a yield strength of 40 ksi (278 MPa). Consistent with previous validations, the bonding between the steel reinforcement and the concrete pier was modeled using the Lagrange_in_solid constraint type.

6.2.2 Collision simulation results of baseline pier

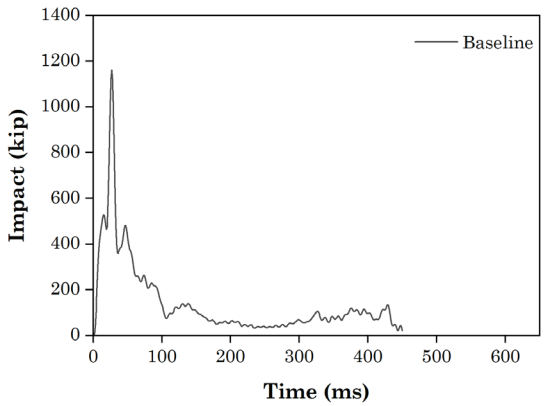

Figure 6-3 Impact history of baseline pier

Figure 6-3 shows the impact history of the baseline pier. The maximum impact force occurred at about 25 ms when the tractor engine reached the pier. The baseline pier failed

completely under the impact of the tractor and the impact resistance dropped nearly to zero. Failure of a pier is defined as the occurrence of uncontrolled deflection, as the pier was not able to stop the vehicle's forward motion, resulting in the deflection to increase continuously, as shown in Figure 6-4(a) and Figure 6-4(b). Although for this case we can easily identify the failure of the pier based on the impact history presented in Figure 6-3, as the impact force during the trailer impact stage was zero; in later sections, we will find that for some piers, uncontrolled deflection occurred, but there was no difference in impact force history compared to that of other piers. This was because these piers failed during the trailer impact stage, consequently, the impact force during the trailer impact stage was not zero.

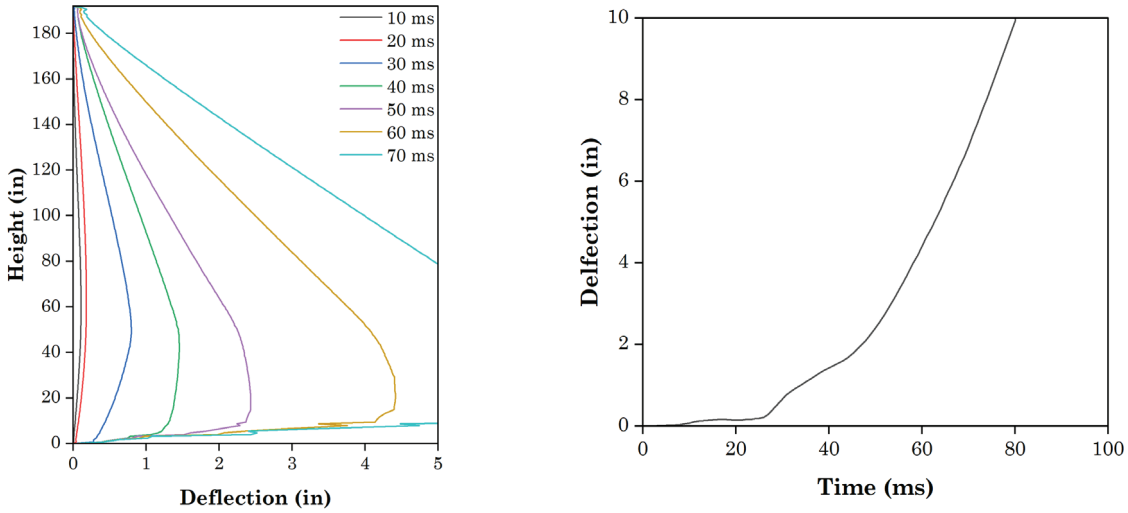

(a) (b)

Figure 6-4 Deflection development of baseline pier: (a) maximum deflection distribution; (b) deflection history at the height of 29 in

The failure process of the baseline pier is displayed in Figure 6-5. The damage here refers to the effective plastic strain, which is a damage index in LS-DYNA that depends on the maximum principle tensile strain and the plastic component of the deformation tensor. It was widely used to represent the damage of materials in the literature. Initially, the damage was mainly concentrated at the rear of the impact point. At 28 ms after the impact of the engine, the damage at the rear intensified, forming a triangular plastic hinge. Further increases in the damage of the plastic hinge could lead to punching shear failure or flexural failure. However, diagonal shear cracks formed first near the bottom and shear failure occurred. And the damage at the upper part of the pier occurred after 40 ms was induced by the uncontrolled deflection at the bottom.

Based on this failure process, it can be seen that the most severe damage observed on bridge piers under heavy tractor-trailer collision primarily occurred below a height of approximately 80 in (2032 mm) in the form of diagonal shear cracks and plastic hinge formation. To enhance the collision resistance of the baseline pier, it is crucial to control these two types of damage. Therefore, the pier should be strengthened up to a height of at least 80 in (2032 mm).

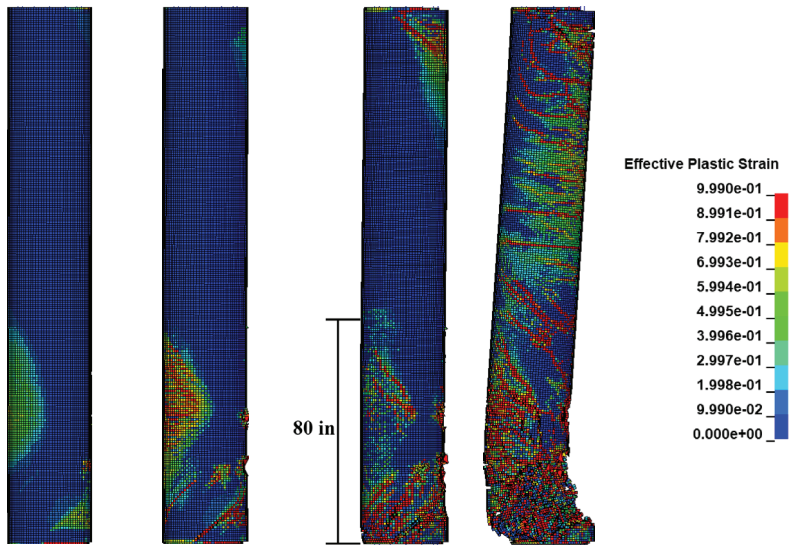

Figure 6-5 Failure process of baseline pier

6.3 RC Collar-strengthened Piers

6.3.1 Modelling details of RC collar-strengthened piers

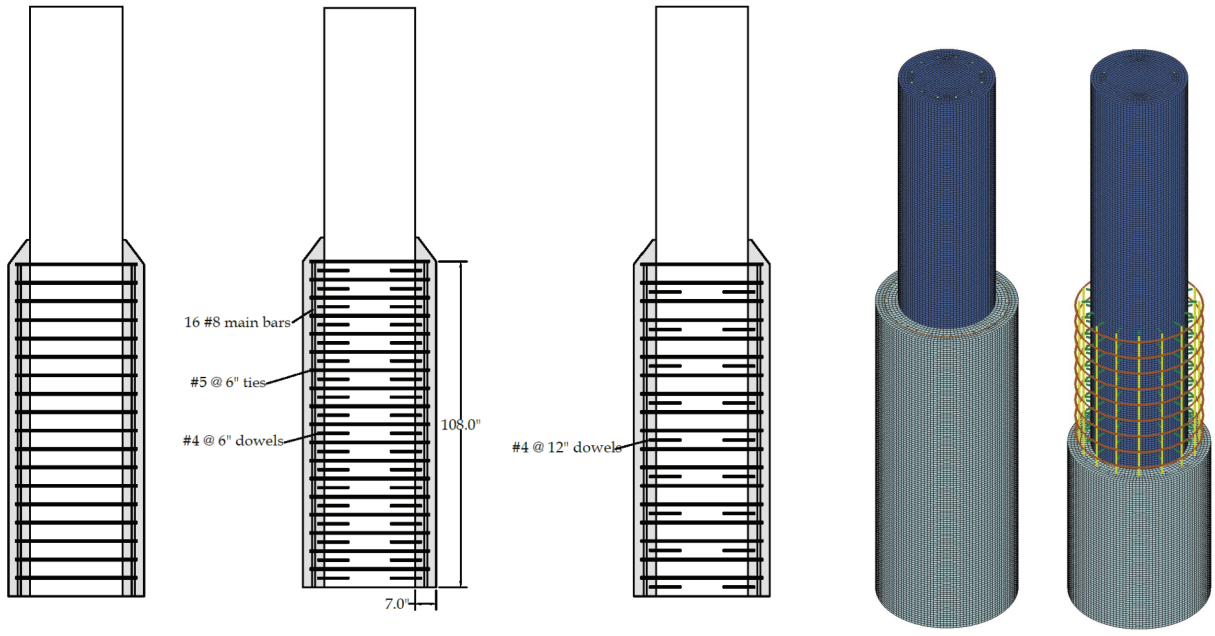

Figure 6-6 Design and FE model of RC collar-strengthened piers

The design and FE model of RC collar-strengthened piers are shown in Figure 6-6. The four cases only differ by interface conditions between the collar and existing pier. The perfect bonding was achieved by node sharing between existing pier and collar, and there were no dowel bars at the interface. For piers with dowel bars at the interface, two configurations were considered: one

adhered to the FDOT Structures Manual (FDOT, 2024) requirement with a spacing of 6 in (152 mm), while the other had a reduced density, with a spacing of 12 in (305 mm). The modelling of the dowel bar was the same as steel reinforcement, which was modelled with beam elements and plastic kinematic material model. And the dowel bars were perfectly bonded with both existing pier and concrete collar through Lagrange_in_solid constraint.

Besides dowel bars, loads could also be transferred across interface between the older concrete and newly cast concrete through adhesive bonding, mechanical interlocking, and friction. Various analytical models have been proposed to describe the failure of this interface. For example, Espeche and Leon (2011) proposed the following failure criterion:

$$\tau \geq ((c - \sigma_n tan\phi)^2 - (c - f_t tan\phi)^2)^{0.5} \quad (6\text{-}1)$$

where τ is the interface shear stress, c is interface cohesion strength, σ_n is the interface normal stress, ϕ is friction angle, and f_t is the splitting tensile strength of the interface.

By applying experimental data and fitting the expression form of Equation (1), Zanotti and Randl (2019) plotted the failure envelopes of concrete with varying strength and steel fiber content, as shown in Figure 6-7. As can be seen, when the normal stress is in tension, the shear strength decreases with increasing tensile stress; when the normal stress is in compression, the shear strength increases with increasing compressive stress. The intersection of the envelope with the σ_n axis corresponds to the tensile strength of the interface, whereas the intersection with τ axis corresponds to the pure shear strength of the interface.

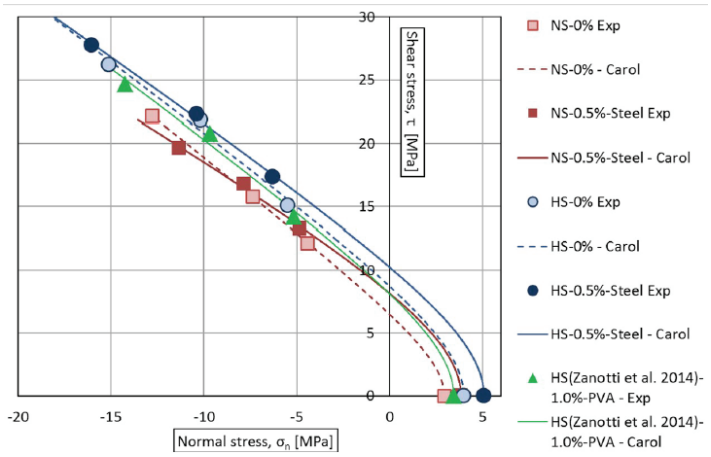

Figure 6-7 Interface failure envelopes by Zanotti and Randl (2019)

Most design codes, e.g., Fib Model Code 2010 (Fib, 2013), adopt a simpler linear model for the interface:

$$\tau \geq c - tan\phi \cdot \sigma_n \quad (6\text{-}2)$$

where σ_n is positive when it is in tension and negative when it is in compression.

For rough interface, e.g. sand blasted, Fib Model Code 2010 (Fib, 2013) provides representative values for c to be 0.22-0.36 ksi (1.5-2.5 MPa), for $tan\phi$ to be 0.7-1.0. For very rough surface, e.g. high pressure water jetted, the representative values of c is 0.36-0.52 ksi (2.5-3.5 MPa), and that for $tan\phi$ is 1.0-1.4. For a concrete surface roughened to an amplitude of 0.25 in (6.35 mm), AASHTO LFRD (AASHTO, 2020a) provides the value for c is 0.24 ksi (1.7 MPa) and for $tan\phi$ is 1. However, AASHTO LRFD (AASHTO, 2020a) explicitly specifies that these values are the lower

bound of experimental data from the literature as this code is primarily for design purposes. In contrast, the Fib Model Code 2010 serves both design and modeling purposes. Therefore, the values provided by the Fib Model Code 2010 are preferred for this study. A value of 0.36 ksi (2.5 MPa) for c and 1.0 for $tan\phi$ is taken. This results in a pure shear strength of the interface of 0.36 ksi (2.5 MPa) (intersection with τ axis) and a tensile strength of 0.36 ksi (2.5 MPa) (intersection with σ_n axis).

To achieve this interface condition in the FE model, the Surface_to_surface_tiebreak contact type in LS-DYNA (referred to as "tiebreak" hereafter) was chosen to define the contact between the existing pier and concrete collar. Under compressive load, this contact type is the same as Automatic_surface_to_surface contact type. Under tensile load, the tiebreak contact follows the following failure criterion where normal and shear failure strengths need to be defined:

$$(|\sigma_n|/NFLS)^2 + (|\tau|/SFLS)^2 \geq 1 \quad (6\text{-}3)$$

where NFLS is the tensile strength of interface and SFLS is the pure shear strength. According to above discussion, both NFLS and SFLS are taken as 0.36 ksi (2.5 MPa).

Comparing Equation (6-3) with Equations (6-1) and (6-2), it can be seen that Equation (6-3) yields a conservative failure envelope, since it does not take into account the shear strength increases when the compressive normal stress increases.

6.3.2 Collision simulation results of RC collar-strengthened piers

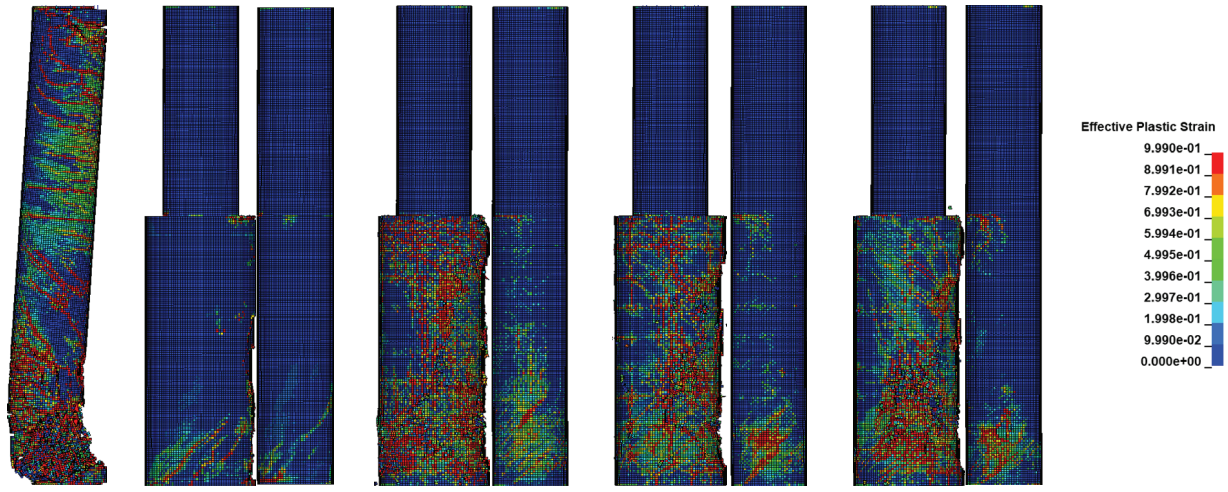

baseline | RC-1 (perfect bonding) | RC-2 (6 in spacing dowel) | RC-3 (12 in spacing dowel) | RC-4 (no dowel)

Figure 6-8 Damage patterns of RC collar-strengthened piers

The damage patterns of RC collar-strengthened piers are displayed in Figure 6-8. None of the four piers showed failure like the baseline pier, where uncontrolled deflection occurred, but with varying degrees of damage. The pier with perfect bonding to the RC collar ,RC-1, showed the least amount of damage, with several diagonal shear cracks developed near the bottom. The other three piers experienced more severe damage.

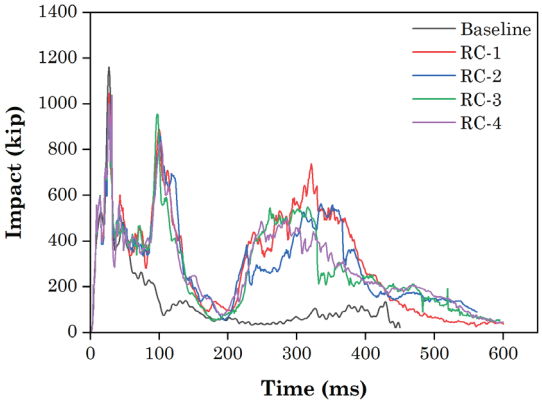

Figure 6-9 Impact histories of RC collar-strengthened piers

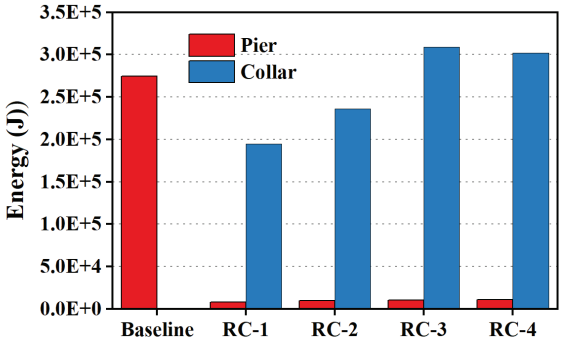

Figure 6-10 Energy absorption of RC collar-strengthened piers during collision

The impact histories of RC collar-strengthened piers, along with that of the baseline pier, are presented in Figure 6-9. Despite variations in their damage patterns, the impact histories of the four piers exhibited similarities. Furthermore, the peak impact force experienced by these strengthened piers was in close proximity to that of the baseline pier, which collapsed due to the collision. This observation suggests that the peak impact force may not be a suitable indicator for evaluating the collision resistance of a pier.

The energy absorbed by the existing piers and collars during the collision is shown in Figure 6-10. It can be observed that in all RC collar-strengthened cases, collars absorbed the majority of the energy, approximately an order of magnitude larger than that of the existing piers. From RC-1 to RC-3, as the interface became weaker, the energy absorbed by the collars increased. The energy absorbed by the existing pier, which can be seen as an indicator of the strengthening effectiveness of the collars, also increased as the interface became weaker. For RC-4, the energy absorbed by the existing pier increased by about 30% compared to that of RC-1 and increased by about 9% compared to that of RC-2. In all RC collar-strengthened piers, the energy absorbed by the existing pier was significantly reduced compared to the baseline pier.

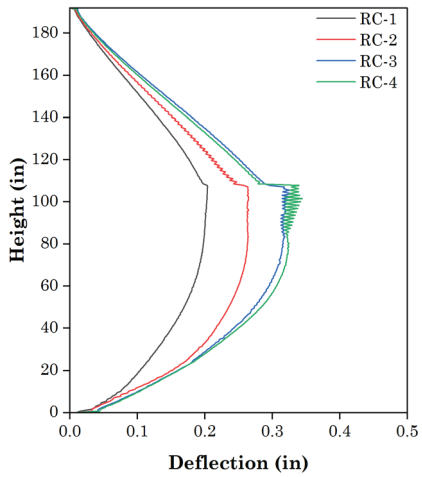

Figure 6-11 Maximum deflections of RC collar-strengthened piers

The maximum deflections are plotted along the height and shown in Figure 6-11. For all four piers, the maximum deflection occurred at about 110 ms when the tractor stopped its forward

motion, and the trailer began to interact with the tractor. The maximum deflection point was located at the end of the strengthened segment (108 in). Piers with perfect bonding with the collar showed the lowest deflection. The maximum deflection increased as the interface bonding condition became weakened. The pier with only a tiebreak interface showed the highest deflection. When comparing RC-4 with RC-2, it can be observed that eliminating dowel bars led to a 30% increase in deflection.

The above results show that the interface bonding had a noticeable influence on the strengthening effectiveness of RC collars. Increasing the interface strength was beneficial in controlling the deflection. A stronger interface was also beneficial in reducing the energy absorbed by the existing pier. This phenomenon can be explained by composite action. When the interface was strong, the existing pier and RC collar acted as a single member, resulting in greater stiffness and consequently reduced deflection and damage to the existing pier. However, when a weaker interface was present, the collar and pier behaved more like a layered structure or deformed separately, leading to lower stiffness and consequently increased deflection and damage to the existing pier.

The FDOT Structures Manual (FDOT, 2024) requires that 6 in (152 mm) spacing dowels should be installed when using RC collar-strengthening, which leads to difficulties in construction. From the results of this section, it can be seen that reducing or eliminating dowels did not necessarily lead to the failure of the pier, although it led to a 30% increase in deflection and a 9% increase in energy absorption by the existing pier. Considering a collision as an extreme event, preventing failure should be the primary concern rather than deflection. On the other hand, the deflection after the increase was 0.34 in, which was still small and was about 0.2% of the total pier height. Therefore, it can be said that the dowel bars could be eliminated.

6.4 UHPC Collar-strengthened Piers

6.4.1 Modelling details of UHPC collar-strengthened piers

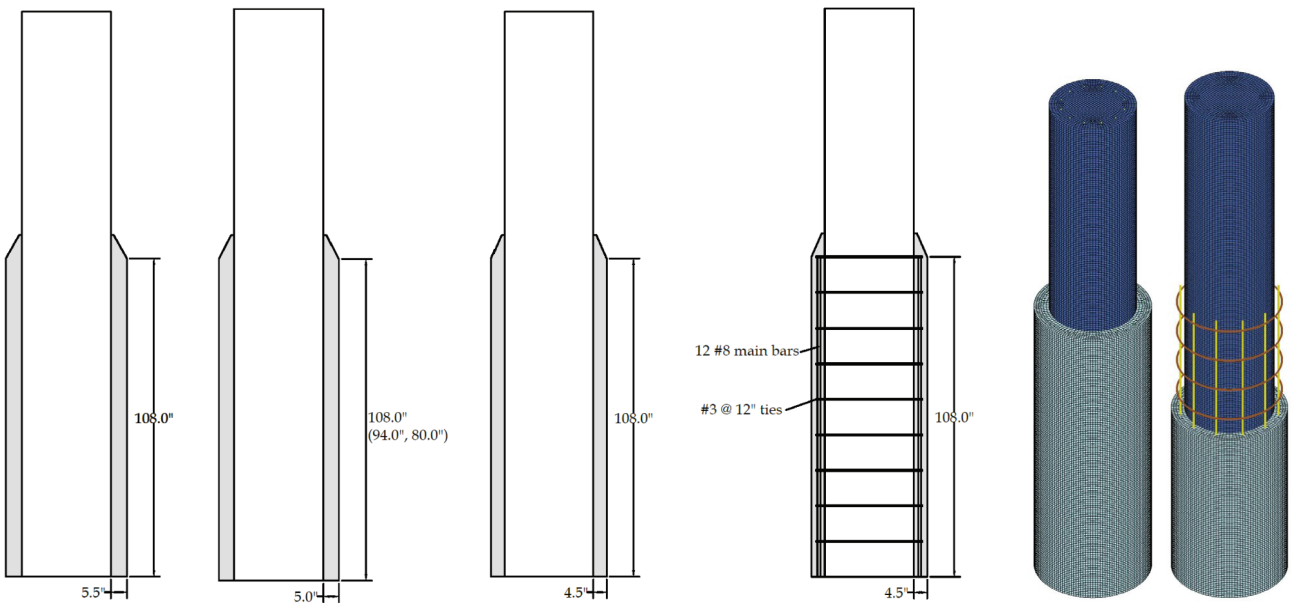

Figure 6-12 Design and FE model of UHPC collar-strengthened piers

The design and FE model of UHPC collar-strengthened piers are shown in Figure 6-12. UHPC collar was modelled with solid elements, and the material model was CSCM with a compressive strength of 18 ksi (124 MPa) which was validated in chapter 5.

Since the results from RC collar-strengthened piers showed that FE model that considered interface conditions gave more conservative results, the same interface modeling technique used in RC collar-strengthened piers was employed here. Previous research (Feng et al., 2020) indicates that the interface strength between newly cast UHPC and existing concrete is stronger than the interface strength between existing concrete and newly cast concrete. However, comprehensive models for describing this strength are currently lacking. Therefore, we applied the same interface conditions used for the RC collar-strengthened piers, with NFLS=SFLS= 0.36 ksi (2.5 MPa), for UHPC collar-strengthening.

6.4.2 Collision simulation results of UHPC collar-strengthened piers

The damage patterns of UHPC collar-strengthened piers with varying collar thickness are shown in Figure 6-13. U-5, which had a UHPC collar thickness of 4.5 in (114 mm), failed during the tractor impact stage; a diagonal shear crack first developed at the bottom, the UHPC collar then split into pieces and became detached from the existing pier, which failed subsequently. This failure mode could be attributed to the weak interface between the collar and the existing pier, preventing a significant amount of impact energy from being transmitted to the interior pier. Additionally, it indicates that the collar, under impact, experienced high tensile stress in the circumferential direction. RU-5, which had a collar longitudinal reinforcement ratio of 0.8% and transverse reinforcement ratio of 0.05%, was created to investigate the effect of small amount of collar reinforcement. As can be seen from the damage pattern, a small amount of reinforcement effectively

prevented the splitting of the collar and failure of the pier. When UHPC collar thickness was increased, as in the case of U-1 and U-2, the damage was mainly shear cracks near the bottom, while flexural damage was also observed on the existing pier. Compared with the damage patterns of RC collar-strengthened pier, the damage of UHPC collar-strengthened pier was noticeably reduced. According to the hand calculation in chapter 4, a UHPC collar thickness of 5.5 in (140 mm) should be sufficient. The simulation results presented here confirmed that the hand calculation method in chapter 4 would yield a conservative design, and the UHPC collar thickness could be further reduced to 5 in (127 mm) based on the FE analysis.

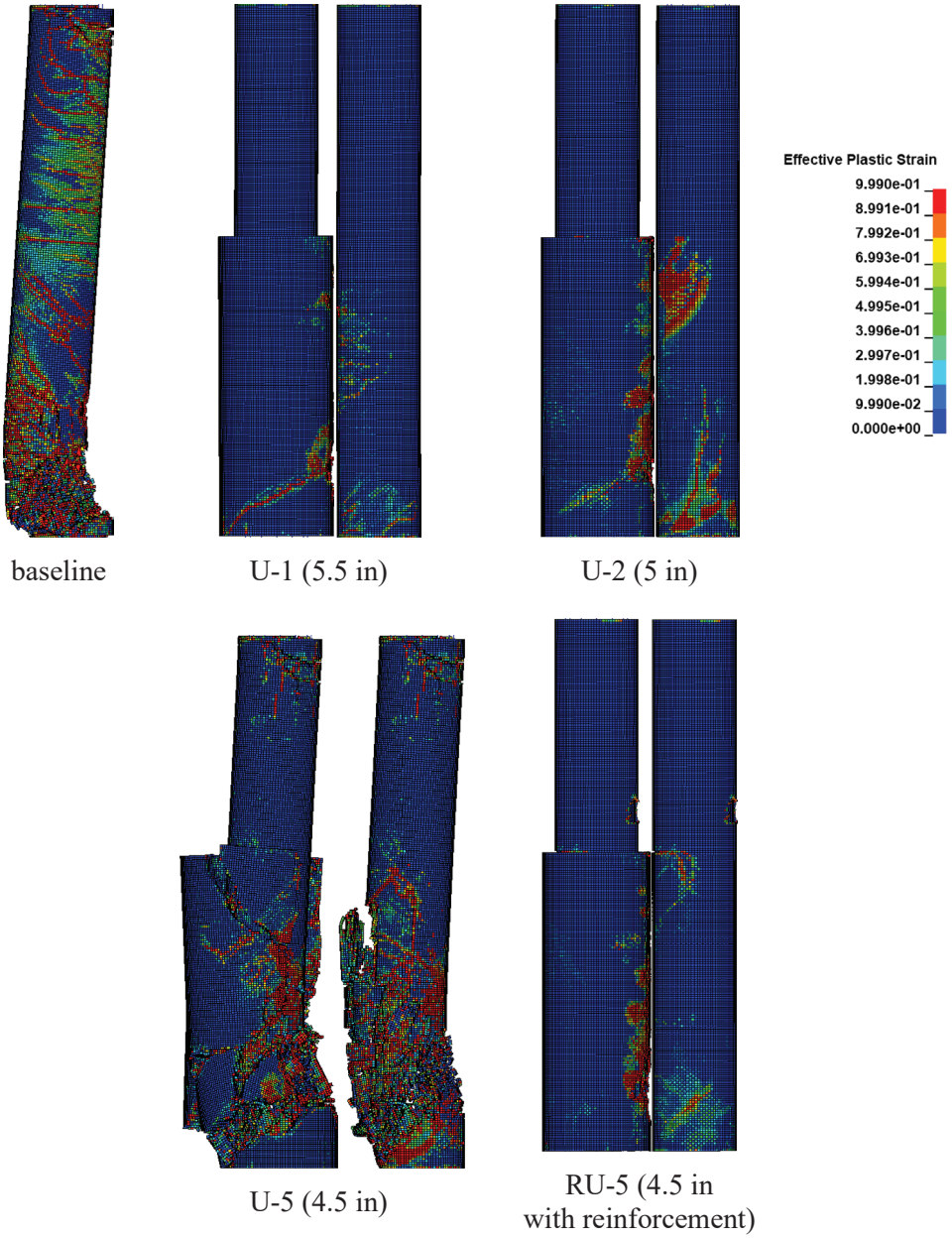

Figure 6-13 Damage patterns of UHPC collar-strengthened piers with varying collar thickness

The impact histories and energy absorption of these four UHPC collar-strengthened piers are displayed in Figure 6-14 and Figure 6-15. The UHPC collar-strengthened piers exhibited similar impact histories, including U-5, which failed during the trailer impact stage. Similar to the results

from RC collar-strengthened piers, there was no improvement in peak impact force compared to the baseline pier. From U-1 to U-5, the energy absorbed by the existing pier increased as the thickness of the collar decreased, leading to the failure of U-5. In the case of RU-5, adding a small amount of collar reinforcement significantly reduced the energy absorbed by the existing pier and increased the energy-absorbing capacity of the collar.

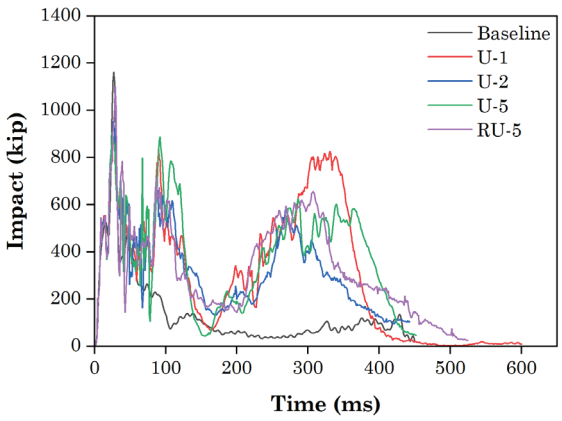

Figure 6-14 Impact histories of UHPC collar-strengthened piers with varying collar thickness

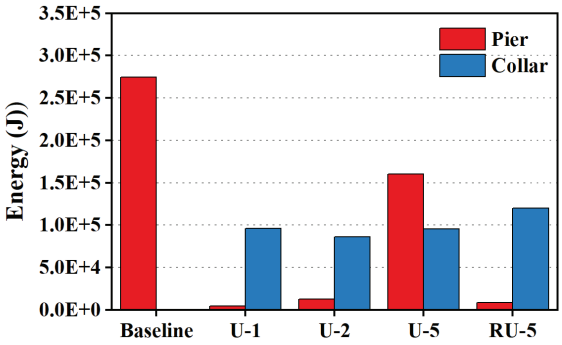

Figure 6-15 Energy absorption of UHPC collar-strengthened piers with varying collar thickness and reinforcement

The maximum deflections of UHPC-collar-strengthened piers are shown in Figure 6-16, while deflection of U-5 was not included since it failed and had uncontrolled deflection. As can be seen, the maximum deflections of the three piers were similar, with no significant differences observed. These results suggest that, in cases of weak interface conditions, increasing collar thickness and adding collar reinforcement were less effective in controlling pier deflection. However, they remained effective in reducing the energy absorbed by the pier.

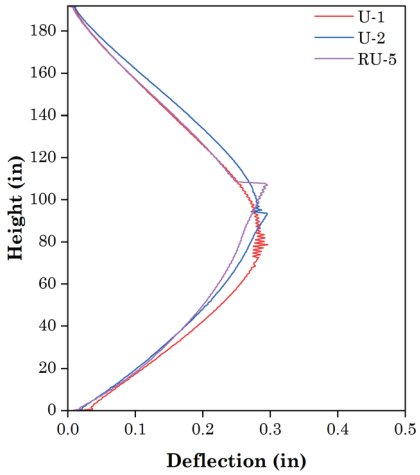

Figure 6-16 Maximum deflections of UHPC collar-strengthened piers with varying collar thickness

The damage patterns of UHPC collar-strengthened piers with different collar heights are shown in Figure 6-17. When the collar height was reduced to 94 in (2388 mm), the damage pattern

did not show visible difference from that observed with a collar height of 108 in. However, when the collar height decreased to 80 in (2032 mm), pier failure occurred.

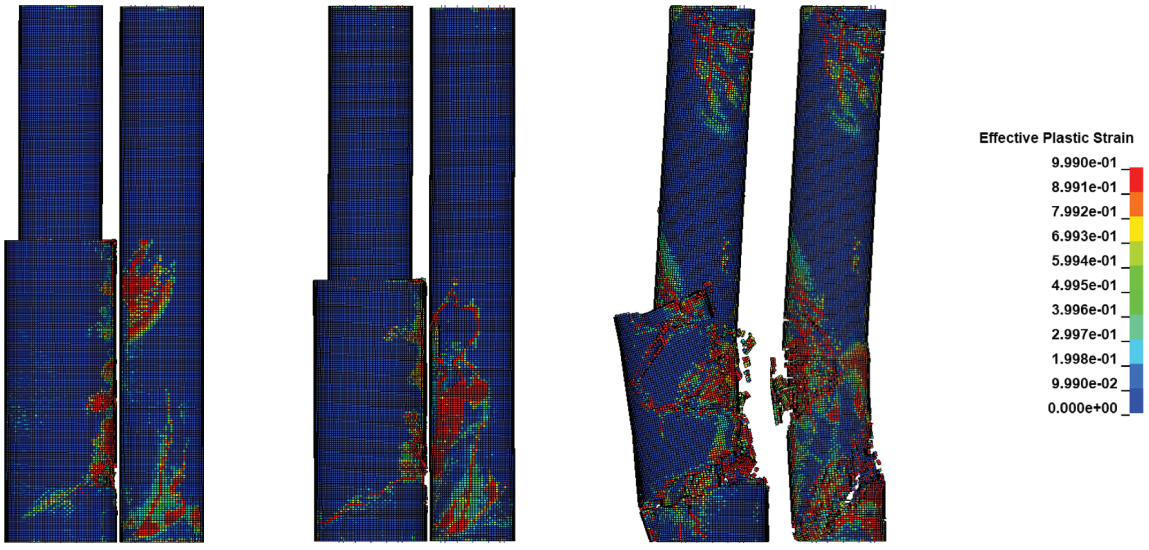

U-2 (108 in) U-3 (94 in) U-4 (80 in)

Figure 6-17 Damage patterns of UHPC collar-strengthened piers with varying collar height

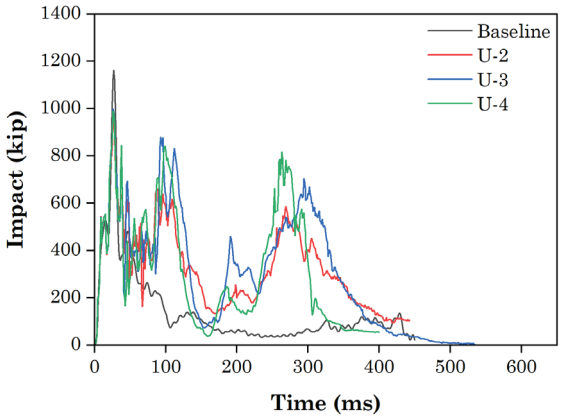

Figure 6-18 Impact histories of UHPC collar-strengthened piers with varying collar height

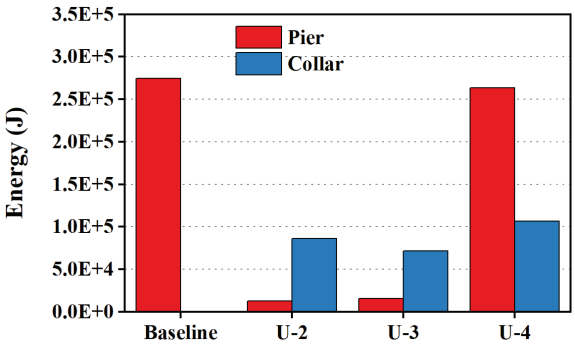

Figure 6-19 Energy absorption of UHPC collar-strengthened piers with varying collar height

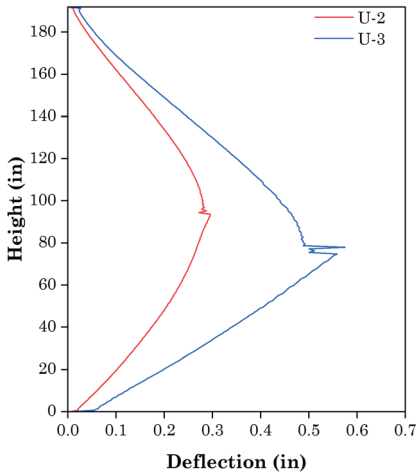

Figure 6-20 Maximum deflections of UHPC collar-strengthened piers with varying collar height

The impact histories and energy absorption of piers with different collar heights are displayed in Figure 6-18 and Figure 6-19. As the collar height decreased, the energy absorbed by the existing pier increased and led to the failure of U-4. Despite the similar energy absorption of U-2 and U-3, the maximum deflections of these two piers are significantly different, as shown in Figure 6-20. U-3, compared to U-2, had a maximum deflection increase of 94%, and the maximum deflection point also shifted downwards. Two reasons can explain this phenomenon. First, the strengthened section had a larger stiffness; thus, a shorter strengthened segment led to increased deflection of the pier. Second, reducing the collar height shifted the unstrengthened section towards the higher bending moment region, as it became closer to the impact position. Consequently, this led to increased deflection. The difference in piers with varying collar heights demonstrates the significant influence of collar height on the response of strengthened piers. Increasing the collar height effectively reduced the deflection of the piers. Although the main damage of the baseline pier was primarily concentrated under the height of 80 in, strengthening to a minimum height of 80 in was shown to be insufficient. The strengthening height should be at least 94 inches, which is about 50% of the pier height in this case. To better control deflection, a strengthening height of 108 in, which is about 55% of the pier total height in this case, is recommended.

6.5 FRP wrap-strengthened Piers

6.5.1 Modelling details of FRP wrap-strengthened piers

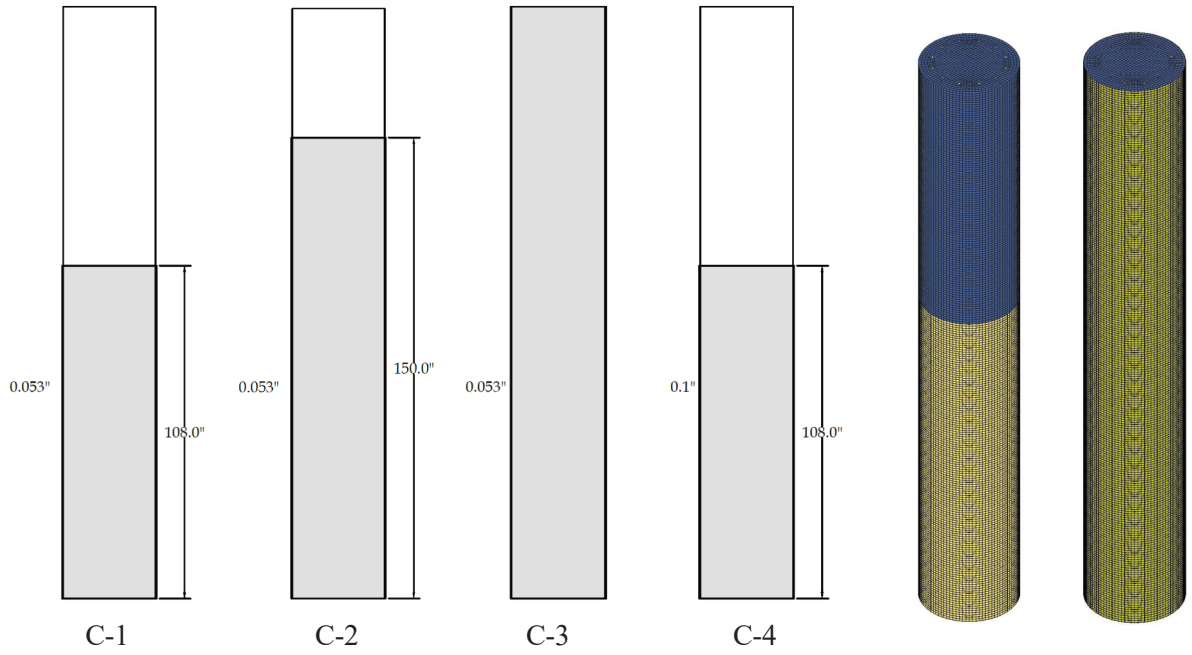

Figure 6-21 Design and FE model of FRP wrap-strengthened piers

The design and FE model of FRP wrap strengthened piers are shown in Figure 6-21. FRP was modelled with shell elements. The material model for FRP was Enhanced_composite_damage model, which was validated in chapter 5. The bonding between FRP and existing pier was also modelled with tiebreak contact type. In real-life applications, FRP wraps are typically attached to concrete using epoxy, which provides a much stronger interface with concrete than that between cementitious materials. In this study, an approximate value of NFLS = SFLS = 0.58 ksi (4.0 MPa) was used, which remains a conservative approach in accordance with the test results (Yao et al., 2005).

6.5.2 Collision simulation results of FRP wrap-strengthened piers

The damage patterns of FRP wraps strengthened piers are shown in Figure 6-22. C-1 and C-2 failed with a damage pattern similar to the unstrengthened baseline pier. In the case of C-3, which was strengthened at full height, the damage was significantly reduced, with most of it concentrated at the bottom. In the case of C-4, which had an increased FRP thickness, the damage level was between that of C-1 and C-3. Despite varying degrees of damage, the impact histories of all three piers were similar, as shown in Figure 6-23.

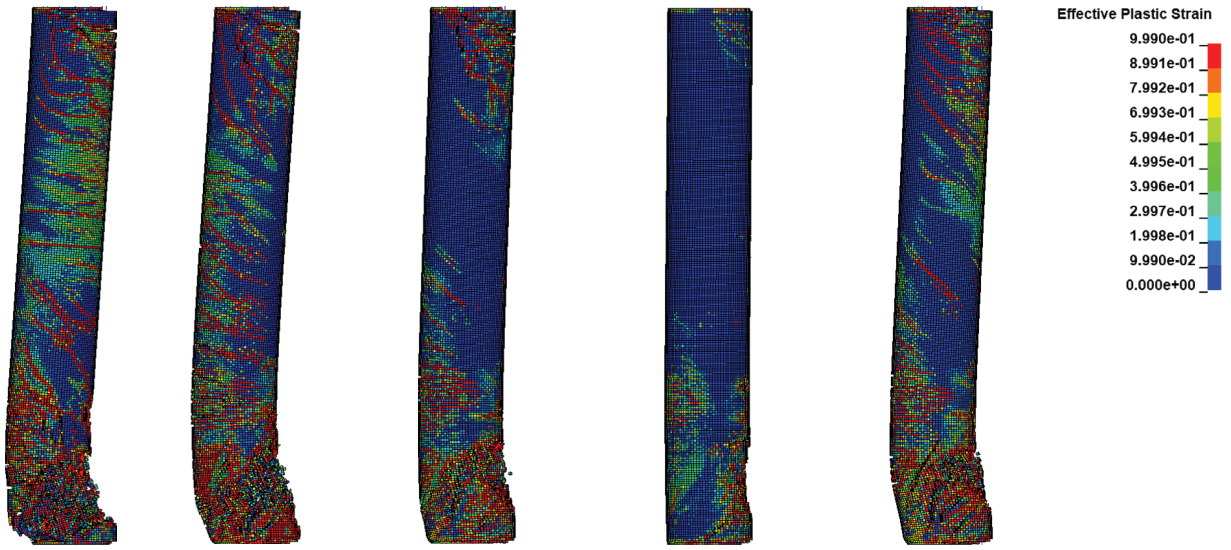

baseline | C-1 (0.053 in thickness, 108 in height) | C-2 (0.053 in thickness, 150 in height) | C-3 (0.053 in thickness, full height) | C-4 (0.1 in thickness, 108 in height)

Figure 6-22 Damage patterns of FRP wrap-strengthened piers

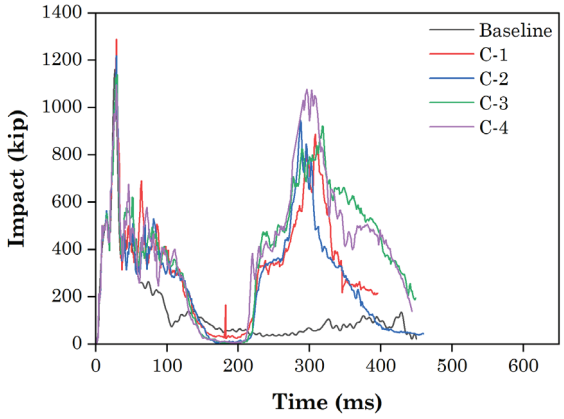

Figure 6-23 Impact histories of FRP wrap-strengthened piers

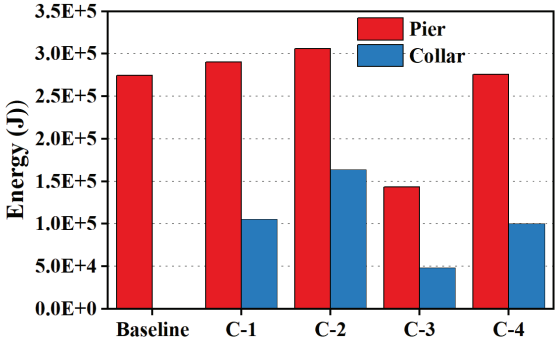

Figure 6-24 Energy absorption of FRP-strengthened piers

The energy absorption of FRP-strengthened piers is shown in Figure 6-24. Except C-3, which was strengthened at full height, the energy absorbed by the existing pier of other three piers all very close to the energy absorption of the baseline pier case. This indicates that increasing the strengthening height and increasing the thickness of FRP wraps were both ineffective in improving the impact resistance of piers.

The maximum deflections of C-3 and C-4 are shown in Figure 6-25. C-1 and C-2 are not included as uncontrolled deflections occurred in these two piers since they were unable to stop the vehicle. The deflection of C-4 was significantly large, approximately 2% of the total pier height. While C-3 exhibited a much smaller deflection, which is about three times smaller than that of C-4.

Based on these results, it can be said that for FRP wrap strengthening, only full height strengthening is recommended. These findings point out the limitations of the hand calculation approach, according to which C-1 and C-2 should have the same collision resistance as C-3. This primarily is because the hand calculations used a sectional approach and does not consider the global response of the pier under dynamic loading, which results in a different internal force distribution compared with static loading.

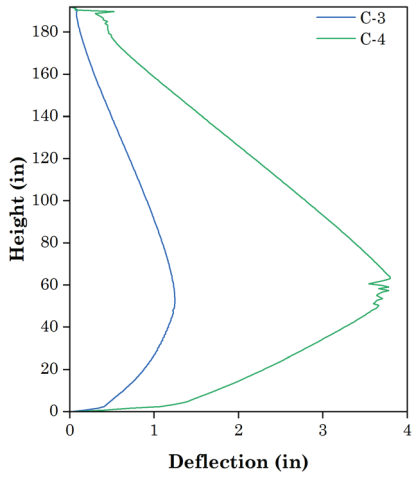

Figure 6-25 Maximum deflections of FRP wrap-strengthened piers

6.6 Comparison of different strengthening methods

The damage pattern, impact history, energy absorption by the existing pier, and maximum deflection, of RC-4, U-2, and C-3 are displayed in Figure 6-26, Figure 6-27, Figure 6-28, and Figure 6-29, respectively. These three piers were chosen because they are proven to be effective strengthening designs while having the smallest thickness in their strengthening groups.

While the impact histories of the three piers were similar, significant differences were observed in damage patterns and deflection histories. The RC collar exhibited the most severe damage, whereas the UHPC collar showed significantly less damage, despite having a smaller collar thickness and the absence of collar reinforcement. In terms of energy absorbed by the existing pier, U-2 was slighter than RC-4. While for the maximum deflection, RC-4 was slightly larger than U-2, but both were smaller than 0.2% of total pier height. It can therefore be said that the strengthening effectiveness of RC-4 and U-2 were on the same level. However, using UHPC allowed for a 29% of reduction in collar thickness and the elimination of collar reinforcement.

In terms of the damage pattern of C-3, a noticeable difference was the occurrence of damage at the top end. This is a result of the significantly larger deflection of C-3, which was 1.25 in (0.65% of total pier height) and about 378% larger compared with RC-4 and U-2, as shown in Figure 6-29. As a result, higher energy was absorbed by the existing pier, as shown in Figure 6-28. Considering that C-3 was strengthened along its full height, it can be concluded that FRP wraps were significantly less effective compared to RC collars and UHPC collars. This can be attributed to the flexural stiffness of a member, which is proportional to the fourth power of the diameter. As a result, increasing the diameter was much more effective in increasing flexural stiffness, resulting in smaller

deflection. Comparing with RC collar-strengthening and UHPC collar-strengthening, FRP strengthening was evidently less promising.

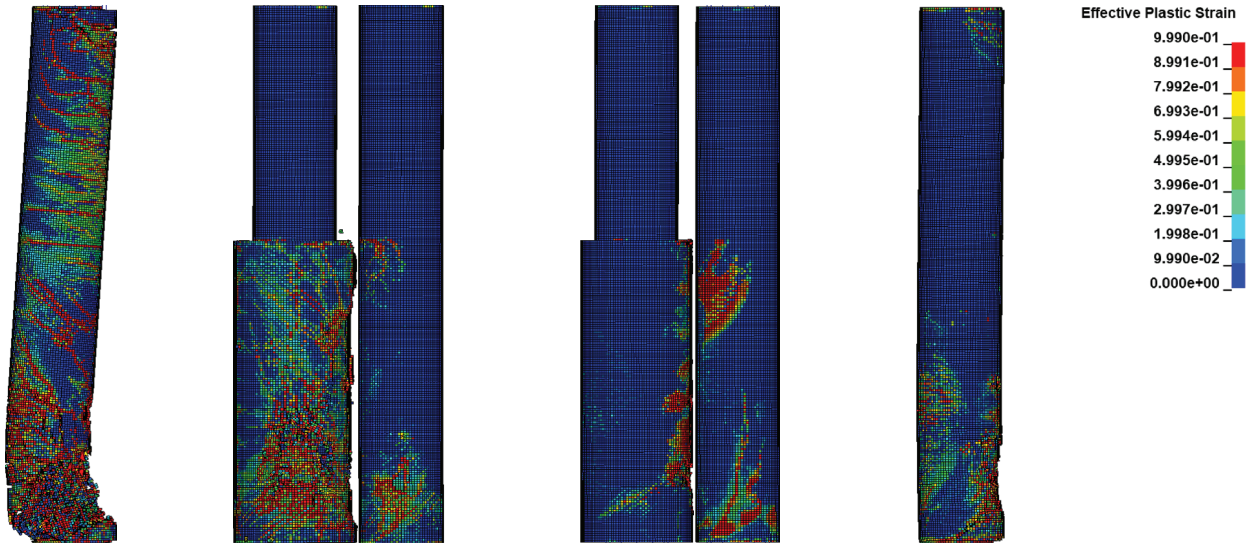

baseline | RC-4 (7 in, no dowel) | U-2 (5 in, no dowel) | C-3 (0.053 in, full height)

Figure 6-26 Comparison of damage patterns of different strengthening methods

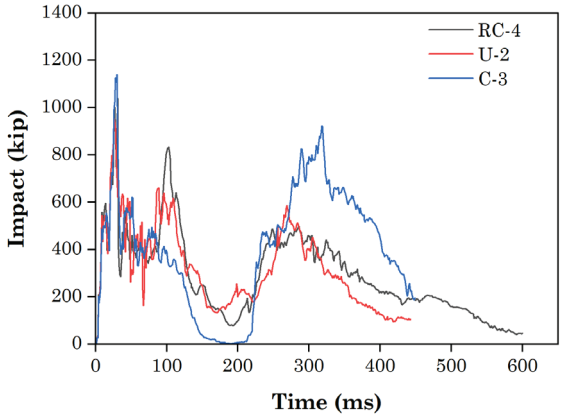

Figure 6-27 Comparison of impact histories of different strengthening methods

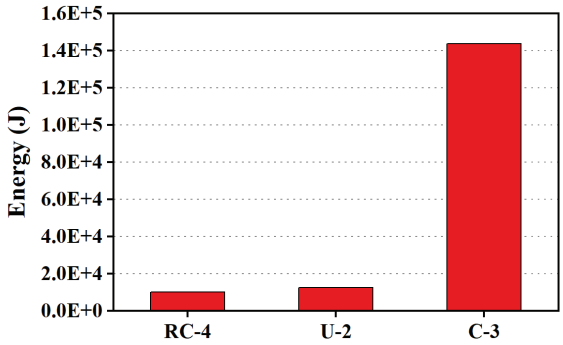

Figure 6-28 Energy absorption of existing piers

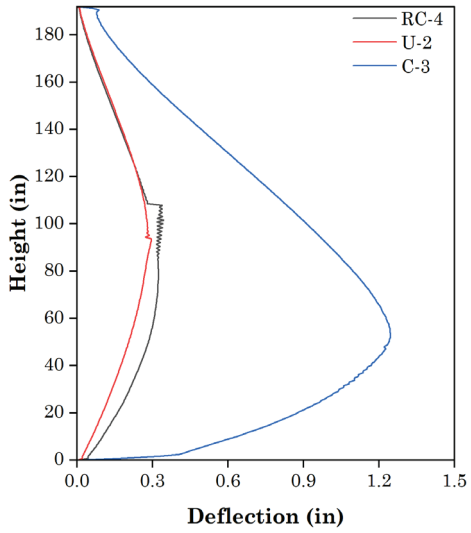

Figure 6-29 Comparison of maximum deflection of different strengthening methods

6.7 Conclusions

Based on the simulation results in this chapter, the following conclusions can be drawn:

- The most severe damage observed on bridge piers under heavy tractor-trailer collision primarily occurred below a height of approximately 80 in (2032 mm) in the form of diagonal shear cracks and plastic hinge formation. However, the results of piers with varying collar heights showed that an 80-in (2032 mm) collar was insufficient. Moreover, increasing collar height was beneficial in reducing deflection. Therefore, for RC collar and UHPC collar-strengthening, the collar height is recommended to be at least 80 in (2032 mm) plus the development length of collar reinforcement when collar reinforcement is present, or over 55% of the total pier height. For FRP strengthening, it is recommended to strengthen the full height of the pier.
- RC collars designed for a 600-kip (2669-kN) equivalent static force were effective in strengthening piers against heavy tractor-trailer collisions. The interface condition between the collar and existing pier had a significant influence on the deflection; a stronger interface resulted in a reduced deflection. Eliminating the 6 in spacing dowels required by FDOT Structures Manual (FDOT, 2024) did not lead to the failure of the pier, but did lead to a maximum deflection increase of 30%. Considering a collision as an extreme event, preventing failure should be the primary concern rather than deflection. On the other hand, the deflection after the increase was 0.34 in, which was still small and was about 0.2% of the total pier height. Therefore, it can be said that the dowel bars could be eliminated.
- The hand calculation method for UHPC collar in chapter 4 could provide a safe design for strengthening piers against heavy tractor-trailer collision. Compared with RC collar, UHPC collar was more effective in controlling damage and results in a 29% reduction in collar thickness and elimination of collar reinforcement. Adding collar reinforcement could further reduce the necessary collar thickness.
- For FRP strengthening, only full-height strengthening is recommended. Although strengthened at full height, FRP wrap strengthening still resulted in a much larger deflection, which was 1.25 in (0.65% of total pier height) and a 378% increase compared with RC collar-strengthening and UHPC collar-strengthening. Compared with RC collar-strengthening and UHPC collar-strengthening, FRP strengthening is evidently less promising. The hand calculation method for FRP in chapter 4 did not guarantee a safe design.

CHAPTER 7 FUTURE TEST MATRIX

In the previous chapter, we compared the performance of piers strengthened with RC collar, UHPC collar, and FRP wraps, and investigated the effect of multiple design parameters including interface condition, strengthening thickness, and height. Based on these results, in this chapter, we selected the two most promising strengthening methods for further experimental investigation. The experimental test program consists of material tests, static tests, and pendulum impact tests. Understanding material properties is the basis for accurately assessing the structure performance. It is also essential for creating accurate FE models before actual tests are carried out. Static tests provide us with insights into how the strengthening system works and the shear strength of the specimens. Impact tests enable us to directly evaluate the impact resistance of specimens and help us find the relationship between impact resistance and static strength.

The experimental program consists of four steps: First, multiple materials tests will be conducted to assess the material behavior under both static and dynamic loading. FE models will be developed based on the material test results to help refine the design of pendulum impact tests and static tests. Second, pendulum impact tests will be conducted on scaled specimens to assess the impact resistance of scaled specimens. Third, static tests will be performed on scaled specimens to determine the static strength of the scaled specimens and establish the relationship between impact resistance and static strength. Finally, static tests will be carried out on full-scale specimens to determine the static strength and estimate the impact resistance based on the relationship established in step two.

7.1 Design of Prototype Specimen

From the results of chapter 6, it is evident that RC collar-strengthening and UHPC collar-strengthening yielded better performance in terms of damage control, control of deflection, and energy absorption. Therefore, RC collar-strengthening and UHPC collar-strengthening were selected for further investigation.

The design of the baseline pier remains unchanged from previous investigations, as it represents the typical bridge piers in Florida that require strengthening. The compressive strength of the concrete is 3.4 ksi (23.33 MPa) and the steel reinforcement is grade 40. The design of the RC collar also remains the same, as it complies with the AASHTO LRFD (AASHTO, 2020a) 600-kip (2669-kN) force requirement, and previous FE analysis demonstrated its ability to protect the pier against collision. The compressive strength of collar concrete is 3.4 ksi (23.44 MPa) and the steel reinforcement is grade 60. The 6-in (152-mm) spacing dowel bars as required by FDOT Structures Manual (FDOT, 2024) will be omitted to facilitate construction process, as FE analysis indicates that eliminating the dowel bars resulted in a 30% increase in deflection but did not lead to failure. For the UHPC collar, the UHPC compressive strength is 18 ksi (124.11 MPa) and the collar thickness is 5 in (127 mm), as indicated by the FE analysis results. The strengthening height of both RC collar and UHPC collar is 108 in (2743 mm), which is about 56% of the total pier height. The material strengths, including concrete, steel reinforcement, and UHPC, remain the same as those in the previous chapters. The design details of these three prototype specimens are shown in Figure 7-1.

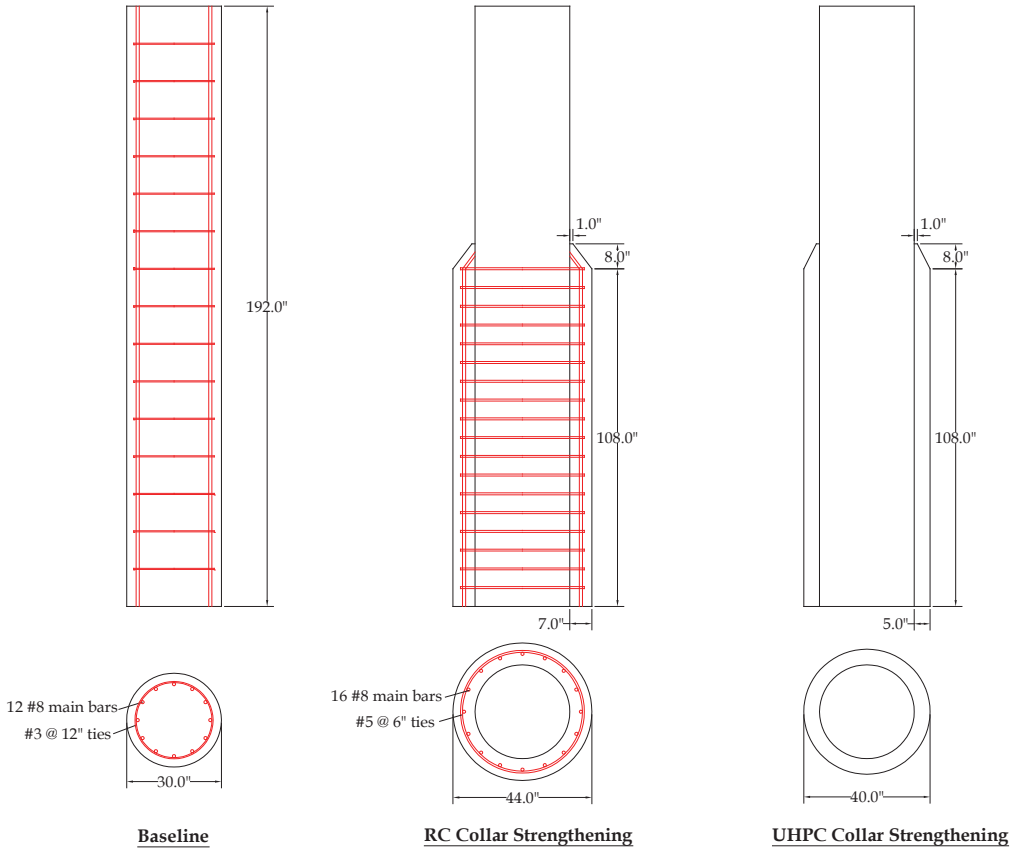

Figure 7-1 Prototype of baseline, RC collar-strengthened, and UHPC collar-strengthened piers

7.2 Material Test

The objective of material tests is to develop FE models which could help refine the structural tests setup and further investigate the design factors that were unable to be covered by structural tests. Material tests involve evaluating the concrete and UHPC behaviors under both static and dynamic loading conditions.

Static loading tests adhere to existing standard testing procedures: Concrete's compressive strength and tensile strength should be determined according to ASTM C39 (ASTM, 2021) and ASTM C496 (ASTM, 2017a), respectively. For UHPC, its compressive behavior should be assessed using ASTM C1856 (ASTM, 2017a), while its tensile behavior should be evaluated in accordance with AASHTO T 397 (AASHTO, 2022).

For dynamic loading tests, there are no standard procedures that could be followed, and the requirements for testing equipment are higher. According to previous FE analysis results, the maximum strain rates of concrete and UHPC were about 40 s^{-1}. Conventional commercial testing machines usually have a maximum strain rate limit of 10 s^{-1}. Therefore, dynamic testing methods should be designed. For dynamic compressive testing, we can utilize the drop weight impact apparatus previously constructed by the research group, as depicted in Figure 7-2. Through adjusting the weight and release height, various strain rate loadings can be achieved. We lack the necessary equipment for dynamic tensile testing. But we will review literature on the dynamic tensile

properties of concrete and UHPC and derive their dynamic tensile behavior based on the static tensile behavior we obtained from static tests.

Finally, we will conduct drop weight impact tests on small-scale beam samples, which involve both tensile and compressive behaviors, using the drop weight impact apparatus in Figure 7-2. to validate the dynamic tensile behaviors we derived.

Figure 7-2 Drop weight impact apparatus

7.3 Pendulum Impact Test

To assess the strength of a specimen under impact loading, failure of the specimen should be achieved under a single swing of the pendulum. According to the FE analysis results in chapter 6, the amount of energy needed to produce the failure of the baseline pier is about 203 kip-ft (275 kN-m). The FDOT pendulum impact test facility, which was designed to accommodate a maximum of 9000-lb (4082-kg) impactor swung from a height of 35 ft (10.67 m), can produce a maximum kinetic energy of 315 kip-ft (427 kN-m). Ideally, this kinetic energy is sufficient for full scale impact tests. However, if we consider the pier is to be impacted at the height of 5 ft (1.52 m) and the height of the footing is 2.5 ft (0.76 m), the maximum elevation of the impactor, relative to the impact point, would be 27.5 ft (8.38 m), which corresponds to a kinetic energy of 247.5 kip-ft (336 kN-m). Moreover, due to various factors such as friction, misalignment of the impactor, and rotational inertia of the winch cable, inevitably there will be energy loss. Assuming this loss is 25%, then the effective energy the pendulum could produce becomes 184 kip-ft (249 kN-m). These all make a full-scale test infeasible. Therefore, scaled models should be used to determine the strength of specimens under impact loading.

7.3.1 Scaled specimen for impact test

The design of scaled models is based on similitude methods. In similitude methods, for a given quantity I, the ratio of the prototype value i_p to the model value i_m is defined as the scaling factor S_i, namely

$$S_i = i_p / i_m \qquad (7\text{-}1)$$

In the case of length l, S is defined as

$S_l = l_p/l_m$ (7-2)

which controls the geometrical similitude to prototype.

In the case of material properties, S is defined as

$S_E = E_p/E_m$ (7-3)

which controls the material similitude.

Other necessary scaling factors of physical quantities involved in structural problems can be determined as functions of S_l and S_E (Noor and Boswell, 1992). A list of all scaling factors is displayed in Table 7-1.

Table 7-1 Scaling factors of physical quantities

Quantities	Scaling factors	Scaling factors for this study
Material properties	S_E	1
Stress	S_E	1
Strain	1	1
Length	S_l	2
Displacement	S_l	2
Angular displacement	1	1
Area	S_l^2	4
2nd moment of area	S_l^4	16
Concentrated load	$S_E S_l^2$	4
Moment	$S_E S_l^3$	8
Shear	$S_E S_l^2$	4
Energy	$S_E S_l^3$	8

The design of half-scale specimens is shown in Figure 7-3. When scaling the steel reinforcement, the principle is to maintain the same reinforcement ratio for the prototype and scaled model (Noor and Boswell, 1992). To meet this requirement, 0.19-in (5 mm) diameter steel wires are needed. The partial strengthening method, as concluded from chapter 6, was not employed. Instead, full-height strengthening was chosen. This decision was based on an FE analysis utilizing previous modeling techniques. Its results indicated that failures are likely to occur at the unstrengthened segment in partially strengthened piers, as illustrated in Figure 7-4(a), which does not align with the objectives of the impact test. The aim of conducting impact tests on these smaller specimens is not to directly evaluate the performance of prototype specimens based on the results from the smaller ones. Rather, it is to comprehend the failure mechanisms of specimens with different strengthening methods and establish a relationship between impact strength and static strength. This relationship allows us to predict the impact strength of prototype specimens based on their static strength. For this objective, it is preferable to allow failure to occur at the strengthened segment. Reinforced concrete footing is included for anchoring of the specimen. According to FE analysis results from chapter 6, the maximum impact force on a full-scale pier was about 1200 kip (5338 kN). Following

the scaling factor of four for concentrated force in Table 7-1, a maximum force of 300 kip (1334 kN) is expected on the half-scale specimen. This 300 kip (1334 kN) produces a bending moment of about 1050 kip-ft (1424 kN-m). The dimensions of the footing were determined to limit the maximum stress caused by this bending moment to a level smaller than the cracking strength of concrete. The closely spaced stirrups are designed to ensure sufficient shear strength. The materials properties for half-scale specimens will remain the same as those of the prototype specimens.

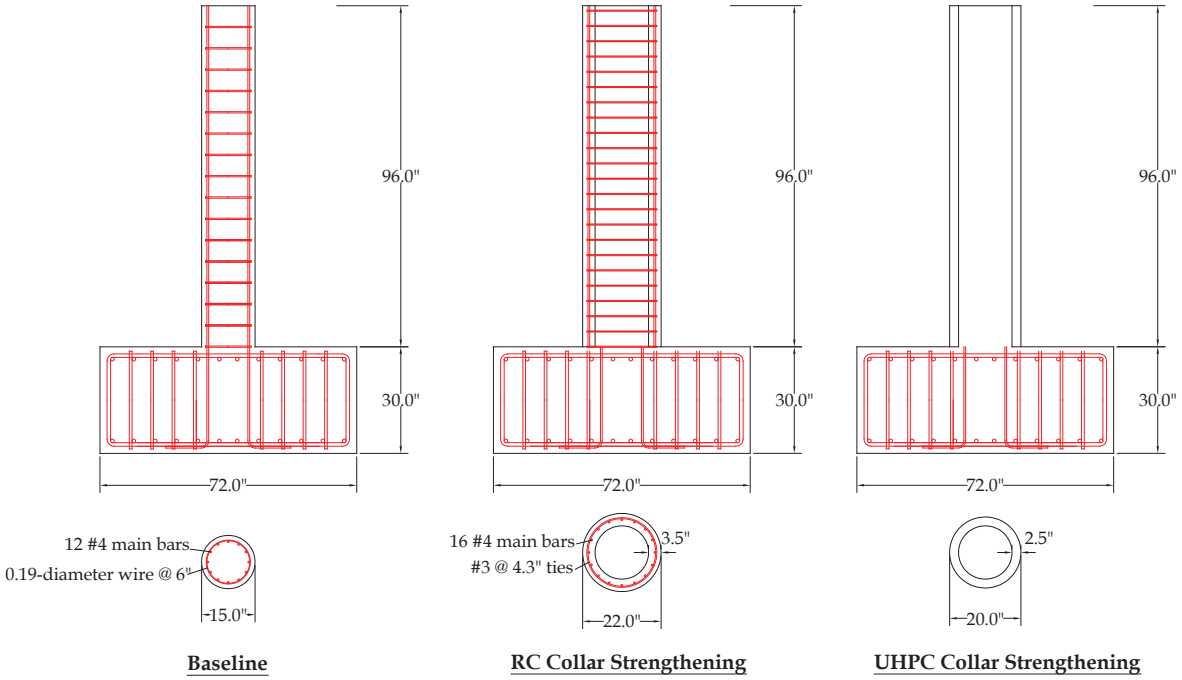

Figure 7-3 Half-scale baseline, RC collar-strengthened, and UHPC collar-strengthened piers for impact test

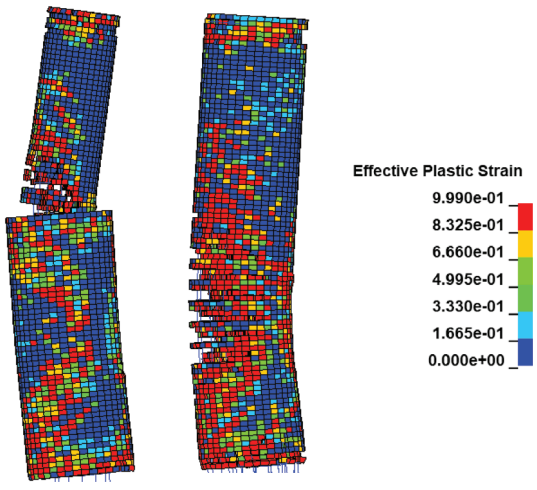

Figure 7-4 FE analysis of half-scale specimen under pendulum impact: (a) strengthening height 54 in; (b) full-height strengthening

7.3.2 Pendulum impact test setup

The impact tests will be performed with the pendulum impact facility at the FDOT Structures Research Center. The test setup is shown in Figure 7-5. The scaled specimens will be mounted to the RC foundation at the ground, which was designed to accommodate the maximum capacity of the pendulum and intended to serve as a permanent component of this test facility (Consolazio et al., 2014). At the back, the specimens will be supported by steel reaction frames both at the top and bottom. The reaction frame consists of three separate frames: the major frame with a height of about 130 in (3302 mm) in the middle, which could prevent horizontal movement of the footing and provide constraint to the pier, and two shorter triangular frames at the sides, which could prevent rotational movement of the footing. These frames are also to be mounted to the RC foundation. Assuming an impact force of 300 kip (1334 kN), the force at each location is within the capacity of each anchoring location, which is approximately 200 kip (890 kN). Tentatively, the reaction frame was planned mainly to be fabricated with W14X176 steel beams. According to a previous study that utilized the same pendulum impact facility (Consolazio et al., 2014), this is sufficient for the impact force. However, to simulate the actual constraint from a bridge, the major frame should be further designed. A detailed design of the reaction frame will be developed in the next phase of the project.

A 5000-lb (2268-kg) concrete-filled steel block with a crushable front nose is to be released from a height of 20 ft (6.10 m) and impact the scaled specimens at a height of 3.5 ft (1.07 m). This height was decided based on AASHTO LRFD (AASHTO, 2020a) specifications, which specify that the equivalent static force should act at a distance of 5 ft (1.52 m) above the ground. If we consider a 2-ft (0.61-m) footing embedment below the ground, then the impact height for the half-scale specimen should be 3.5 ft (1.07 m). By considering a 25% energy loss during the acceleration of the pendulum, the FE analysis results shows that a mass of 5000-lb (2268-kg) of the impactor is sufficient to produce failure in strengthened half-scale piers. A vehicle bumper will be attached to the front of the impactor block to simulate the actual contact between the vehicle and the pier.

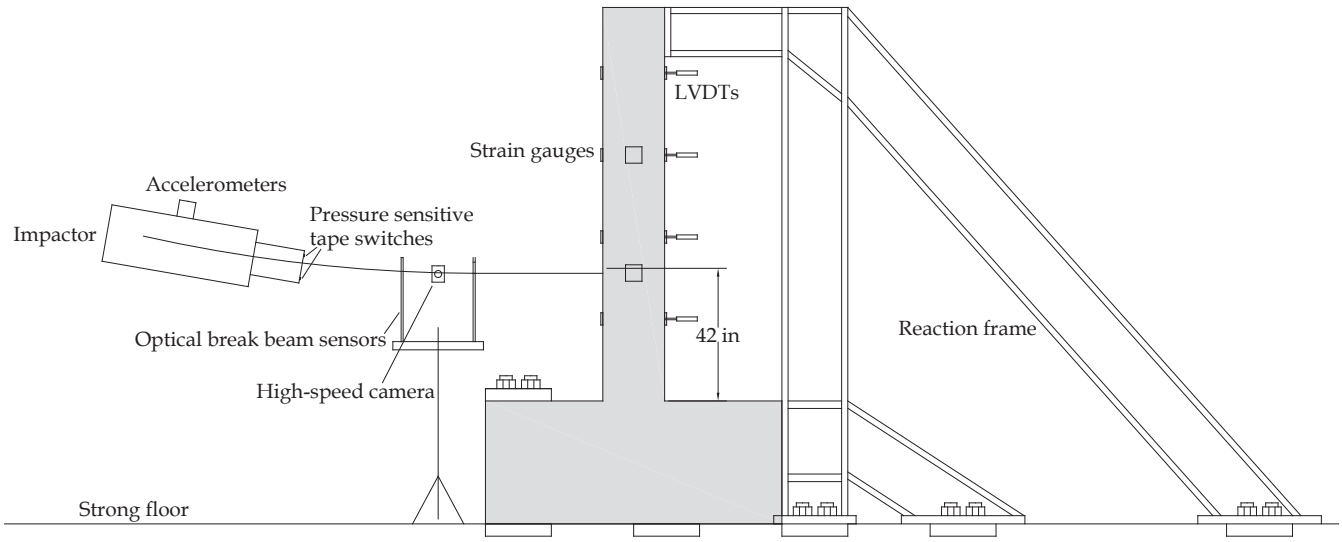

(a)

Figure 7-5 Setup of pendulum impact test program: (a) elevation view; (b) plan view

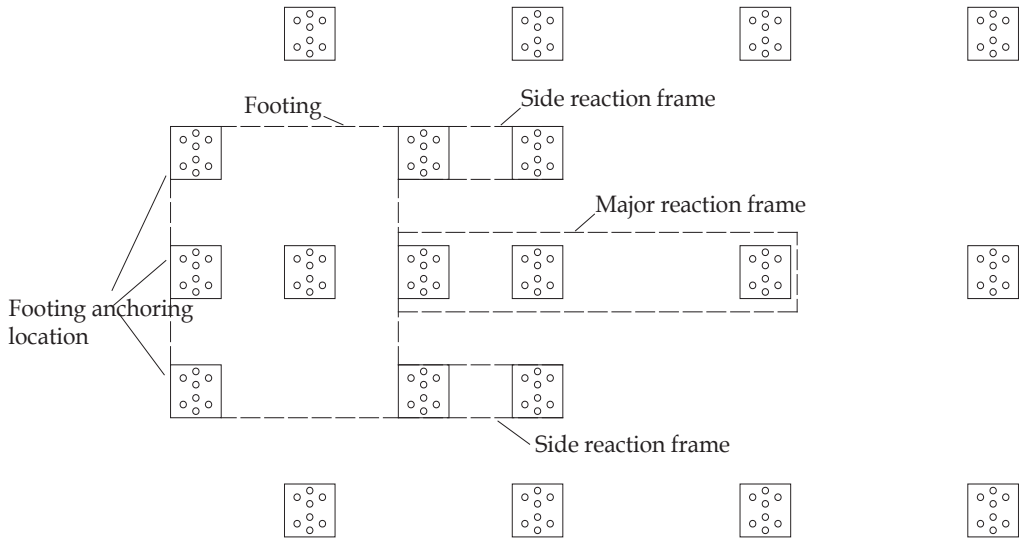

(b)

Figure 7-5 Setup of pendulum impact test program: (a) elevation view; (b) plan view

- Accelerometers with 0 – 500 g measurement range: to indirectly measure the impact force and duration. Three accelerometers are attached to the impactor block, two for impact direction and one for vertical direction. Two accelerometers are also attached to the specimen to measure the acceleration in horizontal direction.
- Pressure sensitive tape switches: attached to the impact surface of the impactor to mark the time point where impactor and pier come into contact.
- Optical break beam sensors: to measure the speed of impactor at the point of contact.
- High-Speed camera: quantitively characterize the impact process.
- LVDTs with measurement range -3.94 – 3.94 in (-100 mm – 100 mm): to measure the deflection along the height.
- Strain gauges: placed at surface, interface at the strengthened segment, and longitudinal rebars of the specimen at a 20-in (508-mm) interval to measure the strain in longitudinal direction.

All instrumentations, except high-speed camera, have a data acquisition frequency of 10 000 Hz.

7.4 Static Test

The primary objective of the static test is to determine the static strength of the baseline pier and strengthened piers at the strengthened section. This allows us to establish a relationship between impact strength and static strength, enabling predictions on the impact strength of full-scale specimens. Ultimately, these findings will inform recommendations on how to strengthen existing piers to withstand vehicle impacts.

7.4.1 Full-scale and scaled specimen for static test

To ensure failure happens at the strengthened section, specimens will be strengthened at full length. For scaled specimen, the design is the same as that used in the impact test. The details of full-scale and scaled specimen for static test are given in Figure 7-6 and Figure 7-7.

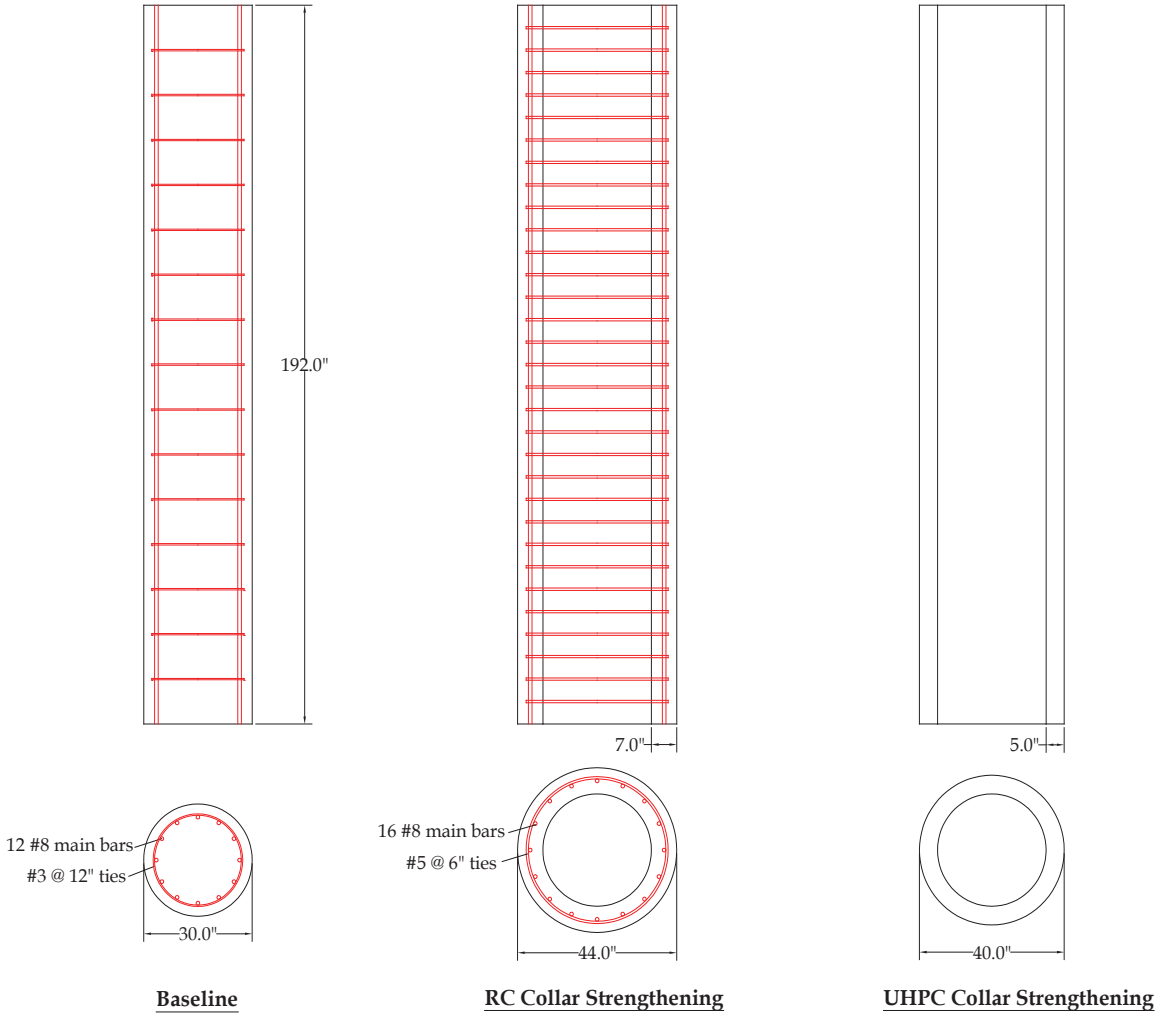

Figure 7-6 Full-scale baseline, RC collar-strengthened, and UHPC collar-strengthened piers for static test

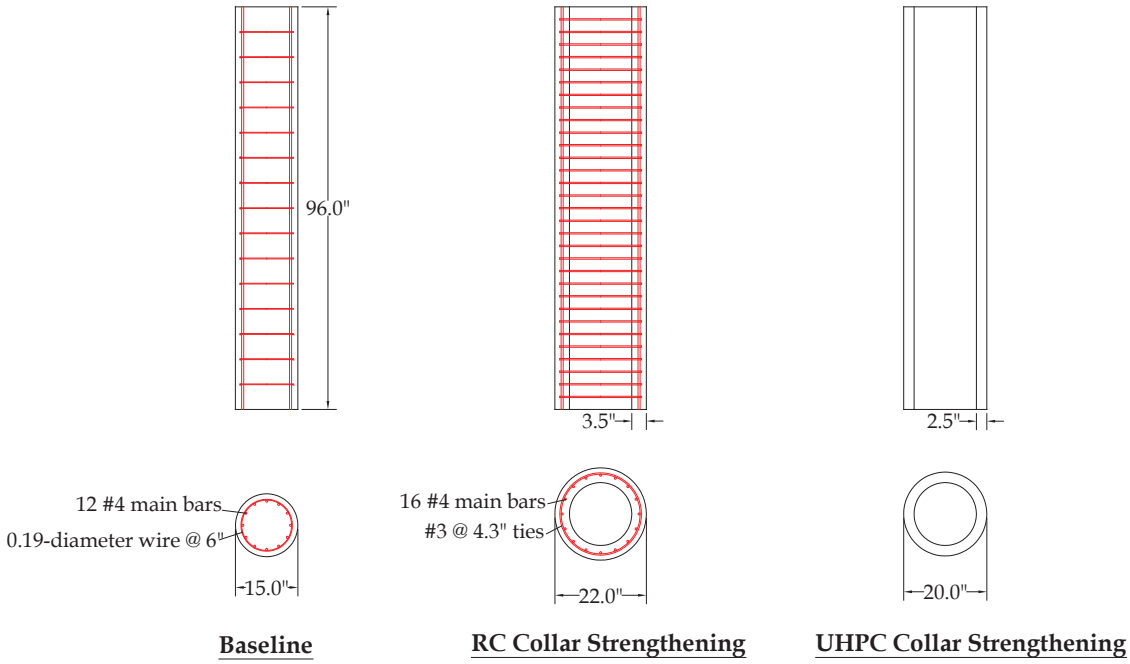

Figure 7-7 Half-scale baseline, RC collar-strengthened, and UHPC collar-strengthened piers for static test

7.4.2 Static test setup

The objective of the static test is to determine the static strength of corresponding failure types observed in the impact testing. If flexural failure is observed from the static test, then the static test should be designed to allow the specimen to exhibit flexural failure. If shear failure is observed from the impact test, then the static test should be designed to allow the specimen to exhibit shear failure. The static test setup is shown in Figure 7-8. A four-point bending setup is employed, and the test will be force-controlled until the failure is reached. Based on the hand calculations in chapter 4, the estimated maximum load is about 700 kip (3114 kN). Flexural failure and shear failure can be achieved by changing the ratio between the length of the shear span and pure bending span. If the desired failure mode is flexural failure, then the length of the shear span will be longer to achieve higher bending moments at the pure bending span. If the desired failure mode is shear failure, then the length of the shear span will be shorter to lower the bending moment at the pure bending span. FE simulation will be performed before the static tests to determine the exact length of the shear span. Detailed setup of the test, including supports, will be designed in next phase.

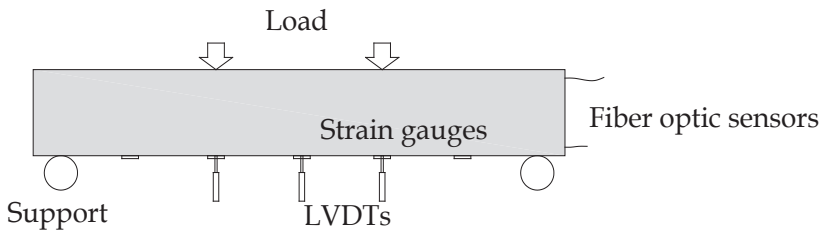

Figure 7-8 Setup and instrumentation of static test program

The instrumentation of the impact test includes the following:

- LVDTs with measurement range -3.94 – 3.94 in (-100 mm – 100 mm): placed at sections of midspan and loading points to measure the specimen vertical deflection.
- Strain gauges: placed at the interface, reinforcing bars, and bottom side at a 15-in (381-mm) interval to measure the strain in longitudinal direction.
- Fiber optic sensors: attached to the longitudinal reinforcement while casting to measure the continuous strain distribution inside the specimen.

7.5 Summary of Test Matrix

In summary, the experimental program will consist of three types of test: material tests on concrete and UHPC, pendulum impact tests, and static tests on the baseline pier, RC-collar-strengthened pier, and UHPC-collar-strengthened pier. A total of nine piers (six half-scale and three full-scale piers) are to be tested. A summary of the test matrix is provided in Table 7-2. It should be noted that the experimental program does not cover factors such as strengthening height and axial force caused by the superstructure. These factors will be investigated through simulating collisions between full-scale bridges and tractor-trailer vehicle using the FE models developed from the experimental program.

The testing sequence will be as follows: we will first conduct the impact test and static test on half-scale baseline piers. After that, we will conduct the impact test and static test on half-scale strengthened piers. The static test on full-scale specimens will be conducted last. For the construction of the specimens, we will construct all the baseline piers first, including those that will be strengthened later. The RC collars and UHPC collars will be constructed one month before their respective tests, following the surface treatment requirements outlined in the FDOT Structures Manual (FDOT, 2024).

Table 7-2 Summary of test matrix

<table>
<tr><th>Test types</th><th colspan="2">Details</th><th>Objectives</th></tr>
<tr><td rowspan="4">Material test</td><td colspan="2">Static compressive</td><td rowspan="3">- Determine static compressive, tensile, and dynamic compressive behaviors of UHPC and concrete.</td></tr>
<tr><td colspan="2">Static tensile</td></tr>
<tr><td colspan="2">Dynamic compressive</td></tr>
<tr><td colspan="2">Small scale beam impact tests</td><td>- Derive dynamic tensile behavior of UHPC and concrete indirectly.
- Develop accurate FE models.</td></tr>
<tr><td rowspan="3">Pendulum impact test</td><td rowspan="3">Half-scale</td><td>baseline</td><td rowspan="3">- Determine the impact strength of each pier.
- Validate the developed FE model.</td></tr>
<tr><td>RC-collar-strengthened</td></tr>
<tr><td>UHPC-collar-strengthened</td></tr>
<tr><td rowspan="6">Static test</td><td rowspan="3">Half-scale</td><td>baseline</td><td rowspan="3">- Determine the static strength of each pier.
- Establish the relationship between static strength and impact strength</td></tr>
<tr><td>RC-collar-strengthened</td></tr>
<tr><td>UHPC-collar-strengthened</td></tr>
<tr><td rowspan="3">Full-scale</td><td>baseline</td><td rowspan="3">- Determine the static strength of full-scale piers and predict the corresponding impact strength based on the established relationship.
- Make design recommendations for pier design to resist vehicle collision based on static strength.</td></tr>
<tr><td>RC-collar-strengthened</td></tr>
<tr><td>UHPC-collar-strengthened</td></tr>
</table>

CHAPTER 8 SUMMARY AND CONCLUSIONS

In this research, we developed dynamic FE models to evaluate the most effective designs for strengthening bridge piers against vehicle collisions. The process began with an extensive literature review to compile existing knowledge on the dynamic responses of bridge piers under vehicle impact, various strengthening methods, and pertinent regulatory codes. Based on the information from the literature review, we first designed a baseline pier representative of the typical bridge piers that need to be strengthened in Florida. Three strengthening methods were selected for investigation: RC collars, UHPC collars, and FRP wraps. Hand calculations were performed to verify the design of the strengthening plans. In the next step, valid dynamic FE models were developed by validating and calibrating a tractor-trailer model and various material constitutive models. The validated FE models were then used to simulate the collision of the tractor-trailer with piers strengthened the proposed strengthening plans. The influence of interface bonding conditions, collar thickness, collar reinforcement, and strengthening height were investigated. Based on the FE analysis, the conclusions are as follows:

- RC collars designed for a 600-kip (2669-kN) ESF were effective in strengthening piers against heavy tractor-trailer collisions. Removing the 6-in spacing dowels required by FDOT Structures Manual (FDOT, 2024) did not lead to the failure of the pier but led to a maximum deflection increase of 30%. Considering the deflection after the increase was still small (about 0.2% of the pier height), it can be concluded that the dowel bars could be eliminated.
- The 600-kip (2669-kN) ESF design approach for UHPC collars resulted in a conservative design. Compared to RC collars, UHPC collars were more effective in controlling damage and led to a 29% reduction in collar thickness and elimination of collar reinforcement. Adding collar reinforcement could further reduce the necessary collar thickness.
- Increasing the height of RC collars and UHPC collars was beneficial in reducing deflection. For RC collars and UHPC collars, the recommended collar height is at least 108 in (2743 mm) (about 55% of the pier height).
- FRP wrap strengthening was less effective in controlling damage and deflection of piers when compared with RC and UHPC collar-strengthening. Based on these findings, FRP wraps are not recommended as a strengthening method.
- Strengthening with RC collars and UHPC collars are identified as the two most promising methods and are recommended to be investigated experimentally.
- An experimental program consisting of material tests, impact tests, and static tests, for future experimental investigations is proposed and summarized as follows:

Table 8-1 Future test matrix

Test types	Details	
Material test	Static compressive	
	Static tensile	
	Dynamic compressive	
	Small scale beam impact tests	
Pendulum impact test	Half-scale	baseline
		RC-collar-strengthened
		UHPC-collar-strengthened
Static test	Half-scale	baseline
		RC-collar-strengthened
		UHPC-collar-strengthened
	Full-scale	baseline
		RC-collar-strengthened
		UHPC-collar-strengthened

REFERENCES

American Association of State Highway and Transportation Officials. (1994). *LRFD Bridge Design Specifications*. (1st ed.). American Association of State Highway and Transportation Officials.

American Association of State Highway and Transportation Officials. (2007). *LRFD Bridge Design Specifications.* (4th ed.). American Association of State Highway and Transportation Officials.

American Association of State Highway and Transportation Officials. (2010). *LRFD Bridge Design Specifications.* (5th ed.). American Association of State Highway and Transportation Officials.

American Association of State Highway and Transportation Officials. (2012). *Guide Specifications for Design of Bonded FRP Systems for Repair and Strengthening of Concrete Bridge Elements* (1st ed.). American Association of State Highway and Transportation Officials.

American Association of State Highway and Transportation Officials. (2020a). *LRFD Bridge Design Specifications.* (9th ed.). American Association of State Highway and Transportation Officials.

American Association of State Highway and Transportation Officials. (2020b). *Guide for Design and Construction of Near-Surface Mounted Titanium Alloy Bars for Strengthening Concrete Structures*. American Association of State Highway and Transportation Officials.

American Association of State Highway and Transportation Officials. (2022). *Standard Method of Test for Uniaxial Tensile Response of Ultra-High Performance Concrete. T 397-22*. American Association of State Highway and Transportation Officials.

Abdelkarim, O. I., & ElGawady, M. A. (2017). Performance of bridge piers under vehicle collision. *Engineering Structures*, *140*, 337-352.

ACI Committee 440. (2002). *Guide For The Design And Construction Of Externally Bonded Frp Systems For Strengthening Concrete Structures*. American Concrete Institute.

ACI Committee 440. (2017). ACI PRC-440.2-17: Guide for the Design and Construction of Externally Bonded FRP Systems for Strengthening Concrete Structures. In *American Concrete Institute*. American Concrete Institute.

Agrawal, A. K., El-Tawil, S., Cao, R., Xu, X., Chen, X., & Wong, W. (2018). *A performance-based approach for loading definition of heavy vehicle impact events*. United States. Federal Highway Administration. Office of Research.

Agrawal, A. K., Liu, G. Y., & Alampalli, S. (2013). Effects of truck impacts on bridge piers. *Advanced Materials Research*, *639*, 13–25.

Agrawal, A. K., Xu, X., & Chen, Z. (2011). *Bridge-vehicle impact assessment*. University Transportation Research Center.

Al-Bukhaiti, K., Yanhui, L., Shichun, Z., Abas, H., & Aoran, D. (2021). Dynamic equilibrium of CFRP-RC square elements under unequal lateral impact. *Materials*, *14*(13), 3591.

ASTM International. (2017a). *ASTM C496/C496M-17: Standard Test Method for Splitting Tensile Strength of Cylindrical Concrete Specimens*. ASTM International.

ASTM International. (2017b). *ASTM C1856/C1856M-17: Standard Practice for Fabricating and Testing Specimens of Ultra-High Performance Concrete*. ASTM International.

ASTM International. (2021). *ASTM C39/C39M-21: Standard Test Method for Compressive Strength of Cylindrical Concrete Specimens*. ASTM International.

Auyeung, S., Alipour, A., & Saini, D. (2019). Performance-based design of bridge piers under vehicle collision. *Engineering Structures*, *191*, 752–765.

Beason, W. L., & Hirsch, T. J. (1989). *Measurement of heavy vehicle impact forces and inertia properties* (No. FHWA-RD-89-120). United States. Federal Highway Administration. Office of Safety and Traffic Operations.

BSI. (2006a). *Eurocode1—Actions on structures—Part 1-7: General actions—Accidental actions. BS EN1991-1-7:2006*. London: BSI.

BSI. (2006b). *National annex to Eurocode 1: Actions on structures—Part 1-7: Accidental actions. NA to BS EN 1991-1-7: 2006*. London: BSI.

Buth, C. E., Brackin, M. S., Williams, W. F., & Fry, G. T. (2011). *Collision loads on bridge piers: phase 2, report of guidelines for designing bridge piers and abutments for vehicle collisions* (No. FHWA/TX-11/9-4973-2). Texas Transportation Institute.

Buth, C. E., Williams, W. F., Brackin, M. S., Lord, D., Geedipally, S. R., & Abu-Odeh, A. Y. (2010). *Analysis of large truck collisions with bridge piers: phase 1, report of guidelines for designing bridge piers and abutments for vehicle collisions* (No. FHWA/TX-10/9-4973-1). Texas Transportation Institute.

Cao, R. (2019). *Heavy truck collision with bridge piers (Doctoral dissertation, The City College of New York)*. New York: The City College of New York.

Cao, R., Agrawal, A. K., El-Tawil, S., Xu, X., & Wong, W. (2019). Heavy truck collision with bridge piers: Computational simulation study. *Journal of Bridge Engineering*, *24*(6), 04019052.

Chang, F. K., & Chang, K. Y. (1987). A progressive damage model for laminated composites containing stress concentrations. *Journal of composite materials*, *21*(9), 834-855.

Chen, L., Fang, L., Fan, W., Liu, T., & Wu, H. (2022). Field test and numerical simulation of a full-scale RC pier under multiple lateral impacts. *Engineering Structures*, *268*, 114747.

Chen, L., El-Tawil, S., & Xiao, Y. (2016). Reduced models for simulating collisions between trucks and bridge piers. *Journal of Bridge Engineering*, *21*(6), 04016020.

Chen, L., Wu, H., & Liu, T. (2021a). Vehicle collision with bridge piers: A state-of-the-art review. *Advances in Structural Engineering*, *24*(2), 385-400.

Chen, L., Wu, H., Fang, Q., & Li, R. (2021b). Full-scale experimental study of a reinforced concrete bridge pier under truck collision. *Journal of Bridge Engineering*, *26*(8), 05021008.

Chopra, A. K. (2011). *Dynamics of structures: Theory and applications to earthquake engineering*. (4th ed.). London: Pearson.

Consolazio, G. R., Getter, D. J., & Kantrales, G. C. (2014). *Validation and implementation of bridge design specifications for barge impact loading (No. BDK75-977-31)*. University of Florida. Dept. of Civil and Coastal Engineering.

Do, T. V., Pham, T. M., & Hao, H. (2018). Dynamic responses and failure modes of bridge columns under vehicle collision. *Engineering Structures*, *156*, 243-259.

Do, T. V., Pham, T. M., & Hao, H. (2019). Impact force profile and failure classification of reinforced concrete bridge columns against vehicle impact. *Engineering Structures*, *183*, 443-458.

Do, V. T. (2019). *Dynamic Analysis and Design of Monolithic and Segmental Concrete Bridge Columns against Impact Loads (Doctoral dissertation, Curtin University)*. Curtin Perth: Curtin University.

El-Tawil, S., Severino, E., & Fonseca, P. (2005). Vehicle collision with bridge piers. *Journal of Bridge Engineering*, *10*(3), 345-353.

Espeche, A. D., & León, J. (2011). Estimation of bond strength envelopes for old-to-new concrete interfaces based on a cylinder splitting test. *Construction and building materials*, *25*(3), 1222-1235.

Fan, W., Shen, D., Yang, T., & Shao, X. (2019). Experimental and numerical study on low-velocity lateral impact behaviors of RC, UHPFRC and UHPFRC-strengthened columns. *Engineering Structures*, *191*, 509-525.

Fan, W., Xu, X., Zhang, Z., & Shao, X. (2018). Performance and sensitivity analysis of UHPFRC-strengthened bridge columns subjected to vehicle collisions. *Engineering Structures*, *173*, 251-268.

FDOT. (2024). *2024 Structures Manual*. FDOT.

Feng, S., Xiao, H., & Li, H. (2020). Comparative studies of the effect of ultrahigh-performance concrete and normal concrete as repair materials on interfacial bond properties and microstructure. *Engineering Structures*, *222*, 111122.

Feyerabend, M. (1988). *Hard transverse impacts on steel beams and reinforced concrete beams (Ph. D. thesis)*. Karlsruhe: University of Karlsruhe.

Fib - federation internationale du beton. (2013). *fib Model Code for Concrete Structures 2010*.

Fuhaid, A. A., Sohel, K. M. A., & Arifuzzaman, M. (2022). The effect of strengthening methods on the performance of reinforced concrete columns against vehicle impact. *Applied Sciences*, *12*(3), 1382.

Fujikake, K., Li, B., & Soeun, S. (2009). Impact response of reinforced concrete beam and its analytical evaluation. *Journal of structural engineering*, *135*(8), 938-950.

Fujikake, K., Senga, T., Ueda, N., Ohno, T., & Katagiri, M. (2006). Effects of strain rate on tensile behavior of reactive powder concrete. *Journal of Advanced Concrete Technology*, *4*(1), 79-84.

Fujikake, K., Uebayashi, K., Ohno, T., Shimoyama, Y., & Katagiri, M. (2002). Dynamic properties of steel fiber reinforced mortar under high-rates of loadings and triaxial stress states. *WIT Transactions on The Built Environment*, *63*.

GB 50367. (2013). *Code for design of strengthening concrete structure*. Beijing: Ministry of Construction of the People's Republic of China & General Administration of Quality Supervision, Inspection and Quarantine of the People's Republic of China. (in Chinese).

GB 50608. (2010). *Technical code for infrastructure application of FRP composites*. Beijing: Ministry of Construction of the People's Republic of China & General Administration of Quality Supervision, Inspection and Quarantine of the People's Republic of China. (in English).

Gholipour, G., & Billah, A. M. (2022). Dynamic behavior of bridge columns reinforced with shape memory alloy rebar and UHPFRC under lateral impact loads. *International Journal of Impact Engineering*, *168*, 104297.

Graybeal, B. A. (2006). *Material property characterization of ultra-high performance concrete* (No. FHWA-HRT-06-103). United States. Federal Highway Administration. Office of Infrastructure Research and Development.

Guo, W., Fan, W., Shao, X., Shen, D., & Chen, B. (2018). Constitutive model of ultra-high-performance fiber-reinforced concrete for low-velocity impact simulations. *Composite Structures*, *185*, 307-326.

Harik, I. E., Shaaban, A. M., Gesund, H., Valli, G. Y. S., & Wang, S. T. (1990). United States bridge failures, 1951–1988. *Journal of Performance of Constructed Facilities*, *4*(4), 272-277.

Heimbs, S., Heller, S., Middendorf, P., Hähnel, F., & Weiße, J. (2009). Low velocity impact on CFRP plates with compressive preload: test and modelling. *International Journal of Impact Engineering*, *36*(10-11), 1182-1193.

Higgins, C. (2013). Development of Titanium Reinforcement for Rehabilitation of Bridges. In *Proceedings of 29th U.S.–Japan Bridge Engineering Workshop*. Tsukuba, Japan.

Higgins, C. (2016). Strengthening R.C. Bridges with Titanium Alloy Bars. *Structural Faults + Repair*. Edinburgh, Scotland.

Higgins, C., Amneus, D., & Barker, L. (2014). Flexural Anchorage Performance and Strengthening Using Titanium for Reinforced Concrete Bridges. *9th International Conference on Short and Medium Span Bridges*. Calgary, Canada.

Higgins, C., Amneus, D., & Barker, L. (2015a). *Methods for strengthening reinforced concrete bridge girders containing poorly detailed flexural steel using near-surface mounted metallics* (No. FHWA-OR-RD-16-02). Oregon. Dept. of Transportation. Research Section.

Higgins, C., Amneus, D., & Barker, L. (2015b). Titanium Alloy Bars for Strengthening a Reinforced Concrete Bridge. In *Proceedings of 8th New York City Bridge Conference*. New York, NY.

Higgins, C., Amneus, D., & Barker, L. (2015c). Titanium Reinforcing for Strengthening Reinforced Concrete Bridges. In *Proceedings of International Bridge Conference*. Pittsburgh, PA.

Higgins, C. (2016). Strengthening RC Bridge Girders for Flexure and Shear Using Titanium Alloy Bars. In *Proceedings of CINPAR 2016*. Porto, Portugal.

Higgins, C., Knudtsen, J., Amneus, D., & Barker, L. (2017). Shear and flexural strengthening of reinforced concrete beams with titanium alloy bar. In *Proceedings of the 2nd World Congress on Civil, Structural, and Environmental Engineering (CSEE'17), Barcelona, Spain* (pp. 2-4).

Higgins, C. C., Barbosa, A., Shrestha, S., Lostra, M., & Belejo, A. (2020). *Seismic Retrofits for Square Reinforced Concrete Columns Using Titanium Alloy Bars*. School of Civil and Construction Engineering, Oregon State University.

Isaac, P., Darby, A., Ibell, T., Evernden, M., & Silva, P. (2011). Response of FRP wrapped RC columns to impact loads. *Advanced Composites in Construction 2011*, 252-263.

Jia, P. C., Wu, H., Wang, R., & Fang, Q. (2021). Dynamic responses of reinforced ultra-high performance concrete members under low-velocity lateral impact. *International Journal of Impact Engineering*, *150*, 103818.

Knudtsen, J., & Higgins, C. (2017). *Application of titanium alloy bars for strengthening reinforced concrete bridge girders (part a: shear)* (No. FHWA-OR-RD-18-01). Oregon. Dept. of Transportation. Research Section.

Li, R., Zhang, N., Wu, H., & Jia, P. (2022a). Vehicular impact resistance of FRP-strengthened RC bridge pier. *Journal of Bridge Engineering*, *27*(8), 04022062.

Li, R. W., Zhang, N., & Wu, H. (2022b). Effectiveness of CFRP shear-strengthening on vehicular impact resistance of double-column RC bridge pier. *Engineering Structures*, *266*, 114604.

Liu, T., Chen, L., Xu, J., Demartino, C., & Kang, T. H. K. (2022). Vehicle collision with reinforced concrete columns wrapped with fiber-reinforced polymer composites. *ACI Structural Journal*, *119*(2), 165-179.

Liu, B., Fan, W., Guo, W., Chen, B., & Liu, R. (2017). Experimental investigation and improved FE modeling of axially-loaded circular RC columns under lateral impact loading. *Engineering Structures*, *152*, 619-642.

Liu, X., Zheng, Y. Z., Fang, Q., Zhou, C., Yang, Y., Xiang, H. B., & Yan, H. C. (2022, September). Anti-collision performance of RC columns strengthened with a composite of FRP grid and UHPC. In *Structures* (Vol. 43, pp. 1682-1691). Elsevier.

Ma, D., Manes, A., Amico, S. C., & Giglio, M. (2019). Ballistic strain-rate-dependent material modelling of glass-fibre woven composite based on the prediction of a meso-heterogeneous approach. *Composite Structures*, *216*, 187-200.

McGuinn, P., Tso, C. F., Donelan, P., Das, P., & Ford, R. (1996). Collisions of HGVs with bridges. In *Proceedings of International Symposium of Safety of Bridges* (pp. 4-5). London.

Micallef, K., Sagaseta, J., Ruiz, M. F., & Muttoni, A. (2014). Assessing punching shear failure in reinforced concrete flat slabs subjected to localised impact loading. *International Journal of Impact Engineering*, *71*, 17-33.

Miele, C. R., Stephens, D., Plaxico, C., & Simunovic, S. (2010). U 26: Enhanced finite element analysis crash model of tractor-trailers (Phase C).

Ministry of Transport of the People's Republic of China. (2015). *General specifications for design of highway bridges and culverts. In: JTG D60-2015*. Beijing. Ministry of Transport of the People's Republic of China.

Mohammed, T. A., & Parvin, A. (2020). Vehicle collision impact response of bridge pier strengthened with composites. *Practice Periodical on Structural Design and Construction*, *25*(4), 04020027.

Murray, Y. D. (2007). *Users manual for LS-DYNA concrete material model 159* (No. FHWA-HRT-05-062). United States. Federal Highway Administration. Office of Research, Development, and Technology.

Nanjing Hitech Composites. 2021. Accessed November 1, 2021. http://cn.hitechfrp.com/.

NCHRP Report 655. (2010). *Recommended guide specification for the design of externally bonded FRP systems for repair and strengthening of concrete bridge elements*. Transportation Research Board. Washington, D.C.

NCHRP Report 678. (2011). *Design of FRP systems for strengthening concrete girders in shear*. Transportation Research Board. Washington, D.C.

Noor, F. A., & Boswell, L. F. (1992). *Small scale modelling of concrete structures*. CRC Press.

Ožbolt, J., & Sharma, A. (2011). Numerical simulation of reinforced concrete beams with different shear reinforcements under dynamic impact loads. *International journal of impact engineering*, *38*(12), 940-950.

Popp, C. (1961). *Der Querstoss beim Aufprall von Kraftfahrzeugen auf Stützen und Rahmenstiele in Strassenunterführungen* (No. 14). Stahlbau-Verlag.

Queiroz, F. O., & Horowitz, B. (2016). Shear strength of hollow circular sections. *Revista IBRACON de Estruturas e Materiais*, *9*(2), 214-225.

Russell, H. G., Graybeal, B. A., & Russell, H. G. (2013). *Ultra-high performance concrete: A state-of-the-art report for the bridge community (No. FHWA-HRT-13-060)*. United States. Federal Highway Administration. Office of Infrastructure Research and Development.

Saatci, S., & Vecchio, F. J. (2009). Effects of shear mechanisms on impact behavior of reinforced concrete beams. *ACI structural Journal*, *106*(1), 78.

Sha, Y., & Hao, H. (2015). Laboratory tests and numerical simulations of CFRP strengthened RC pier subjected to barge impact load. *International Journal of Structural Stability and Dynamics*, *15*(02), 1450037.

Sharma, H., Gardoni, P., & Hurlebaus, S. (2014). Probabilistic demand model and performance-based fragility estimates for RC column subject to vehicle collision. *Engineering Structures*, *74*, 86-95.

Sharma, H., Hurlebaus, S., & Gardoni, P. (2008). Development of a bridge bumper to protect bridge girders from overheight vehicle impacts. *Computer-Aided Civil and Infrastructure Engineering*, *23*(6), 415-426.

Sharma, H., Hurlebaus, S., & Gardoni, P. (2012). Performance-based response evaluation of reinforced concrete columns subject to vehicle impact. *International Journal of Impact Engineering*, *43*, 52-62.

Sohel, K. M. A., Al-Jabri, K., & Al Abri, A. H. S. (2020, August). Behavior and design of reinforced concrete building columns subjected to low-velocity car impact. In *Structures* (Vol. 26, pp. 601-616). Elsevier.

Takahashi, Y., Muto, I., Tadokoro, Y., & Tagomori, N. (1994). Application of titanium to construction and civil engineering. In *Nippon Steel Technical Report* (pp. 9-15). Nippon Steel Corp.

Thilakarathna, H. M. I., Thambiratnam, D. P., Dhanasekar, M., & Perera, N. (2010). Numerical simulation of axially loaded concrete columns under transverse impact and vulnerability assessment. *International Journal of Impact Engineering*, *37*(11), 1100-1112.

UEDA, M., HIRAGA, A., & NISHIMURA, T. (2011). Compressive strength of a carbon fiber in matrix. *Journal of the Japan Society for Composite Materials*, *37*(3), 103-110.

Vavra, E., & Higgins, C. (2017). *Application of Titanium Alloy Bars for Strengthening Reinforced Concrete Bridge Girders. Part B: Flexure*. FHWA-OR-18-03. Oregon Department of Transportation, Salem, OR.

Wardhana, K., & Hadipriono, F. C. (2003). Analysis of recent bridge failures in the United States. *Journal of performance of constructed facilities*, *17*(3), 144-150.

Wei, J., Li, J., & Wu, C. (2023). Study on hybrid fibre reinforced UHPC beams under single and repeated lateral impact loading. *Construction and Building Materials*, *368*, 130403.

Wei, J., Li, J., Wu, C., Liu, Z. X., & Li, J. (2021). Hybrid fibre reinforced ultra-high performance concrete beams under static and impact loads. *Engineering Structures*, *245*, 112921.

Williams, E. M., Graham, S. S., Reed, P. A., & Rushing, T. S. (2009). Laboratory characterization of Cor-Tuf concrete with and without steel fibers.

Xu, J. J., Demartino, C., Shan, B., Heo, Y. A., & Xiao, Y. (2020). Experimental investigation on performance of cantilever CFRP-wrapped circular RC columns under lateral low-velocity impact. *Composite Structures*, *242*, 112143.

Yao, J., Teng, J. G., & Chen, J. F. (2005). Experimental study on FRP-to-concrete bonded joints. *Composites Part B: Engineering*, *36*(2), 99-113.

Zanotti, C., & Randl, N. (2019). Are concrete-concrete bond tests comparable?. *Cement and Concrete Composites*, *99*, 80-88.

Zhang, X., Hao, H., & Li, C. (2016). Experimental investigation of the response of precast segmental columns subjected to impact loading. *International Journal of Impact Engineering*, *95*, 105-124.

Zhou, D., & Li, R. (2018). Damage assessment of bridge piers subjected to vehicle collision. *Advances in structural engineering*, *21*(15), 2270-2281.

Zhou, S. C., Demartino, C., Xu, J. J., & Xiao, Y. (2021). Effectiveness of CFRP seismic-retrofit of circular RC bridge piers under vehicular lateral impact loading. *Engineering Structures*, *243*, 112602.

APPENDIX A: HORSE HM-60 CARBON FIBER FABRIC PROPERTIES

Dry fiber properties

Tensile strength	710.68 ksi (4900 MPa)
Tensile modulus	37061.39 ksi (255530 MPa)
Elongation	0.016

Laminated fiber properties

Tensile strength (ASTM D3039)	598.05 ksi (4123.43 MPa)
Tensile modulus (ASTM D3039)	33671.96 ksi (232160 MPa)
Elongation (ASTM D3039)	0.0169
Flexural strength (ASTM D7264)	151.44 ksi (1044.15 MPa)
Shear strength (ASTM D2344)	11.60 ksi (80 MPa)
FRP with concrete bonding strength	$\geq$ 0.36 ksi (2.5 MPa)
Density	112.37 lb/ft^3 (1800 kg/m^3)
Fiber thickness	0.013 in (0.333 mm)